

TRANSPORT AND FORMATION PROCESSES FOR FINE AIRBORNE ASH
FROM THREE RECENT VOLCANIC ERUPTIONS IN ALASKA:
IMPLICATIONS FOR DETECTION METHODS AND TRACKING MODELS

By

Peter G. Rinkleff

RECOMMENDED:

Kenneson G. Dean

James E. Beget

Jonathan Dehn, Advisory Committee Co-Chair

Catherine F. Cahill, Advisory Committee Co-Chair

Sarah J. Fowell, Co-Chair, Department of Geology and
Geophysics

Anupma Prakash, Co-Chair, Department of Geology and
Geophysics

APPROVED:

Paul W. Layer, Dean, College of Natural Science and
Mathematics

Lawrence K. Duffy, Interim Dean of the Graduate School

Date

TRANSPORT AND FORMATION PROCESSES FOR FINE AIRBORNE ASH
FROM THREE RECENT VOLCANIC ERUPTIONS IN ALASKA:
IMPLICATIONS FOR DETECTION METHODS AND TRACKING MODELS

A
THESIS

Presented to the Faculty
of the University of Alaska Fairbanks

in Partial Fulfillment of the Requirements
for the Degree of

DOCTOR OF PHILOSOPHY

By

Peter G. Rinkleff

Fairbanks, Alaska

December 2011

© Peter G. Rinkleff

UMI Number: 3530096

All rights reserved

INFORMATION TO ALL USERS

The quality of this reproduction is dependent upon the quality of the copy submitted.

In the unlikely event that the author did not send a complete manuscript and there are missing pages, these will be noted. Also, if material had to be removed, a note will indicate the deletion.



UMI 3530096

Published by ProQuest LLC (2012). Copyright in the Dissertation held by the Author.

Microform Edition © ProQuest LLC.

All rights reserved. This work is protected against unauthorized copying under Title 17, United States Code



ProQuest LLC.
789 East Eisenhower Parkway
P.O. Box 1346
Ann Arbor, MI 48106 - 1346

Abstract

Airborne fine volcanic ash was collected during the eruptions of Augustine Volcano in 2006, Pavlof Volcano in 2007, and Redoubt Volcano in 2009 using Davis Rotating Unit for Measurement (DRUM) cascade impactors to observe atmospheric processes acting on ash as an atmospheric particle. During the Redoubt eruption, samples were also collected by Beta Attenuation Mass (BAM-1020) and Environmental Beta Attenuation Mass (EBAM) monitors. BAM-1020s and EBAMs provided real-time mass concentration data; DRUM samplers provided samples for post-eruptive analysis. DRUM samples were retrospectively analyzed for time-resolved mass concentration and chemistry. EBAM and BAM-1020s reported near real-time, time-resolved mass concentrations. Scanning Electron Microscopy with Energy Dispersive Spectroscopy was conducted to determine particle size, shape, and composition. Image processing methods were developed to determine particle size distributions and shape factors.

Ash occurred as single grains, ash aggregates, and hybrid aggregates. Ash aggregates occurred in plumes from pyroclastic flows and were found in a discrete aerodynamic size range (2.5-1.15 μm). Hybrid ash was common in all samples and likely formed when downward mixing ash mingled with upward mixing sea salt and non-sea salt sulfate. The mass concentration of sulfate did not vary systematically with ash which indicated that the source of sulfate was not

necessarily volcanic. Ash size distributions were log-normal. Size distribution plots of ash collected from the same plume at different transport distances showed that longer atmospheric residence times allowed for more aggregation to occur which led to larger but fewer particles in the plume the longer it was transported. Ash transport and dispersion models forecasted ash fall over a broad area, but ash fall was only observed in areas unaffected by topographic barriers. PM_{10} (particulates $\leq 10 \mu\text{m}$ in aerodynamic diameter or O_A) ash was detected closer to the volcano when no $PM_{2.5}$ (particulates $\leq 2.5 \mu\text{m}$ O_A) ash was observed. Further downwind, $PM_{2.5}$ ash was collected which indicated that the settling rates of PM_{10} and $PM_{2.5}$ influenced their removal rates. Diurnal variations in ash mass concentrations were controlled by air masses rising due to solar heating which transported ash from the sampling site, or descending due to radiative cooling which brought ash to the sampling site. Respirable ($PM_{2.5}$) ash was collected when there were no satellite ash detections which underscored the importance of ash transport and dispersion models for forecasting the presence of ash when mass concentrations are below satellite detection limits.

Table of Contents

	Page
Signature Page	i
Title Page	ii
Abstract	iii
Table of Contents	v
List of Figures	xi
List of Tables	xxix
Dedication Page	xxx
Chapter 1 Introduction	1
1.1 The Atmospheric Fate and Transport of Volcanic Ash	3
1.1.1 Atmospheric Influences on Particle Growth	4
1.1.2 Particle Settling and Stokes' Law	6
1.1.3 Ash Particle Composition	10
1.1.4 Changes to Aerosol Shape, Size, and Density	11
1.1.5 The Influence of Volcanic Plume Regions on Aggregation	12
1.1.6 The Influence of Tropospheric Transport on Aggregation	14
1.1.7 The Influence of PBL Transport on Aggregation	15
1.2 Collection Methods and Analytical Techniques	16
1.2.1 Davis Rotating Unit for Measurement (DRUM) Samplers	16
1.2.2 Beta Attenuation Mass (BAM-1020) Monitors and Environmental Beta Attenuation Monitors (EBAM)	17

	Page
1.2.3 Scanning Electron Microscopy (SEM) and Energy Dispersive Spectroscopy (EDS).....	17
1.2.4 Digital Image Processing Techniques.....	18
1.3 The 2006 Eruption of Augustine Volcano.....	18
1.4 The 2007 Eruption of Pavlof Volcano.....	21
1.5 The 2009 Eruption of Redoubt Volcano.....	21
1.6 References.....	25
1.7 Figures.....	30
1.8 Tables.....	35
Chapter 2 Particle Morphologies and Formation Processes for Fine Ash Aerosol Collected During the 2006 Eruption of Augustine Volcano, Alaska.....	36
Abstract.....	36
2.1 Introduction.....	38
2.2 Geologic Setting and Eruptive History.....	41
2.3 Augustine 2006 Eruption.....	41
2.4 Sampling and Analytical Techniques.....	43
2.4.1 Davis Rotating Unit for Measurement (DRUM) Sampler.....	43
2.4.2 SEM and EDS Analysis Techniques.....	44
2.4.3 Image Analysis Techniques.....	47
2.5 Results.....	48
2.5.1 Volcanic Ash Aerosol Types.....	48

	Page
2.5.1.1 Single Grain Ash.....	49
2.5.1.2 Ash Aggregates.....	49
2.5.1.3 Hybrid Aggregates.....	49
2.5.2 Volcanic Ash Particle Size Distributions.....	51
2.5.2.1 Initial Eruption Phase.....	51
2.5.2.2 Pyroclastic Flow Particles.....	52
2.6 Discussion.....	52
2.6.1 Potential Aggregation Processes.....	53
2.6.2 Implications of Ash Aggregation Processes for Transport Models and Satellite Detection Methods.....	55
2.7 Acknowledgements.....	56
2.8 References.....	58
2.9 Figures.....	64
2.10 Tables.....	81
Chapter 3 Daily Variation in PM_{2.5} Volcanic Ash Concentration Reaching Sand Point, AK from the 2007 Eruption of Pavlof Volcano	82
Abstract.....	82
3.1 Introduction.....	84
3.2 Satellite Ash Detection Methods.....	85
3.3 Tephra Studies.....	86
3.4 Eruptive Chronology and Geologic Setting.....	88

	Page
3.5 Aerosol Collection	89
3.6 SEM and EDS Spectroscopy	91
3.7 HYSPLIT Air Mass Tracking Method	93
3.8 Results.....	93
3.8.1 Identification and Description of Ash.....	93
3.8.2 Sulfur and Sea Salt Maritime Aerosols.....	95
3.8.3 Meteorological Influences	98
3.9 Conclusions.....	99
3.10 Acknowledgements.....	100
3.11 References.....	101
3.12 Figures.....	106
3.13 Tables.....	118
Chapter 4 Characterization of Airborne Volcanic Ash Aerosols Collected During the 2009 Redoubt Volcano Eruption.....	121
Abstract.....	121
4.1 Introduction.....	124
4.1.1 Geologic Setting and Eruptive History.....	124
4.1.2 Redoubt Volcano 2009 Eruption	125
4.1.3 Sampling Sites	126
4.2 Sample Collection Techniques	128

	Page
4.2.1 Environmental Beta Attenuation Monitors (EBAMs) and Beta Attenuation Mass Monitors (BAM-1020s).....	128
4.2.2 Davis Rotating Unit for Measurement (DRUM) Sampler.....	129
4.2.3 Tephra Sampling.....	131
4.3 SEM Sample Analysis	131
4.3.1 DRUM Sample Analysis.....	131
4.3.2 EBAM and BAM-1020 Sample Analysis.....	132
4.4 SEM and EDS Analysis Techniques.....	134
4.5 Discussion	135
4.6 Conclusion	137
4.7 Acknowledgments.....	138
4.8 References.....	140
4.9 Figures.....	146
Chapter 5 Conclusion.....	168
5.1 Ash Aggregation Processes.....	168
5.2 Fine Ash Volume and Settling Rate Underestimation	169
5.3 Satellite Detection Method Limitations	171
5.4 References.....	173
Appendix A Augustine DRUM SEM Images.....	DVD
Appendix B Augustine EDS Particle Measurements and Shape Descriptors...DVD	
Appendix C Augustine DRUM EDS Spectra Graphs and Tables	DVD

	Page
Appendix D Augustine DRUM EDS Element Maps.....	DVD
Appendix E Pavlof DRUM SEM Images and EDS Element Maps.....	DVD
Appendix F Pavlof EDS Particle Measurements and Shape Descriptors	DVD
Appendix G Pavlof DRUM EDS Spectra Graphs and Tables.....	DVD
Appendix H Pavlof DRUM EDS Element Maps.....	DVD

List of Figures

	Page
Chapter 1 Figures	
Figure 1.1. Study map showing the locations of Augustine, Pavlof, and Redoubt volcanoes with selected populated places in Alaska	30
Figure 1.2. Schematic diagram of volcanic plume interacting with atmospheric features. Figure is from McGee et al. (1997)	31
Figure 1.3. Representative regional vertical distribution of tropospheric aerosol mass concentration. Most of the aerosol content in the troposphere is within the first few kilometers of the atmosphere. Figure is from Jaenicke (1993)	32
Figure 1.4. An irregular particle and its equivalent spheres. Figure is from Reist, 1993	33
Figure 1.5. Schematic steps involved in the transfer of SO ₂ from the gas phase to the aqueous phase of an atmospheric water droplet and its oxidation in the liquid phase. SO _{2(g)} = gas phase SO ₂ , SO _{2(l)} = SO ₂ at water-gas interface. The sequence of steps is as follows: 1) Transport of gas to the surface of the droplet, 2) Transfer of gas across the gas-water interface, 3) Formation of aqueous phase equilibria of the dissolved species, 4) Transport of the dissolved species from the surface to the bulk aqueous phase of the droplet, 5) Reaction in the droplet. Figure and caption after Finlayson-Pitts and Pitts (1986).....	34

Chapter 2 Figures

- Figure 2.1. Location map of Augustine Volcano and the sampling location near Homer, Alaska. Augustine is located in Cook Inlet 275 km west-southwest of Anchorage and 110 km west of Homer64
- Figure 2.2. Silicon mass concentration relative to time. The initial eruptive phase from 13 to 22 January (blue box) is dominated by larger aerosols ($35.0\text{-}1.15\ \mu\text{m}\ \text{O}_A$). Smaller size fractions have essentially no silicon present. The eruptive style for the period starting on 28 January through 5 February (orange box) was dominated by pyroclastic flows. While significant ash mass concentrations were present in the larger size fractions, significant ash mass concentrations were also present in smaller size fractions ($1.15\text{-}0.26\ \mu\text{m}\ \text{O}_A$)65
- Figure 2.3. Silicon mass concentration relative to time ($1.15\text{-}0.09\ \mu\text{m}\ \text{O}_A$). The initial eruptive phase indicated by the blue box had very little ash present due to the explosive ash-forming processes that occurred during this phase. Over the pyroclastic flow-dominated phase (orange box) clast-to-clast milling produced fine ash $1.15\text{-}0.26\ \mu\text{m}\ \text{O}_A$ 66

Figure 2.4. An An 8-stage DRUM cascade impactor. Arrows indicate the flow direction. The inlet pictured is a standard $10\ \mu\text{m}\ \text{O}_A$ configuration. The inlet, Stage 1 (inlet to $5.0\ \mu\text{m}\ \text{O}_A$) and Stage 8 ($0.26\text{-}0.09\ \mu\text{m}\ \text{O}_A$) are indicated by arrows. The inlet shown here imparts a $10\ \mu\text{m}\ \text{O}_A$ initial size cut. The yellow arrow indicates the flow direction through the sampler. Image courtesy of T. Cahill and the Delta Group, University of California, Davis67

Figure 2.5. The 8-stage DRUM impactor installed at the University of Alaska Homer, AK Field Station. The sampler was inverted from its normal deployment configuration and was fitted with a special inlet (white pipe) for collecting $35.0\ \mu\text{m}\ \text{O}_A$ and smaller aerosol68

Figure 2.6. An example drum with collected aerosol. This drum (not from this study) has been used to collect aerosol over an extended period. The dark lines are likely heavy industrial pollutants and carbon soot. The lines on the drum surface result from the internal slotted orifice directing aerosols to impact on the drum surface over a discrete time interval69

- Figure 2.7. SEM DRUM sample image mosaic. The large particles are hybrid aggregates or ash comingled with non-sea salt sulfates and sea salts; smaller particles are individual ash grains and sea salt particles. Each individual image represents 3 hours of sampling time based on a drum rotation rate of 4 mm/day. The entire mosaic represents about 8.5 hours of sampling time taking image overlaps into account.....70
- Figure 2.8. EDS element map image pre-processing steps. The corresponding secondary electron image (A) is analyzed by EDS for Si element composition (B). The resulting element map is inverted to more clearly show EDS X-ray detects71
- Figure 2.9. Particles digitally segmented by the ‘watershed’ method. Some particles were segmented while others retained their original dimensions. Figures are from Ferreria and Rasband (2011)72
- Figure 2.10. Post thresholding image selection. After the inverted element map is thresholded by the three methods indicated in the text and segmented, manual review of the threshold results is conducted. The original inverted element map is visually compared to the threshold results and the result most closely matching the inverted image (A) is retained. The other two images (B & C) are discarded73

Figure 2.11. Single ash SEM images. These images (A and B) show the general features of individual glassy ash grains. These images were obtained from DRUM samples collected on 30 January 2006. The images from Stage 5 and 7 (C and D) are included to show the lack of ash present. The particles present in these stages are non-sea salt sulfate aerosol74

Figure 2.12. Particle size distribution for single grain ash. Single grain ash particle size distributions for ash collected on 14 (A and B) and 17 January 2006 (C and D) shown here are log-normal. The plume sampled on 14 January was sampled again on 17 January due to favorable weather conditions. Comparison of early plume and late plume distributions show enrichment in larger particles possibly due to either particle aggregation or the plume settling low enough to be sampled at a higher mass concentration near the ground level75

Figure 2.13. Ash aggregate images. Ash aggregates were only observed in the 2.5-1.15 $\mu\text{m } \text{Ø}_A$ Stage 3 aerosols collected from plumes from pyroclastic flows. These images are of samples collected during 30 January 2006 and show ash aggregates present with individual ash grains.....76

Figure 2.14. Hybrid ash aggregate images. Hybrid ash aggregates were found in all stages. Ash imaged in A was collected in Stage 1 on 14 January 2006, B was collected in Stage 3 on 31 January 2006, C was collected in Stage 5 on 3 February 2006, and D was collected by Stage 7 on 30 January 2006. In the larger sizes ($35.0-1.15 \mu\text{m } \text{Ø}_A$) the dominant aerosol was sea salt that had mingled with ash. Smaller size fractions were mostly non-sea salt sulfate that had combined with volcanic ash.....77

Figure 2.15. Non-ash aerosols collected by DRUM sampler. The aerosols, shown in A and B were collected on 26 January 2006 in Stage 1 and 5 respectively, are mostly sea salt with minor amounts of non-sea salt sulfate. Aerosols shown in C and D were collected in Stage 5 on 16 January and 23 January 2006 respectively. Aerosols shown in E were collected in Stage 7 on 26 January 2006. Images C, D, and E show non-sea salt sulfates. It is interpreted that the dendritic forms shown in C were the result of a wet sulfate droplet drying on the sample surface after being sampled78

Figure 2.16. HYSPLIT back trajectory showing the path of the plume sampled first on 14 January and again on 17 January 2006. Note how the altitude of the plume descends over the transport path. This is due to modeled air parcel isentropic movement, not by HYSPLIT modeling ash settling rates.....79

Figure 2.17. Pyroclastic flow elutriation plume particle size distributions. Ash was present in Stages 1-7. The particle size distributions shown here are from Stages 1, 3, 5 and 7. The total distribution in log-normal as are those from Stages 1-5. Stage 7 shows a bimodal distribution possibly due to the smallest particle sizes ($\leq 0.01 \mu\text{m}^2$) being the result of image noise. The second mode centered at $0.02 \mu\text{m}^2$ may represent the very fine end of the particle size distribution for the elutriation plume.....	80
--	----

Chapter 3 Figures

Figure 3.1. Location map of Pavlof Volcano and the sampling location in Sand Point, Alaska. Pavlof is located on the Lower Alaska Peninsula between the Pacific Ocean and the Bering Sea 90 km west of Sand Point.....	106
--	-----

Figure 3.2. Three stage DRUM sampler, sample drum, and installation at Sand Point, Alaska. The dark lines on the sample drum (A) pictured here (not from this study) are likely heavy industrial pollutants and carbon soot. Three sample drums fit in the chambers in the DRUM sampler (B). For installation at Sand Point (C), the sampler was wrapped in a plastic bag and attached to the red cooler which contained the vacuum pump. The plastic bag gave a measure of weather resistance to the sampler. Holes in the cooler allowed air circulation necessary for keeping the pump cool. The entire sampler assembly was attached with bungee cords to a wooden pallet weighted with rocks to give the sampler set-up some stability. The sampler was connected to local AC power and operated unattended for 6 weeks. The entire sampler assembly was transported in the red cooler.....107

Figure 3.3. SEM DRUM sample image mosaic. The large particles are sea salts; smaller particles are volcanic ash. Each individual image represents 1.4 hours of sampling time based on a rotation rate of 4 mm/day. The entire mosaic represents 4 hours of sampling time taking the image overlaps into account108

Figure 3.4. Si, Al, Ca, Fe, Mg, K, and Ti concentrations versus time (2.5-1.15 μm O_A) showing diurnal variation109

Figure 3.5. HYSPLIT back trajectories for 29-31 August 2007 over Sand Point, Alaska	110
Figure 3.6. Silicon concentration versus time showing diurnal variation.....	111
Figure 3.7 A and B. SEM Images and EDS maps from Stage 1 (2.5-1.15 μm O_A). A, collected at 17:00 AKDT on 27 August 2007, shows abundant volcanic ash along with large sea salt particles. B, collected at 23:00 AKDT on 27 August 2007, shows infrequent ash particles along with abundant sea salt particles. Both images have minor sulfate aerosols....	112
Figure 3.7 C and D. SEM images and EDS maps from Stage 2 (1.15-0.34 μm O_A). C was collected at 18:00 AKDT on 30 August 2007 and shows sparse volcanic ash along with abundant sulfate. D was collected at 02:00 AKDT on 31 August 2007 and shows abundant volcanic ash and sulfate. Both images show little sea salt	113
Figure 3.7 E and F. SEM images and EDS maps from Stage 3 (0.34-0.1 μm O_A). E was collected at 18:00 AKDT on 30 August 2007 and shows sparse volcanic ash along with occasional sulfate. F was collected at 05:00 AKDT on 31 August 2007 and shows abundant volcanic ash and sulfate. Both images show no sea salt. The dark patch in the upper left-hand corner of the Cl map in F is the result of contamination on the sample mount	114

Figure 3.8. Wind direction and speed data from Cold Bay, AK from 26 August – 8 September 2007. Source: Weather Underground www.wunderground.com accessed on 13 May 2011, based on unofficial National Weather Service station Sand Point PASD weather data. The nearest official data are available from the Cold Bay PACD station which show similar conditions over these intervals115

Figure 3.9. AVHRR BTD split-window images showing ash clouds at Pavlof Volcano. The left image was taken on 28 August 2007 at 11:48PM AKDT (29 August 07:48 UTC) and the right image was taken almost ten hours later on 29 August at 09:20 AKDT (17:20 UTC). Areas that may contain ash are colored blue through light green. The earlier image shows the ash plume during an explosive phase of the eruption. The later image show the remnants of that earlier plume as detached ash clouds. Other blue areas scattered along the peninsula are algorithm artifacts not related to ash. Image and caption credit: Rick Wessels. Image courtesy of AVO/USGS.....116

Figure 3.10. Photo of steam and ash erupting from Pavlof volcano on 29 August 2007, from 13:10-13:15, AKDT. This image was taken from the northwest. The plume is weak and bent over. Steam is evident near the summit, but only diffuse ash is visible downwind of the volcano. Image credit: Guy Tytgat. Image courtesy of AVO/USGS117

Chapter 4 Figures

- Figure 4.1. Location map of Redoubt Volcano, Alaska and sampling locations used in this study. Redoubt is located on Cook Inlet 170 km southwest of Anchorage 146
- Figure 4.2. Exterior view of an EBAM equipped with a meteorological station. The unit consists of a louvered inlet (top) which is attached to the sampler cabinet. Attached to the sampler cabinet by two horizontal arms are weather station components. A communications unit is also attached to the main sampler cabinet. Photo credit: Drew Grimes, U.S. Fish and Wildlife Service 147
- Figure 4.3. Interior view of the EBAM filter tape, β -source and detector. The assembly shown in the upper center of the cabinet contains the base of the inlet tube shown in Figure 4.2 and a ^{14}C source which emits a constant source of β -particles. The β -particles are attenuated as they collide with particles collected on the filter tape. Two dark sample spots are visible on the take-up roll of the filter tape spool. Aerosols are the filter tape which is located between the base of the inlet and the β -particle detector assembly. Photo Credit: MetOne Inc 148

Figure 4.4 A and B. EBAM filter sample spots from the MOA Garden site

PM_{2.5} configured EBAM with Redoubt ash present. These spots are about 1 cm in diameter and represent a one hour interval. 4A shows a close-up of individual filter spots. The dark spot was collected over the 11:00 (AKDT) hour during a high mass loading episode while the lighter and virtually blank spots were collected during low mass loading episodes. B shows an entire 24 hour sample period. Note the arrows bracketing the 24 hour period. At each 24 hour interval, the EBAM advances 2 spaces to indicate the date change..... 149

Figure 4.5. Three-stage DRUM sampler (A), sample drum (B), and chamber inlet (C).

The sampler (A) connects to a vacuum pump and inlet/cyclone unit which imparts the initial size cut. The 3 circular chambers contain rotating drums that provide the sampling impaction surface. The first chamber (opened) collects the largest size fraction (2.5-1.15 $\mu\text{m } \text{\textcircled{A}}$). Subsequent stages collect smaller aerosol (1.15-0.34 and 0.34-0.1 $\mu\text{m } \text{\textcircled{A}}$). The outer case is 30 x 20 x 10 cm. The sample drum (B) has a MylarTM strip affixed to the outer surface. The dark lines on the outer drum surface are combustion aerosol particles that have collected on the MylarTM strip 150

- Figure 4.6. SEM DRUM sample image mosaic. The large particles are salts, smaller particles are volcanic ash. Each individual image represents about 3.5 hours of sampling time based on a rotation rate of 4 mm/day. The entire mosaic represents about 9 hours of sampling time after taking the image overlaps into account..... 151
- Figure 4.7. SEM secondary electron (SE) image and EDS element maps of EBAM filter tape. Si, Ca, and Al element maps are shown. The entire filter media is silica rich, while the thicker fibers also contain significant amounts of Ca and Al 152
- Figure 4.8. Secondary electron image of PM₁₀ EBAM filter tape and aerosol sample collected on 28 March 2009 at 05:00 AKDT at the MOA Air Quality Monitoring Program Garden site and corresponding EDS spectra from circled particles. Note the prominent silicon, aluminum, and calcium peaks in each spectrum regardless of particle composition. Particles indicated by 1 and 3 are likely salt aerosols due to the high chlorine counts, but the spectra are still dominated by background silicon counts. Particles indicated by 2 and 3 are possibly volcanic ash particles. Silicon is detected in all particles since the background (filter media) is made of silicon, aluminum, and calcium-rich glass fibers..... 153

- Figure 4.9. Secondary electron image of PM₁₀ EBAM filter tape and aerosol sample collected on 28 March 2009 at 18:00 AKDT at the MOA Air Quality Monitoring Program Garden site. Image A is the filter tape before analysis. Image B is the same area imaged after the collection of a 6 minute EDS spectra scan of approximately 25,000 counts per second, with the largest beam spot size setting and maximum accelerating current. Note the extensive fusing of aerosols and filter media. Some minor shifting of filter fibers is also present. Scan time, spot size, and accelerating current were set to collect sufficient x-ray counts to produce element maps with enough resolution for reliable image processing154
- Figure 4.10. Secondary electron image of PM_{2.5} EBAM filter tape and aerosol sample collected on 28 March 2009 at 05:00 AKDT at the MOA Air Quality Monitoring Program Garden site. Few particles are present in the sample due to the low PM_{2.5} mass concentration (3 µg/m³). Those particles that are present are found on the surface of thick fiber mats (A) or imbedded in the media (B, C, and D)155
- Figure 4.11 A. Hourly EBAM PM₁₀ levels in Soldotna, Alaska from 22 through 26 March 2009. Mass concentration spikes on 23 March are due to Redoubt ash at the sampling site. Mass concentrations after March 23 are from non-volcanic aerosols.....156

Figure 4.11 B. Hourly BAM-1020 PM ₁₀ and PM _{2.5} levels in Anchorage, Alaska from 22 through 26 March 2009. Mass concentration spikes on 23 March are due to Redoubt ash at the sampling site. Non-volcanic aerosol was responsible for the elevated aerosol mass concentrations after 23 March 2009	157
Figure 4.11 C. Hourly BAM-1020 PM ₁₀ and PM _{2.5} levels in Wasilla, Alaska from 22 through 26 March 2009. No distinct increase in mass concentration coincides with HYSPLIT model predictions for 23 March. Non-volcanic aerosol was responsible for the elevated aerosol mass concentrations after 23 March 2009	158
Figure 4.11 D. Hourly BAM-1020 PM ₁₀ and PM _{2.5} levels in Palmer, Alaska from 22 through 26 March 2009. No mass concentration spikes were observed on 23 March despite HYSPLIT predicted arrival of air masses from Redoubt. Non-volcanic aerosol was responsible for the elevated aerosol mass concentrations after 23 March 2009	159
Figure 4.12. Relative hourly PM ₁₀ levels in Soldotna, Anchorage, Wasilla, and Palmer, Alaska from 23 to 26 March 2009. Mass concentration spikes (indicated by the box) on 23 March are due to Redoubt ash at the sampling site in Soldotna and Wasilla. No mass concentration spikes were observed in Palmer and Wasilla on 23 March. Aerosol mass concentrations after March 23 are from non-volcanic aerosol	160

- Figure 4.13. HYSPLIT backward trajectories for Soldotna, Anchorage, Wasilla/Palmer, and DNP&P HQ for the 23 March 2009 Redoubt eruption events. Trajectory altitudes are in meters above ground level.....161
- Figure 4.14. Time series of Si aerosol concentration collected by the DRUM sampler located at DNP&P HQ from 20 March-11 April 2009. The mass concentrations in boxes 1–3 are likely due to volcanic ash from Redoubt. This is confirmed by HYSPLIT trajectories presented in Figure 4.16. Silicon mass concentrations indicated in boxes 4–6 are from non-volcanic sources such as glacial dust and windblown river sediments. Note the relatively low silicon mass concentrations in the smallest ($0.34\text{-}0.09\ \mu\text{m}\ \varnothing_A$) size fraction relative to the other stages.....162
- Figure 4.15 A. SEM secondary electron image and EDS element maps of aerosol collected at DNP&P HQ by DRUM sampler in the $2.5\text{-}1.15\ \mu\text{m}\ \varnothing_A$ stage at 09:00 AKDT 23 March 2009. Sampling direction is from right to left. Volcanic glass shards are visible in the SE image and are visible in the EDS Si map. Some large sulfate particles are also present and evident in the S map. Minor chlorine salts are present, but most of the field of view is below the detection limit for Cl. No aggregation of particles is observed.....163

Figure 4.15 B. SEM secondary electron image and EDS element maps of aerosol collected at DNP&P HQ by DRUM sampler in the 1.15-0.34 μm O_A stage at 08:00 AKDT 23 March 2009. Sampling direction is from right to left. Some volcanic ash particles are visible in the SE image and the EDS Si map, but are very small and do not distinctly show shard shapes. Many large sulfate particles are also present and evident in the S map. No Cl is evident. The concentration of Si particles increases from right to left indicating a change in aerosol mass load. The sulfate mass load does not seem to change systematically with Si indicating that S and Si mass concentrations in this sampling interval are independent.....164

Figure 4.15 C. SEM secondary electron image and EDS element maps of aerosol collected at Ninilchik, Alaska by DRUM sampler in the 2.5-1.15 μm O_A stage at 17:00 AKDT 26 March 2009. Sampling direction is from right to left. Some Si is present and associated with S particles. Circular, ellipsoid, and rod-shaped Cl sea salt particles are abundant in the field of view. The S+Si particles are separate from the Cl particles indicating that Si and S aerosols combined to form hybrid aerosol while the sea salt particles did not. It is possible that the sulfate particles were liquid and sea salt particles were crystalline when aggregation occurred which could influence the aggregation process.....165

Figure 4.15 D. SEM secondary electron image and EDS element maps of aerosol collected at Ninilchik, Alaska by DRUM sampler in the 1.15-0.35 μm stage at 09:00 AKDT 27 March 2009. Sampling direction is from right to left. Large sulfate particles exhibiting distinct crystal shapes are evident in this image. There is no Cl aerosol present. Si aerosol is ubiquitous throughout the field of view. Sulfate may have been a dry aerosol when it was sampled due to the crystal shapes present in the image and that Si seems to be evenly distributed in the sample and not partitioned in sulfate particles. Sulfate particle sizes seem to decrease and particles become less crystalline as sampling progresses166

Figure 4.16. HYSPLIT backward trajectories for Denali National Park and Preserve (DNP&P) for 28-30 March 1 April and 7 April 2009. Trajectories from the 28-30 March show air masses transporting from Redoubt to DNP&P. Trajectories from 1 and 7 April 2009 show air masses transporting from the northeast and north, respectively167

List of Tables

	Page
Chapter 1 Tables	
Table 1.1 Magma Compositions and Constituents	35
Chapter 2 Tables	
Table 2.1. Shape Descriptors	81
Chapter 3 Tables	
Table 3.1. Satellite Sensors Used for Brightness Temperature Difference Ash Detection	118
Table 3.2. Composition of Sea Salt Particles in Clean Atmospheres	119
Table 3.3. Atmospheric Sulfur Aerosols.....	120

Dedication

Accomplishments are made with the support of others.

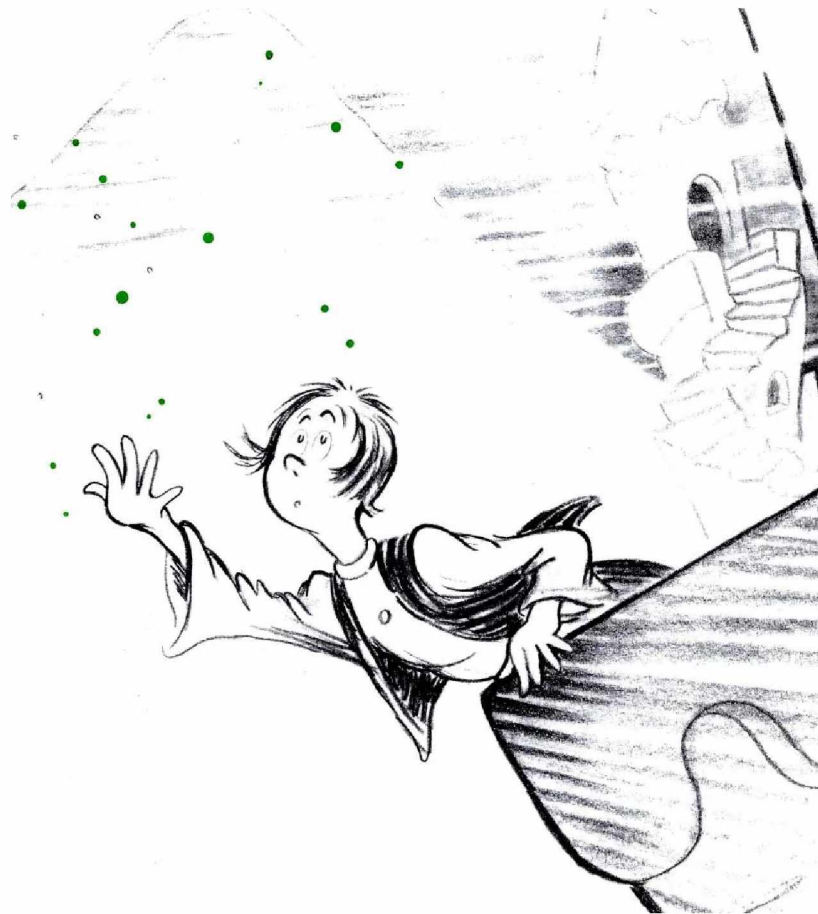
Without the constant encouragement and perspective of my wife, Wendy, I would not have been able to complete this dissertation. It is to her that I dedicate this work.

And to my children, Cecilia and Colin, from whom I have gained a renewed appreciation of the world at large that I further dedicate this volume.

And to my parents who developed and nurtured my initial sense of interest in the natural world, I owe my heartfelt gratitude.

And those teachers, professors, colleagues, and friends who have shared with me their enthusiasm and interest, I owe my sincere thanks.

And lastly, to those who have reviewed and edited this work I owe my sincere thanks. Their thoughtful comments and suggestions made this work possible.



“I wish,” spoke the King, “to have you make something fall from my skies that no other kingdom has ever had before. What can you do? What will you make?”

For a moment they stood thinking, blinking their creaky eyes. Then they spoke a word...one word...“Oobleck.”

“Oobleck...?” asked the King. “What will it look like?”

*“Won’t look like rain. Won’t look like snow.
Won’t look like fog, that’s all we know.
We just can’t tell you any more.
We’ve never made oobleck before.”*

*Excerpt and illustration from Oobleck, by Dr. Seuss.
1949. Random House Publishers, New York, NY.*

Chapter 1 Introduction

Volcanoes are constantly erupting around the world. Every year, an average of 20-30 explosive eruptions are observed worldwide (Siebert and Simkin, 2002-). Ash from these eruptions can impact human health (Horwell and Baxter, 2006), aviation (Casadevall, 1994), climate (Darteville et al., 2002), ecosystems (Langman et al., 2010), and visibility (Blong, 1984). Large eruptions, greater than Volcanic Explosivity Index (VEI) 3, occur about three times per year (Siebert and Simkin, 2002-; Newhall and Self, 1982). Ash from these eruptions can be injected high into the atmosphere, undergo long range transport, and cause effects far from the eruption source (Mather et al., 2003). Some notable examples of such eruptions include the Eyjafjallajökull eruption in 2010 which closed commercial airspace over Europe (Gudmundsson et al., 2010), the eruption of Mt. Pinatubo in 1992 which affected global temperatures (Darteville et al., 2002), and the 1985 eruption of Mt. St. Helens which produced measurable ash in several Western U.S. states (Sarna-Wojcicki et al., 1981). While these large eruptions capture headlines and the collective conscious, smaller eruptions are far more numerous and can produce ash clouds which can undergo long range transport (Mather et al., 2003; Schneider et al., 1995) and cause impacts on a local and regional scale (Blong, 1984).

Few studies, however, have examined ash particles while they are suspended in the atmosphere (Mather et al., 2003; Rose et al., 2000). Those studies that have sampled volcanic ash undergoing atmospheric transport were conducted over short

intervals, at single locations, or examined the chemistry of soluble aerosols but did not address the chemistry or morphology of volcanic ash (e.g. Hunton et al., 2005). Modeling studies have been conducted to understand how fine volcanic ash aerosol behaves as it is transported, but these studies are often purely mathematical or use data from tephra studies that focus on larger particles with short (<hours) atmospheric lifetimes that fall out near the volcano (Mastin et al., 2009). These studies tend to omit respirable particulate matter that is small enough to be transported hemispherically. While proximal fallout may have implications near the volcano such as structural loading from ash fall and impact hazards from ballistics, these effects are relatively localized in time and geographic area (Blong, 1984). Long-range transport of fine volcanic ash particulates may have impacts on respiratory and ecosystem health, aircraft and aerodrome operations, climate, visibility, and other impacts at distances far from the erupting volcano (Mather et al., 2003; Rose et al., 2000).

Observations and analysis of airborne volcanic ash collected during three volcanic eruptions in Alaska (Figure 1.1) are presented in this dissertation including the eruptions of Augustine Volcano (2006), Pavlof Volcano (2007), and Redoubt Volcano (2009). These studies attempt to address issues associated with the long-range transport of volcanic ash, specifically how ash concentration and particle size vary with transport distance, what physical and chemical processes transform ash as it is transported, and how ash aggregates during transport. The Augustine study also provides aerosol size distribution and concentration data for future use in volcanic ash distribution models and for validation and calibration of satellite remote sensing ash

detection and retrieval methods. These data are contained in the DVD that accompanies this dissertation.

1.1 The Atmospheric Fate and Transport of Volcanic Ash

Beyond its source, formation processes, and emplacement in the atmosphere, airborne volcanic ash is no different than other atmospheric aerosols in regard to fate and transport (Sparks et al., 1997). Atmospheric transport of volcanic ash is influenced by qualities of the particle itself, the strength of the eruption, and the atmosphere into which it is erupted. The altitude to which ash is erupted dictates the type of atmospheric environment the ash initially encounters, the residence time the ash particle has in the atmosphere, and the evolution of the particle as it is transported. The type of atmosphere into which ash is erupted depends largely on the geographic location of the erupting volcano and the time of year of the eruption.

Pyroclasts are formed as volcanic rocks are explosively erupted and can range in diameter from several meters to sub-micron (Fisher and Schminke, 1984). Larger pyroclasts fall out of the plume near the vent in a matter of seconds to minutes while smaller pyroclasts can have atmospheric lifetimes of hours to weeks and can be transported globally before removal. Pyroclast formation during volcanic eruptions has been described in depth by various authors (e.g. Sparks et al., 1997; Cashman and Mangan, 1994; Fisher and Schminke, 1984). The process, in condensed form, is as follows: pyroclasts are formed when magmatic gases (H_2O , SO_2 , CO_2 , etc.) rapidly form bubbles which grow at a rate that exceeds the yield strength of the magmatic

fluid, causing the bubbles to burst and shatter. The release of gas from these bubbles drives the resulting particles from the volcanic vent. The volume of gas released during an eruption and the release rate play a significant role in the rate of pyroclast production, particle sizes produced, and the eruptive plume height (Sparks et al., 1997; Newhall and Self, 1982; Walker, 1973). The fracturing process can impart an electrostatic charge to the resulting pyroclasts which may play an important role in particle aggregation. James et al. (2002) simulate a process which creates a significant electrostatic charge by fracto-emission during pyroclast formation.

1.1.1 Atmospheric Influences on Particle Growth

The altitude of plume emplacement, latitude of the volcano, and the time of year when an eruption occurs all have a significant role in ash aggregation processes and rates. Figure 1.2 from McGee et al., (1997) shows a host of atmospheric constituents interacting with a volcanic plume and results of those interactions. Since ash can be transported globally, it can encounter a variety of atmospheric conditions before it is ultimately removed. Explosive eruptions can produce a range of plume types depending on the overall energy of the eruption and other factors such as volatile content, the composition of the erupted magma, vent size, etc. (Sparks et al., 1997; Newhall and Self, 1982; Walker, 1973). In general, volcanic eruptions can produce large, energetic plumes that can reach the stratosphere and upper troposphere, weak, bent-over plumes which do not go much higher than the elevation of the vent, or pyroclastic flows which propagate down the sides of volcanoes (Sparks

et al., 1997). High plumes can encounter the upper troposphere-lower stratosphere, while low plumes are erupted into the lower troposphere (Sparks et al., 1997). The upper troposphere-lower stratosphere is a non-turbulent, cold, generally dry region with low levels of aerosol and reactive chemical species while the lower troposphere is relatively turbulent and moist, and contains a host of aerosol (Figure 1.3) and reactive gases (Seinfeld and Pandis, 2006; Jaenicke 1993). The geographic location of the erupting volcano also has an influence on the type of atmospheric environment acting on ash. For example, warm, maritime tropical air masses present different chemical and physical influences than would dry, continental polar air masses (Seinfeld and Pandis, 2006; Finlayson-Pitts and Pitts, 1986). The time of year of an eruption can also have significant influence on the atmosphere into which the plume is emplaced. A summertime atmosphere contains more reactive species and higher aerosol levels than a wintertime atmosphere. Furthermore, during high latitude winter, ultraviolet solar flux, an important source of energy for some atmospheric reactions, can be very low or absent which can limit or prevent some important photochemical processes such as the conversion of SO_2 to sulfate (Seinfeld and Pandis, 2006; Finlayson-Pitts and Pitts, 1986).

In the most basic sense, large, dense aerosols are removed from the atmosphere more rapidly than small, less dense ones (Reist, 1993). Volcanic ash particles are defined to be 2 mm in diameter and smaller (Fisher and Schminke, 1984). Along with ash, other particle sizes are produced ranging from blocks and bombs (>64 mm) to lapilli (<64 mm - >2 mm). Generally lapilli and larger particles

fall out of a plume near the vent and do not undergo long range transport (Sparks et al., 1997). Because large pyroclastic particles ($>10 \mu\text{m } \varnothing_A$) are quickly removed from a volcanic plume by ballistic trajectories, they are not considered further in this discussion because their atmospheric residence time is too short for much atmospheric interaction (Shipley and Sarna-Wojcicki, 1982). However, smaller particles ($<10 \mu\text{m } \varnothing_A$) can remain suspended in the atmosphere for hours to days, undergo significant atmospheric reactions, and experience long range transport (Reist, 1993).

1.1.2 Particle Settling and Stokes' Law

If no forces other than fluid dynamics acted upon volcanic ash, residence time would be purely a function of Stokes' Law (Reist, 1993; Fuchs, 1964) which states that particles settling in a viscous medium are influenced by particle size and density along with the viscosity of the medium in which they are suspended. A further stipulation is that the particles are settling in a non turbulent fashion when the particle Reynolds number is less than 1 (Hinds, 1999). In its most basic form, Stokes' Law is as follows:

$$F_D = 3\pi\eta Vd$$

where F_D is the force of drag on a spherical particle, η is the viscosity of the medium, V is the velocity of the particle, and d is the density of the particle. According to this version of Stokes' Law, the initial height from which the particle is released into the atmosphere, particle density, and the viscosity of air would be the only factors

dictating settling rates and thus atmospheric residence time. Stokes' Law in this form assumes that all particles are spherical and do not change shape, size, or density and the medium is not flowing nor changing its viscosity. But the atmosphere is a turbulent flow regime, and aerosols are not inert objects (Seinfeld and Pandis, 2006; Finlayson-Pitts and Pitts, 1986). If settling rate solely dictated the removal of volcanic ash from the atmosphere, micrometer-sized ash erupted to 10-20 km would remain suspended for hundreds of years and fill the atmosphere (Cahill et al., 2010). Instead, physical and chemical processes act upon aerosols and alter the aerosol in several ways. To adequately model the settling rate for a particle in the atmosphere, each of the terms in Stokes' Law would have to be recast as dynamic values that can change as the particle is transported. Because there are many processes acting on aerosols, it is necessary to discuss physical and chemical processes separately to more clearly examine their individual influences on settling rates and aerosol removal.

Very fine volcanic ash, defined by Rose and Durant (2009) to be less than 10 μm in diameter, enters the atmosphere as a solid, angular, elongate, platy, or non-spherical isometric particle (Heiken and Wohletz, 1985). The influence of non-spherical particle shape on particle settling rates is addressed by Reist (1993), Wilson and Huang (1979), and Fuchs (1964). For non-spherical particles, it is necessary to represent the required diameter term in Stokes' Law with a shape factor to properly account for the effects of non-sphericity on particle motion. When particles are elongate, a dynamic shape factor reduced to a statistical average is needed to completely describe particle motion because particles change their orientation due to

Brownian and shear rotation. The shape factor is used to determine an equivalent diameter sphere referred to as the Stokes' equivalent sphere (Figure 1.4) which is a theoretical sphere that has the equivalent settling velocity and mass as the original non-spherical particle (Reist, 1993). Wilson and Huang (1979) presented an exhaustive empirical study on the settling rates of volcanic particles with a variety of shapes and densities. While the particle sizes they investigated were larger than the particles sampled in the studies presented in this dissertation, their data show that as long as the Reynolds number, the measure of the ratio of inertial forces to viscous forces, remains <1 , the settling rate for an ash particle closely resembles the settling rate for a cylinder with a diameter equal to the arithmetic mean of the three principle axes of the ash particle (Wilson and Huang, 1979). Since a volcanic cloud contains a range of ash particle sizes and shapes, it is necessary to determine the particle size range and shapes contained in the cloud to properly model the range of settling velocities of particles in the cloud.

Particle density is another important term in Stokes' Law. Volcanoes produce a range of rock compositions with different densities ranging from $0.7\text{-}2\text{ g/cm}^3$ for pumice, $2.35\text{-}2.45\text{ g/cm}^3$ for glass shards, $2.7\text{-}3.2\text{ g/cm}^3$ for dense rock and $2.6\text{-}5.2\text{ g/cm}^3$ for crystals (Shipley and Sarna-Wojcicki, 1982; Wilson and Huang, 1979). Higher density particles of an equivalent diameter will settle at rates faster than those that are less dense according to Stokes' Law. To more easily incorporate particle density, size, and shape into one basic term, the use of the aerodynamic diameter equivalent sphere is used to calculate particle motion (Reist, 1993). An aerodynamic

diameter equivalent sphere is a virtual sphere that has a density of 1 g/cm^3 and a diameter scaled to give the spherical particle the same settling velocity as the actual particle. Depending on the particle shape and density, the actual particle could be larger or smaller than its aerodynamic diameter. Aerodynamic diameter is used to simplify particle motion calculations and plays a major descriptive role in aerosol research (Reist, 1993).

The above discussion is primarily focused on the motion of single volcanic particles, but volcanic plumes and clouds composed of many individual particles move as one entity at least during the initial period of their existence (Sparks et al., 1997; Fuchs, 1964). Clouds are regions where the composition, density, and temperature are different than that of the surrounding atmosphere. A rising volcanic plume is a region of expansion due to eruptive decompression and ingestion of air (Sparks et al., 1997). According to Fuchs (1964), plume rise is generally due to differences in temperature and humidity between the interior of the plume and that of the surrounding atmosphere. Plumes rise because the temperature of the plume exceeds the temperature of the surrounding atmosphere, resulting in buoyant rise. The density of the particles contained in the plume have a secondary role in controlling plume rise, except when cloud density overwhelms thermal buoyancy and the rising column collapses, which produces pyroclastic flows. The density of the plume plays a significant role in the rate of mixing with the surrounding atmosphere. As the plume mixes with the surrounding atmosphere and volcanic gases are dispersed, the plume becomes more dilute and the environment in which the ash is

suspended becomes more similar to the ambient atmosphere than a volcanic plume (Sparks et al., 1997).

1.1.3 Ash Particle Composition

As stated earlier, airborne volcanic ash is subject to the same processes as any other atmospheric aerosol. To understand what atmospheric processes act on volcanic ash, it is necessary to fully describe ash in terms of its physical and chemical characteristics. As a further definition, volcanic ash is one type of mineral aerosol like desert dust, loess, and windblown river or glacial sediment. Ash is comprised of primarily volcanic glass which is chiefly silica with some aluminum, calcium, iron, and sodium. Minerals can also form ash (Heiken and Wohletz, 1985; Shipley and Sarna-Wojcicki, 1982). Common volcanic minerals include plagioclase feldspar, pyroxene, amphibole, olivine, mica, apatite, quartz, magnetite, and ilmenite. Most explosive ash-producing eruptions occur at volcanoes that are erupting basaltic to rhyolitic magmas. Table 1.1 shows the relative compositions of magmas and their names. In general, silicic magmas erupt more explosively than do silica poor magmas. Historically there have been more explosive dacitic and rhyolitic eruptions than basaltic ones (Siebert and Simkin, 2002-). Information about the magma composition of the erupting volcano may provide useful input parameters for volcanic ash transport and dispersal models (Mastin et al., 2009; Webley and Mastin, 2009).

1.1.4 Changes to Aerosol Shape, Size, and Density

Up to this point of this discussion, ash aerosols have been assumed to remain a constant size and shape. Particles described in this work and by others (e.g. Taddeucci et al., 2011; Rose and Durant, 2011; Durant and Rose, 2009; James et al., 2002; Vietch and Woods, 2001; Sorem, 1982) show that airborne ash can undergo aggregation processes due to the presence of a liquid phase or electrostatic aggregation in the absence of a liquid phase. Fuchs (1964) explains that particle aggregation is extremely efficient when particles are extremely fine. These aggregations explain how volcanic ash is incorporated into larger aerosols and is removed from the atmosphere at rates considerably faster than the settling rate of individual ash particles. For example, small aerosols commonly serve as cloud condensation nuclei and grow into larger particles by the addition of water. Also, aerosols commonly have an electrostatic charge which can attract other aerosols and cause them to stick together and form wet or dry aggregates (James et al., 2002; Fuchs, 1964). Aerosols provide volumes in which or surfaces on which chemical reactions can occur. For example, sulfur dioxide reacting with liquid water droplets (Figure 1.5) forms sulfuric acid droplets or sulfur dioxide and water can react on the surface of an ash particle to form a sulfate coating on the ash (Finlayson-Pitts and Pitts, 1986). As these reactions occur, individual primary aerosols form larger secondary hybrid particles. The resultant secondary particles have settling properties different than their constituents. In general, as particles aggregate and grow, they attain faster settling rates and are removed from the atmosphere. In some cases

however, large fluffy particles can have slower settling rates than their constituents due to an overall large aspect ratio and low density. A prime example of this is large carbon chain soot aerosols (Reist, 1993; Fuchs 1964) and large fluffy aggregate ash particles first described by Sorem (1982) in the Mt. St. Helens 18 May 1980 eruptive plume.

Particle growth is not the only fate of aerosols. Ash aggregate break-up during descent was observed by Taddeucci et al. (2011) in the Eyjafjallajokull 2010 eruption plume. A droplet may be transported to a drier atmosphere than the one in which it formed. This could cause the particle to dry and become smaller. The process of hydration and subsequent drying can produce particles that are different sizes at the same relative humidity. This discrepancy, or hysteresis, adds another element to the complex nature of aerosol behavior as it evolves and ages during its atmospheric lifetime (Fuchs 1964).

1.1.5 The Influence of Volcanic Plume Regions on Aggregation

Sparks et al. (1997) describe in depth and detail the dynamics of volcanic plume behavior. Their description is referenced here as it pertains to ash particle dynamics within the plume. As ash is erupted, it is initially a hot particle, but it rapidly cools due to decompression and, to a greater extent, radiative cooling as it is ejected. The initial jet phase of the eruption is extremely energetic and is the result of violent degassing at the vent. In this region, ash is predominantly under the influence

of volcanic processes, but this changes once it enters the convective region of the column.

In the convective region, the pyroclast has cooled from magmatic temperatures. Expansion of plume gases due to decompression and mixing with the atmospheric causes the plume to rise until the temperature of the plume equals that of the surrounding atmosphere (Sparks et al., 1997; Fuchs, 1964). The particle motion is turbulent and the particles collide with other particles in the plume. Collisions in this region may lead to the production of smaller pyroclasts from abrasion. Clast-to-clast milling may also form electrostatic charges on particles (Darteville et al., 2002). In this region, electrostatic charge may cause particles to form aggregates with other volcanic particles (James et al., 2002).

The convective region of the plume is where the plume begins to ingest and mix with the surrounding atmosphere (Sparks et al., 1997). The atmosphere into which a plume erupts is a dynamic system containing any number of aerosol types (sea salt, non-sea salt sulfate, reactive hydrocarbons, water vapor, black carbon, soil, desert dust, etc.) and reactive gases (Seinfeld and Pandis 2006; Finlayson-Pitts and Pitts, 1986). Once ash is erupted it is, by the very fact of its atmospheric presence, an atmospheric particle whose atmospheric lifetime will be governed by atmospheric physics and chemistry (Reist, 1993; Fuchs, 1964). Likewise, the gases in the plume will undergo dilution and reaction with atmospheric gases and aerosol by the same atmospheric pathways. The length of time the particle exists in the atmosphere, its individual chemistry, particle shape, size, and electrostatic charge will all influence

what processes the pyroclast experiences before it is eventually removed from the atmosphere.

1.1.6 The Influence of Tropospheric Transport on Aggregation

The troposphere is the region into which most volcanoes emit their plumes (Sparks et al., 1997). Depending on latitude, the troposphere can range in thickness from 20 km at the equator to 8 km at the poles. The troposphere is divided into three main regions based on general characteristics of each region (Seinfeld and Pandis, 2006; Sparks et al., 1997; Finlayson-Pitts and Pitts, 1986). The lower troposphere, also referred to the Planetary Boundary Layer (PBL), is the region closest to the Earth's surface. It contains a broad mix of reactive gases and aerosols, and is moist, turbulent, and generally warmer than the other levels of the troposphere. Above the PBL, the main part of the troposphere, called the free troposphere, is a region of relatively low aerosol and reactive gas content. It is generally drier and colder than the PBL. The upper troposphere-lower stratosphere is the third zone of the troposphere. It is a transition zone from the troposphere to the stratosphere. During the summertime, this transition zone may exist as a distinct boundary which can impede the rise of air masses from the troposphere into the stratosphere, at other times, this region is undefined by temperature differences and flow from one level to another is relatively unrestricted.

In the free troposphere and at the upper troposphere/lower stratosphere boundary, the relatively dry, cold, aerosol-free conditions do not allow for extensive aggregation to occur outside that which is caused by conditions in the volcanic plume

(Sparks et al., 1997). Plumes entering the free troposphere contain ash, volcanic gases and atmospheric constituents ingested by the plume in the PBL. Any aggregation in the free troposphere is limited by the contents of the plume which is also expanding and becoming colder and more dilute. This plume expansion limits the ability of aggregates to form and reactions to occur because aggregation due to collision and electrostatic attraction is heavily influenced by particle proximity (Fuchs, 1964). Dry conditions in the free troposphere may cause wet particles formed in the PBL to effloresce or lose water and crystallize. Particle charge relaxation and wind shear, especially at the margins of a plume and in dilute plumes, may cause ash aggregates to lose cohesion and break apart (Taddeucci et al., 2011; James et al., 2002; Fuchs, 1964). The volcanic water vapor in the plume and atmospheric water vapor ingested by the plume may condense on ash particles to form water droplets or glaciolate to form ice particles (Durant and Rose, 2009).

1.1.7 The Influence of PBL Transport on Aggregation

All volcanic ash erupted into the atmosphere encounters the PBL before it settles out of the plume. Any particle in the PBL is subject to a range of processes that can strongly influence aggregation. Moist, aerosol-laden air containing reactive gases can be ingested by a convecting plume and add reactive components to the plume. These components may influence the particle aggregation occurring in the plume as it rises into the free troposphere. Ash settling from a dispersed plume or a downward mixing plume, either by advection or isentropic flow, may encounter

upward mixing PBL air masses. Maritime aerosols containing sea salt and non-sea salt sulfate in a moist atmosphere can readily combine with ash aerosols via collision or electrostatic attraction (Rose and Durant, 2009). Continental air masses can also contain reactive gases and aerosols such as OH⁻, SO₂, sulfate, desert dust, and carbon soot which can interact with volcanic ash and form complex secondary aerosols.

1.2 Collection Methods and Analytical Techniques

During the eruption of Augustine Volcano in 2006 and the eruption of Pavlof in 2007, Davis Rotating Unit for Measurement (DRUM) cascade impactors were used to collect airborne volcanic ash. During the eruption of Redoubt Volcano in 2009, DRUM samplers and Beta Attenuation Mass monitors (BAM-1020) and Environmental Beta Attenuation Monitors (EBAM) collected airborne ash.

1.2.1 Davis Rotating Unit for Measurement (DRUM) Samplers

DRUM samplers collect time-resolved aerosol samples in discrete size increments over a timed interval (Raabe et al., 1988; Cahill and Wakabayashi, 1993). In these studies, the samplers provided a temporal resolution of 3 hours over a 6 week period. For the Augustine eruption an 8 stage DRUM cascade impactor was used. The size increments were 35-5, 5-2.5, 2.5-1.15, 1.15-0.75, 0.75-0.56, 0.56-0.34, 0.34-0.26 and 0.26-0.09 μm (in aerodynamic diameter or \AA_A). For the Pavlof and Redoubt eruptions, 3-stage DRUM samplers were used. The size increments for the 3-stage DRUMs were 2.5-1.15, 1.15-0.34, and 0.34-0.9 μm \AA_A . The collected samples were

analyzed for mass concentration and chemistry as a function of time. The aerosol mass concentration is determined by β -particle attenuation and reported as mass concentration at a given time (Reist, 1993). Quantitative elemental concentrations for selected elements between Na and Pb are determined using synchrotron X-ray fluorescence (S-XRF) and reported as elemental concentration at a given time (Cahill, 2003; Cahill et al., 1999).

1.2.2 Beta Attenuation Mass (BAM-1020) Monitors and Environmental Beta Attenuation Monitors (EBAM)

The BAM-1020 and EBAM instruments operate by filtering particulate matter through a glass fiber filter tape and measuring β -particle attenuation over a set time increment, typically 1 hour, based on established sampling protocol (Alaska Department of Environmental Conservation 2009a; 2009b; Municipality of Anchorage, 2009; MetOne, 2009). The devices report the beta particle attenuation as mass concentration per unit of time in real-time by telemetered communications. These data are routinely used by public officials as a measure of air quality for regulatory purposes and to advise populations about potential air quality hazards.

1.2.3 Scanning Electron Microscopy (SEM) and Energy Dispersive Spectroscopy (EDS)

Scanning Electron Microscopy (SEM) was also conducted to determine particle morphologies, particle counts, and size distributions at different times during

eruptions. Energy Dispersive Spectroscopy (EDS) was conducted along with the SEM analysis to determine individual particle composition. These analyses were conducted at the University of Alaska Fairbanks Advanced Instrumentation Laboratory.

1.2.4 Digital Image Processing Techniques

Grain size distributions and shape descriptors for ash particles from the Augustine eruption were determined from EDS element maps by digital image processing methods. While the measurements and shape descriptors presented here are similar to those presented by Riley et al. (2003), the image collection method and image processing software used for this study are commonly available at relatively low cost. SEM instruments equipped with EDS spectrometers are commonly available at most scientific research institutions. The image processing software package used, Image J (Ferreira and Rasband, 2011), is an open-source public-domain program available without cost from the National Institutes of Health.

1.3 The 2006 Eruption of Augustine Volcano

The 2006 eruption of Augustine Volcano provided the first opportunity where a DRUM sampler was deployed specifically to collect ash from an erupting volcano (Cahill et al., 2010). The sampler was located at the University of Alaska Research Station in Homer, AK, and ran continuously from 11 January, when the volcano began erupting, to 11 February, 2009 when it returned to repose. Cahill et al. (2010)

reported on the results of this sampling and showed that the DRUM sampler was a viable method for collecting time and size resolved airborne volcanic ash undergoing atmospheric transport and that the mass concentration and elemental concentration data obtained could be used for volcanic ash transport model inputs.

The Augustine eruption work presented in Chapter 2 expands upon those results by presenting new results from SEM and EDS studies conducted on the DRUM samples collected by Cahill et al. (2010). The SEM analysis revealed a variety of volcanic particle types in the samples ranging from individual glassy volcanic ash shard grains to complex aggregates of ash mingled with background sulfate and sea salt aerosols. The particle counts, size distributions, and shape descriptors of ash shards and aggregates determined by image analysis techniques are useful as possible volcanic ash transport and distribution model inputs (Mastin et al., 2009; Riley et al., 2003). Aggregate ash particulates observed in SEM images show two distinct morphologies: ash aggregates and hybrid aggregates. Ash aggregates were only sampled from elutriation plumes from pyroclastic flows and consist exclusively of ash particles. Hybrid aggregates were commonly sampled from the Augustine and Redoubt eruption plumes and consist of ash particles mingled with either sea salts or non-sea salt sulfates. Several formation pathways for ash aggregates have been suggested including the attraction of dry, electrostatically-charged ash (James et al., 2002), wet aggregation (Vietch and Woods, 2001), and ice hydrometeor aggregation (Durant and Rose, 2009). Upward-mixing of sea salt and

non-sea salt sulfate maritime aerosols combining with downward mixing of volcanic ash (Rose et al., 2000) may explain the formation of hybrid aggregates.

Particle size distributions determined by low-cost image processing methods show that ash produced by the initial central vent eruption of Augustine produced ash $35.0\text{-}1.15\ \mu\text{m}\ \text{Ø}_A$, and likely larger. The distribution of particle sizes over this size range was log normal; most particles are small, but most of the mass is contained in fewer large particles. Particle distributions for ash collected from pyroclastic flow plumes show that ash was present over the same size range as ash from the central vent eruption pulses but in much smaller size fractions ($0.75\text{-}0.56$, and $0.34\text{-}0.26\ \mu\text{m}\ \text{Ø}_A$). This observation is consistent with those of Darteville et al. (2002) for the production of fine ash observed in the Mt. Pinatubo 1991 eruption cloud. Ash was also sampled from a single plume at different travel times. During 14 January, a plume from Augustine was sampled at Homer about an hour after the eruption pulse began. On 17 January, some 3 days later, the same plume was again sampled in Homer because the plume had been caught up in a cyclone which brought the ash plume back to the sampling site. Particle size distributions show that the particles present in the plume on 17 January were more numerous than on 14 January. This may have occurred because the main mass of the ash cloud was erupted higher in the atmosphere than the sampling site elevation on January 14, hence the air masses that were sampled were relatively ash poor. During the next 3 days, the ash would have had time to settle from higher altitudes by downward mixing, increased settling rate

due to aggregation and/or isentropic transport which may account for higher ash mass loads on 17 January.

1.4 The 2007 Eruption of Pavlof Volcano

Pavlof Volcano (Chapter 3) presented another opportunity to use DRUM samplers to collect airborne volcanic ash. Compared to the Augustine 2006 eruption, the Pavlof eruption was less energetic (VEI 2 vs. VEI 3 for Augustine) (Siebert and Simkin, 2002-) and had no pyroclastic flows. Even so, analysis of the aerosols showed some interesting processes, specifically: 1) diurnal variations in ash concentration at the sampling site, 2) the presence of ash downwind of the volcano during the waning phase of the eruption, 3) the presence of observable ash in the absence of satellite ash detections, and 4) no hybridization of volcanic ash with the background maritime aerosols. The Pavlof eruption underscores the importance of ash forecasting models when ash mass concentrations and particle sizes are below the detection limit of satellite detection methods but could pose a hazard downwind of the volcano. It should be mentioned, however, that the determination of possible hazards associated with specific mass concentrations of respirable ash was outside the scope of this work. These results also demonstrate that local weather conditions can influence ash concentrations downwind of an erupting volcano in a manner independent of the actual ash production rate at the volcanic vent.

1.5 The 2009 Eruption of Redoubt Volcano

Redoubt Volcano (Chapter 4) provided yet another opportunity to sample airborne volcanic ash. Unlike Augustine and Pavlof, airborne ash sampling from Redoubt occurred at several sites. The Denali National Park Headquarters and Ninilchik School were outfitted with 3-stage DRUM impactors. In addition to the DRUM samplers, Beta Attenuation Mass monitors (BAM-1020) were operating in Anchorage, Wasilla, and Palmer, Alaska while an Environmental Beta Attenuation Monitor (EBAM) was set up by the U.S. Fish and Wildlife Service (FWS) in Soldotna, Alaska in anticipation of the eruption. The BAM-1020s were part of the instruments used for an ongoing air quality monitoring program conducted by the Municipality of Anchorage (MOA) and the Alaska Department of Environmental Conservation (Alaska Department of Environmental Conservation, 2009a; 2009b; Municipality of Anchorage, 2009). The EBAM in Soldotna, usually used by the FWS for monitoring particulate matter levels from wildfire smoke, was also fortuitously employed for monitoring particulate matter levels during the Redoubt eruption since it was otherwise idle. The samplers located in Anchorage, Wasilla and Palmer collected PM_{10} and $PM_{2.5}$ (Alaska Department of Environmental Conservation, 2009a; 2009b; Municipality of Anchorage, 2009); the EBAM in Soldotna collected PM_{10} . PM_{10} refers to particulate matter $\leq 10 \mu m \text{ } \varnothing_A$ while $PM_{2.5}$ refers to particulate matter $\leq 2.5 \mu m \text{ } \varnothing_A$.

S-XRF elemental concentration analysis and β -attenuation analysis from DRUM samples show distinct mass loading events corresponding with eruption

events. Elemental concentrations of these mass loading events are consistent with volcanic ash transport from the volcano. Accompanying these data, HYSPLIT backward trajectories (Draxler and Rolph, 2011; Rolph, 2011) confirmed that air masses sampled during these times were transported from Redoubt volcano.

Analysis of DRUM, BAM-1020 and EBAM mass concentration data show a systematic removal of particles with increasing distance from the volcano and atmospheric transport time as the plume became more dilute and traveled across the Alaska Range. SEM analysis shows that ash occurred as either single grain glass shards or as hybrid aggregates similar to those observed from the Augustine 2006 eruption samples. Hybrid aggregate ash consists of ash associated with either sea salts or sulfate. Hybrid aggregates were present at all sampling locations, but are most common in the Ninilchik samples because the sampling location was on the southeastern shore of Cook Inlet.

The BAM-1020s operated by the MOA and the EBAM operated by the FWS recorded an increase of PM_{10} consistent with HYSPLIT model predictions. No corresponding $PM_{2.5}$ increase was observed, however. This may have been because the eruptive ash particle distribution was low in $PM_{2.5}$ or because of the slower settling rate of these particles relative to the sampling locations and longer transport distances.

The Redoubt eruption study demonstrates that a suite of sampling techniques is needed to address both the real-time reporting requirements during an eruption and the need for scientific investigation of ash particles. DRUM samplers are found to be

suitable for sampling respirable volcanic ash for detailed post-eruption analysis, but they are not designed to report real-time information about aerosol mass concentrations. BAM-1020s and EBAMs are ideal for reporting real-time respirable ash mass concentrations, but they are not suitable for post eruptive analysis because the filter media contaminated the spectra of the sample and the sample and filter media fused from the heat produced by the electron beam in the SEM. Furthermore, neither instrument collects particles larger than total suspended particulate, or particles larger than $100 \mu\text{m } \phi_A$.

Since no single technique or instrument successfully samples all the components of an eruptive plume, the use of a combination of instruments and collection techniques is needed to satisfy aerosol research and warning requirements. A sampling suite could be configured to allow for real-time telemetered reporting of aerosol mass concentrations using EBAMs or BAM-1020s, DRUM samplers for post-eruptive mass and chemical evaluation of PM_{10} and $\text{PM}_{2.5}$, TSP high volume samplers for the overall aerosol volume, standard tephra collection methods for measuring fall volumes and particle sizes, and passive collection methods such as settling plates to collect and preserve delicate ash aggregates that would otherwise be degraded or destroyed by energetic collection techniques.

1.6 References

Alaska Department of Environmental Conservation, Division of Air Quality, Air Monitoring and Quality Assurance Section, 2009a. Alaska's 2009 Air Monitoring Network Plan. www.dec.state.ak.us/air/am/am_airmonplan.htm (last accessed on 10 March 2012).

Alaska Department of Environmental Conservation, Division of Air Quality, Air Monitoring and Quality Assurance Section, 2009b. MetOne Instruments Beta Attenuation Mass (BAM) Monitor Model 1020. www.dec.state.ak.us/air/am/am_sops1.htm (last accessed on 10 March 2012).

Blong, R.J., 1984. *Volcanic Hazards: A sourcebook on the effects of eruptions*. Academic Press, Sidney, Australia.

Cahill, C.F., 2003. Asian aerosol transport to Alaska during ACE-Asia. *Journal of Geophysical Research*. 108, 8664-8872.

Cahill C.F., Rinkleff, P., Dehn, J., Webley, P., Cahill, T., Barnes, D., 2010. Aerosol measurement from a recent Alaskan volcanic eruption: Implications for volcanic ash transport predictions. *Journal of Volcanology and Geothermal Research*. 198, 76-80.

Cahill, T.A., Wakabayashi, P., 1993. Compositional analysis of size-segregated aerosol samples. In: Newman, L. (Ed.), *Measurement Challenges in Atmospheric Chemistry*, American Chemical Society, pp. 211-228.

Cahill, T.A., Cliff, S., Perry, K., Jimenez-Cruz, M., McHugo, S., 1999. Size and time resolved anthropogenic components of aerosols via synchrotron x-ray fluorescence: Application to Asian aerosol transport. Abstracts, American Geophysical Union 1999 Fall Meeting, December. San Francisco, California, pp. 13-17.

Casadevall, T.J., 1994. The 1989–1990 eruption of Redoubt Volcano Alaska: Impacts on aircraft operations. *Journal of Volcanology and Geothermal Research*. 62, 301-316.

Cashman, K.V., Mangan, M.T., 1994. Physical aspects of magma degassing II. Constraints on vesiculation processes from textural studies of eruptive products. In: Carroll, M.R., Holloway, J.R. (Eds.), *Volatiles in Magmas. Reviews in Mineralogy*, Volume 30. Mineralogical Society of America, Washington, D.C., pp. 447-478.

Darteville, S., Ernst, G.J., Stix, J., Bernard, A., 2002. Origin of the Mount Pinatubo climactic eruption cloud: Implications for volcanic hazards and atmospheric impacts. *Geology*. 30, 663-666.

Draxler, R.R., Rolph, G.D., 2011. HYSPLIT (HYbrid Single-Particle Lagrangian Integrated Trajectory). NOAA Air Resources Laboratory, Silver Spring, MD. Model access via NOAA ARL READY Website: <http://ready.arl.noaa.gov/HYSPLIT.php> (last accessed on 10 March 2012).

Durant, A.J., Rose, W.I., 2009. Sedimentological constraints on hydrometeor-enhanced particle deposition: 1992 eruptions of Crater Peak, Alaska. *Journal of Volcanology and Geothermal Research*. 186, 40–59.

Ferreria, T., Rasband, W., 2011. Image J user guide. <http://imagej.nih.gov/ij/docs/user-guide.pdf> (last accessed on 10 March 2012).

Finlayson-Pitts, B.J., Pitts J.N., 1986. *Atmospheric Chemistry: Fundamentals and Experimental Techniques*. Wiley-Interscience, New York, NY.

Fisher, R.V., Schminke, H.-U., 1984. *Pyroclastic Rocks*. Springer-Verlag, New York, NY.

Fuchs, N.A., 1964. *The Mechanics of Aerosols*. Dover Publications, New York, NY.

Gudmundsson, M., Pederson, R., Vogfjörð, K., Thorbjarnardóttir, B., Jakobsdóttir, S., Roberts, M., 2010. Eruptions of Eyjafjallajökull Volcano, Iceland. *Eos*. 91, 190-191.

Heiken, G., Wohletz, K., 1985. *Volcanic Ash*. University of California Press, Berkeley, CA.

Hinds, W.C., 1999. *Aerosol Technology: Properties, Behavior, and Measurement of Airborne Particles*, 2nd Edition. Wiley Interscience, New York, NY.

Horwell, C.J., Baxter, P.J., 2006. The respiratory health hazards of volcanic ash: A review for volcanic risk mitigation. *Bulletin of Volcanology*. 69, 1-24.

Hunton, D.E., Viggiano, A.A., Miller, T.M., Ballenthin, J.O., Reeves, J.M., Wilson, J.C., Lee, S.-H., Anderson, B.E., Brune, W.H., Harder, H., Simpas, J.B., Oskarsson, N., 2005. In-situ aircraft observations of the 2000 Mt. Hekla volcanic cloud: Composition and chemical evolution in the Arctic lower stratosphere. *Journal of Volcanology and Geothermal Research*. 145, 23–34.

James, M.R., Gilbert, J.S., Lane, S.J., 2002. Experimental investigation of volcanic particle aggregation in the absence of a liquid phase. *Journal of Geophysical Research*. 107, 148-227.

- Jaenicke, R. 1993. Tropospheric aerosols. In: Hobbs, P.V. (Ed.), *Tropospheric Aerosols*. Academic Press, San Diego, CA, pp. 1-31.
- Langman, B., Zatsek, K., Hort, M., 2010. Atmospheric distribution and removal of volcanic ash after the eruption of Kasatochi volcano: A regional model study. *Journal of Geophysical Research*. 115, 1-10.
- Mastin, L.G., Guffanti, M., Servranckx, R., Webley, P.W., Barsotti, S., Dean, K., Durant, A., Ewert, J.W., Neri, A., Rose, W.I., Schneider, D.J., Siebert, L., Stunder, B., Swanson, G., Tupper, A., Volentik, A., Waythomas, C.F., 2009. A multidisciplinary effort to assign realistic source parameters to model of volcanic ash-cloud transport and dispersion during eruptions. In: Mastin, L.G., Webley, P.W. (Eds.), *Journal of Volcanology and Geothermal Research: Special Issue on Volcanic Ash Clouds*. 186, 10–21.
- Mather, T.A., Pyle, D.M., Oppenheimer, C., 2003. Tropospheric Volcanic Aerosol. In: Robock, A., Oppenheimer, C. (Eds.), *Volcanism in the Earth's Atmosphere*. American Geophysical Union, Washington D.C., pp. 189-212.
- McGee, K.A., Doukas, M.P., Kessler, R., Gerlach, T., 1997. Impacts of volcanic gases on climate, the environment, and people. U.S. Geological Survey Open-File Report, 97-262, 2 p.
- MetOne Inc., 2009. E-BAM datasheet. http://www.metone.com/documents/E-BAM_Datasheet_Rev_Aug09.pdf (last accessed on 10 March 2012).
- Municipality of Anchorage, Air Quality Program, Environmental Services Division, Department of Health and Human Services, 2009. *Air Quality in Anchorage, A Summary of Air Quality Monitoring Data and Trends, 1980–2008*. [http://www.muni.org/Departments/health/environment/AirQ/Documents/2009report final.pdf](http://www.muni.org/Departments/health/environment/AirQ/Documents/2009report%20final.pdf) (last accessed on 10 March 2012).
- Newhall, C.G., Self, S., 1982. The Volcanic Explosivity Index (VEI): An estimate of explosive magnitude for historical volcanism. *Journal of Geophysical Research*. 87, 1231-1238.
- Raabe, O.G., Braaten, D.A., Axelbaum, R.L., Teague, S.V., Cahill, T.A., 1988. Calibration studies of the DRUM impactor. *Journal of Aerosol Science*. 19, 183-195.
- Reist, P.C., 1993. *Aerosol Science and Technology*. Second Edition. McGraw-Hill, New York, NY.

Riley, C.M., Rose, W.I., Bluth, G.J.S., 2003. Quantitative shape measurements of distal volcanic ash. *Journal of Geophysical Research*. 108, 2504-2519.

Rolph, G.D., 2011. Real-time Environmental Applications and Display sYstem (READY). NOAA Air Resources Laboratory, Silver Spring, MD. <http://ready.arl.noaa.gov> (last accessed on 10 March 2012).

Rose, W.I., Durant, A.J., 2011. Fate of volcanic ash: Aggregation and fallout. *Geology*. 39, 895-896.

Rose, W.I., Durant, A.J., 2009. Fine ash content of explosive eruptions. *Journal of Volcanology and Geothermal Research*. 186, 32-39.

Rose, W.I., Bluth, G.J.S., Ernst, G.G.J., 2000. Integrating retrievals of volcanic cloud characteristics from satellite remote sensors: a summary. *Philosophical Transactions of the Royal Society of London*. 358, 1585-1606.

Sarna-Wojcicki, A.M., Shipley, S., Waitt Jr., R.B., Dzurisin, D., Wood, S.H., Lipman, P.W., Mullineaux, D.R., 1981. Aerial distribution, thickness, mass, volume, and grain size of air-fall ash from the six major eruptions of 1980. In: Lipman, P.W. and Mullineaux, D.R. (Eds.), *The 1980 Eruptions of Mount St. Helens, Washington*. U.S. Geological Survey Professional Paper 1250, pp. 577-600.

Schneider, D., Rose, W., Kelley, L., 1995. Tracking of 1992 eruption clouds from Crater Peak vent of Mount Spurr Volcano, Alaska, using AVHRR. In: Keith, T.E.C. (Ed.), *The 1992 eruptions of Crater Peak vent, Mount Spurr Volcano, Alaska*. U.S. Geological Survey Bulletin B 2139, pp. 27-36.

Seinfeld, J.H., Pandis, S.N., 2006. *Atmospheric Chemistry and Physics*. Wiley, Hoboken, NJ.

Shipley, S., Sarna-Wojcicki, A.M., 1982. Distribution, thickness, and mass of Late Pleistocene and Holocene tephra from major volcanoes in the northwestern United States: A preliminary assessment of hazards from volcanic ejecta to nuclear reactors in the Pacific Northwest: U.S. Geological Survey Miscellaneous Field Studies Map MF-1435.

Siebert, L., Simkin, T., 2002-. *Volcanoes of the World: An Illustrated Catalog of Holocene Volcanoes and their Eruptions*. Smithsonian Institution, Global Volcanism Program, Digital Information Series, GVP-3. <http://www.volcano.si.edu/world/> (last accessed on 10 March 2012).

Sorem, D.K., 1982. Volcanic ash clusters: Tephra rafts and scavengers. *Journal of Volcanology and Geothermal Research*. 13, 63-71.

Sparks, R.S.J., Bursik, M.I., Carey, S.N., Gilbert, J.S., Glaze, L.S., Sigurdsson, H., Woods, A.W., 1997. *Volcanic Plumes*. John Wiley, Hoboken, N. J.

Taddeucci, J., Scarlato, P., C. Montanaro, C., Cimarelli, C., Del Bello, E., Freda, C., Andronico, D., Gudmundsson, M.T., Dingwell, D.B., 2011. Aggregation-dominated ash settling from the Eyjafjallajökull volcanic cloud illuminated by field and laboratory high-speed imaging. *Geology*. 39, 891-894.

Vietch, G., Woods, A.W., 2001. Particle aggregation in volcanic plumes. *Journal of Geophysical Research*. 106, 26-42

Walker, G.P.L., 1973. Explosive volcanic eruptions - a new classification scheme, *Geologisches. Rundschau*. 62, 431-446.

Webley, P., Mastin, L., 2009. Improved prediction and tracking of volcanic ash clouds. *Journal of Volcanology and Geothermal Research*. 186, 1-9.

Wilson, L., Huang, T.C., 1979. The influence of shape on the atmospheric settling velocity of ash particles. *Earth and Planetary Science Letters*. 44, 311-324.

1.7 Figures

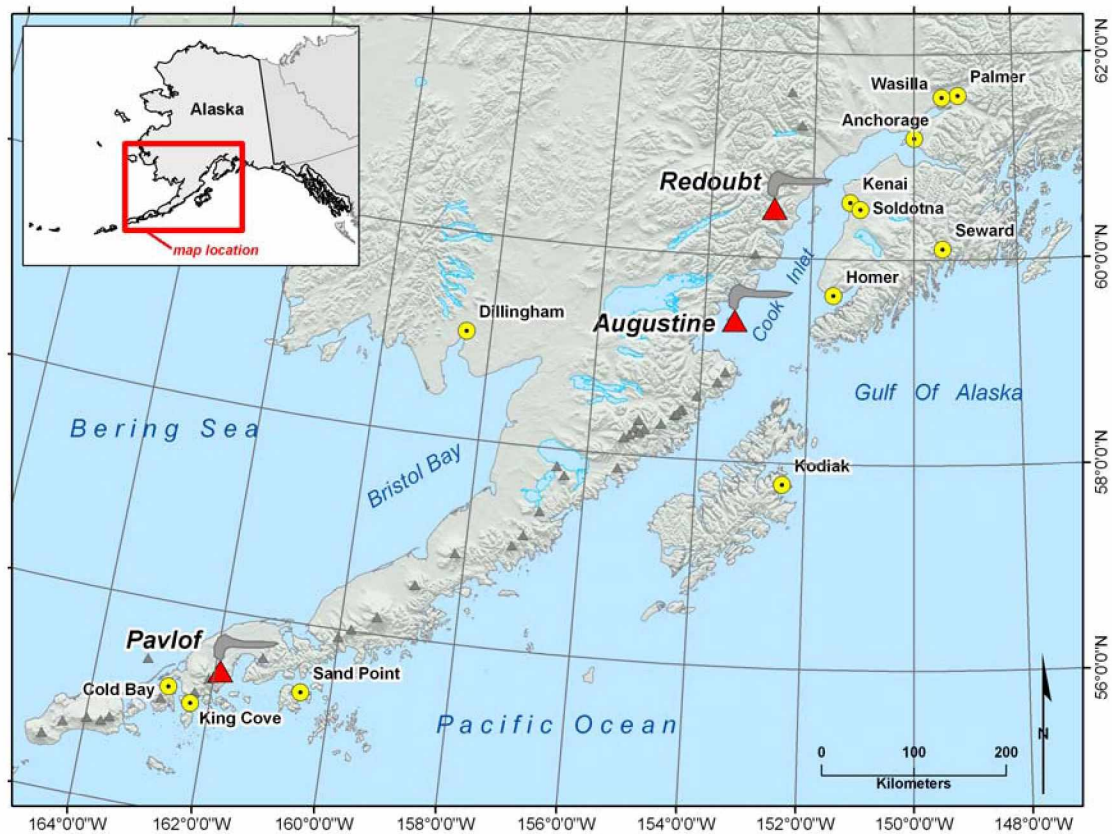


Figure 1.1. Study map showing the locations of Augustine, Pavlof, and Redoubt volcanoes with selected populated places in Alaska.

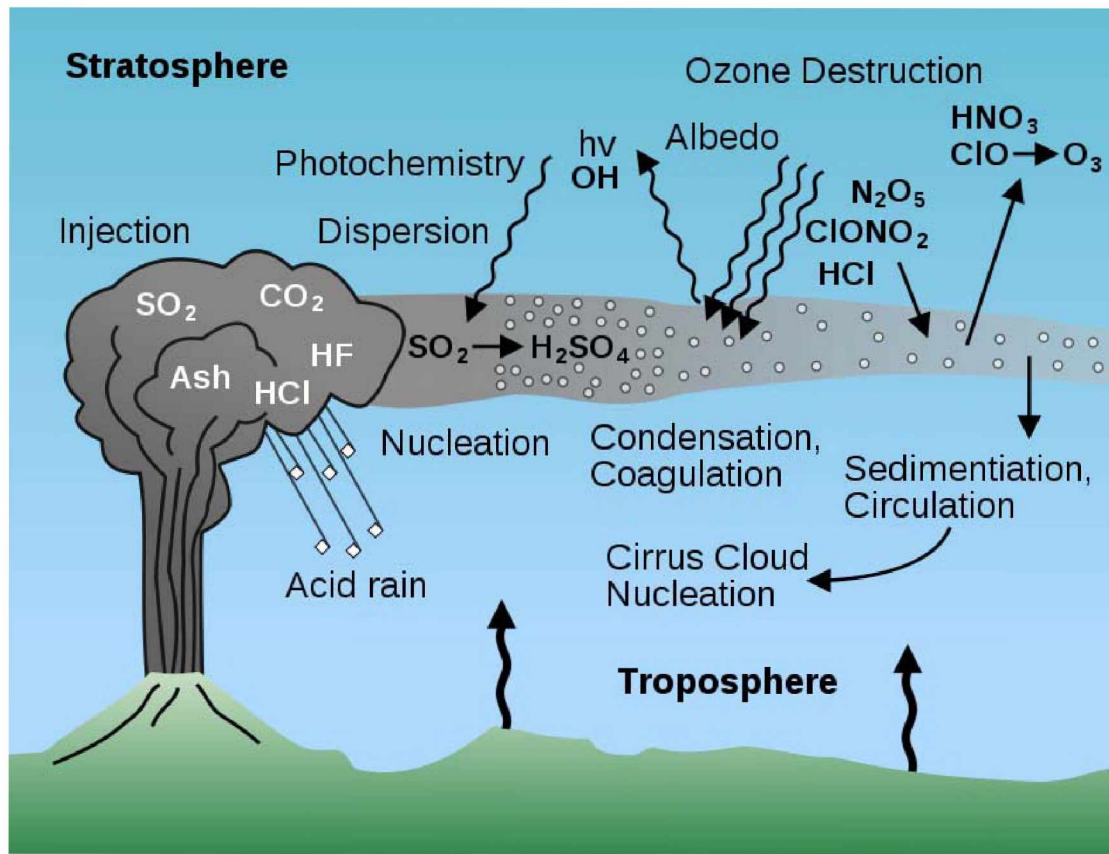


Figure 1.2. Schematic diagram of volcanic plume interacting with atmospheric features. Figure is from McGee et al. (1997).

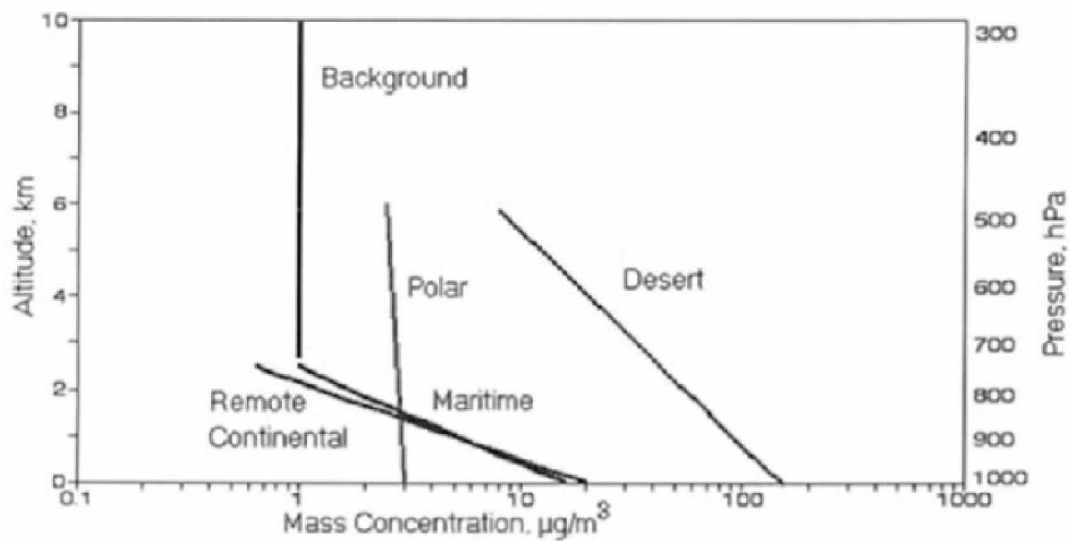


Figure 1.3. Representative regional vertical distribution of tropospheric aerosol mass concentration. Most of the aerosol content in the troposphere is within the first few kilometers of the atmosphere. Figure is from Jaenicke (1993).

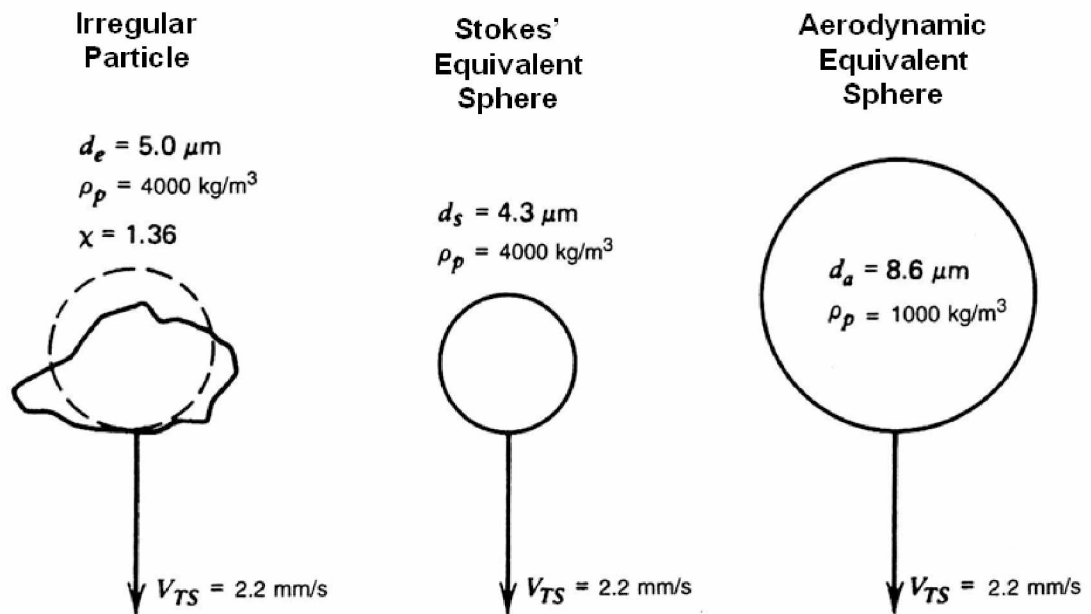


Figure 1.4. An irregular particle and its equivalent spheres. Figure is from Reist, 1993.

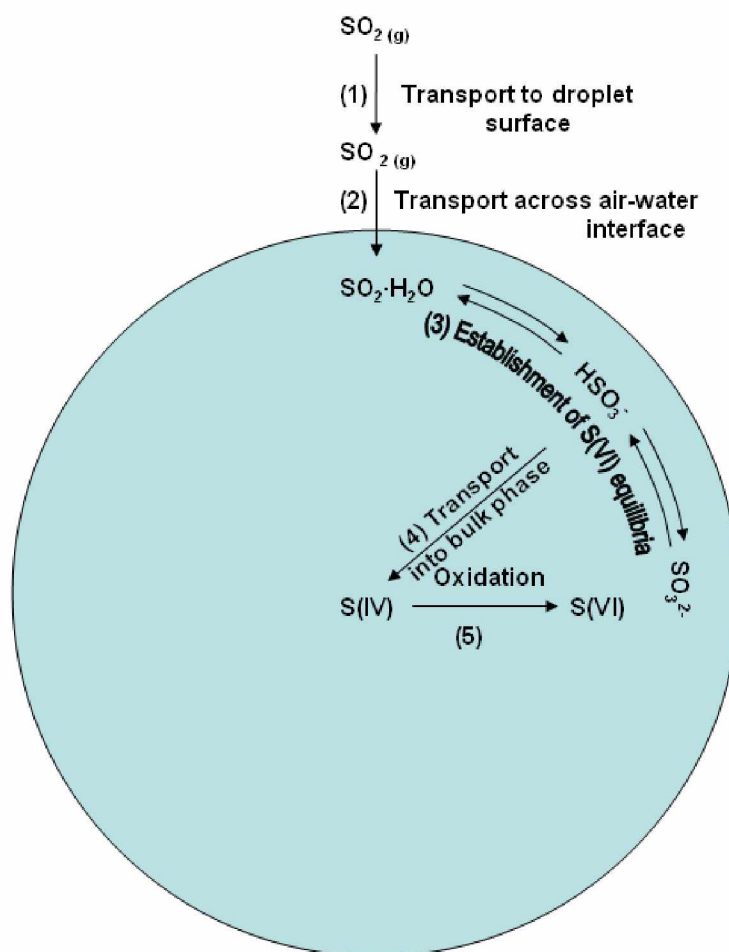


Figure 1.5. Schematic steps involved in the transfer of SO₂ from the gas phase to the aqueous phase of an atmospheric water droplet and its oxidation in the liquid phase. SO_{2(g)} = gas phase SO₂, SO_{2(i)} = SO₂ at water-gas interface. The sequence of steps is as follows: 1) Transport of gas to the surface of the droplet, 2) Transfer of gas across the gas-water interface, 3) Formation of aqueous phase equilibria of the dissolved species, 4) Transport of the dissolved species from the surface to the bulk aqueous phase of the droplet, 5) Reaction in the droplet. Figure and caption after Finlayson-Pitts and Pitts (1986).

1.8 Tables

Table 1.1 Magma Compositions and Constituents.

Type	Silica Content	Mineral phases ⁺	Explosivity*
Basalt	Low	Ol, Px, Il, Mt	Low
Basaltic Andesite	Low to Medium	Ol, Px, Mt, Il, Mt	Low to Medium
Dacite	Medium to High	Px, Mt, Il, Plag, Amp, Ap	Medium to High
Rhyolite	High	Px, Biot, Mt, Il, Plag, Qz, Amp, Ap	High

*The degree of explosivity is a function of several factors. The values listed here are general characteristics. For a more detailed discussion of explosivity and magma types, see Pyle (2000) and Newhall and Self (1982). General petrologic mineralogical assemblages are from Deer et al. (1996). ⁺Ol = olivine, Px = pyroxene, Mt = magnetite, Il = ilmenite, Plag = plagioclase feldspar, Amp = amphibole, Ap = apatite = Qz = quartz.

Chapter 2 Particle Morphologies and Formation Processes for Fine Ash Aerosol Collected During the 2006 Eruption of Augustine Volcano, Alaska¹

Abstract

Fine airborne volcanic ash (35-0.09 μm in aerodynamic diameter or O_A) from the 2006 eruption of Augustine volcano located in south-central Alaska was collected with a DRUM cascade impactor and analyzed by scanning electron microscopy (SEM) and energy dispersive spectroscopy (EDS) for chemistry and morphology. The sampler continuously collected aerosol in 8 size ranges (35.0-5.0, 5.0-2.5, 2.5-1.15, 1.15-0.75, 0.75-0.56, 0.56-0.34, 0.34-0.26, 0.26-0.09 μm O_A) from 11 January to 11 February, 2006, during the explosive and continuous emission phase of the eruption. The 35-5.0, 2.5-1.15, 0.75-0.56 and 0.34-0.26 μm O_A stages were imaged and analyzed in their entirety by SEM and EDS. A low-cost digital image processing method was used to measure particle dimensions and determine shape factors for the ash. These analyses show that ash particles in the eruptive plumes existed as single ash particles and ash aggregates. Individual ash particles were angular silicate glass shards with traces ($\ll 1\%$) of crystals and were not combined with sea salt and non-sea salt sulfate. Aggregate particles occurred as two types: 1) ash aggregates and 2)

¹ Rinkleff, P.G., Cahill, C.F., in prep. Particle morphologies and formation processes for fine ash Aerosol collected during the 2006 eruption of Augustine Volcano, Alaska. Prepared for submission to the Journal of Volcanology and Geothermal Research.

hybrid aggregates. Ash aggregates were only found on the 2.5-1.15 μm O_A stage along with individual ash grains and were not observed with sea salts or non-sea salt sulfates. Ash aggregates were only present in elutriation clouds formed by pyroclastic flows. Hybrid aggregates occurred as ash particles mixed with sea salt and/or non-sea salt sulfate. Three formation processes for these ash aerosol types are proposed: 1) Individual ash aerosol occurs when the ash has not aggregated or has become disaggregated during transport or sampling. 2) Ash aggregates form by the attraction of electrostatically charged ash particles, when ash was swept up by water droplets, by ice particles which dried during transport, or after sampling. 3) Hybrid ash aggregates form when ash is swept up by droplets containing sea salt and/or non-sea salt sulfate that are mixed upward from the marine boundary layer into downward mixing ash.

Particle size distributions determined by digital image processing confirmed the presence of fine ash in the 35-1.15 μm O_A stages and the absence of ash in smaller fractions. Ash clouds produced by pyroclastic flows contained ash in all but the 0.26-0.09 μm O_A stage. Ash particle size distributions were log normal; most of the particles were small, but the bulk of the mass was contained in few large particles. Favorable weather transported ash in a single plume from Augustine to the sampling site on 14 January and later on 17 January. Particle distributions and mass concentrations show that more and larger particles were collected on 17 January, possibly due to longer atmospheric residence time which allowed particles to aggregate and settle out of the plume.

2.1 Introduction

Airborne volcanic ash is a well known hazard to human health (Horwell and Baxter, 2006; Baxter, 2000) and aviation-based activities (Casadevall, 1994; Przedpelski and Casadevall, 1994). It also can impact ecosystem health (e.g. Langman et al., 2010; Óskarsson, 1980), have climatological effects (e.g. Grainger and Highwood, 2003), and affect visibility (Blong, 1984). Volcanic ash satellite detection and observation methods combined with atmospheric volcanic ash transport and dispersion (VATD) models provide information on the location and height of ash clouds, provide forecasts of where ash clouds will be transported, and estimate downwind mass concentrations of ash (Mastin et al., 2009). These forecasts are critical elements of the information needed by incident response personnel to institute an effective protective posture for communities in the path of volcanic clouds (Neal et al., 2010). To facilitate accurate forecasting, VATD models require information about the size, composition, and concentration of ash in plumes (Mastin et al., 2009). However, direct measurements of airborne ash particle size, composition, concentration, and morphology are rare. Mather et al. (2003) and Rose et al. (2000) review the limited number of tropospheric volcanic ash measurements reported in the literature. Most airborne ash studies referenced are of limited duration (hours to days) and contain limited compositional information. For example, Hunton et al. (2005) describe a NASA DC-8 sampling aircraft encounter with the Hekla 2000 eruption ash cloud. The aerosol they collected over the 10 minute encounter with the plume was divided into 2/3 soluble and 1/3 non-soluble fractions; the soluble fraction

was analyzed in-depth while the non-soluble aerosols or volcanic ash were not. The Mt. St. Helens, Redoubt, and Masaya volcano studies presented in Leifer et al. (1981), Hobbs et al. (1982; 1991), and Mather et al. (2003) provide four of the best records of volcanic aerosols but none provide the information needed for model validation or detection method calibration.

Model inputs from ash particle characteristics have usually come from data derived from standard tephra collection studies on fall deposits (Mastin et al., 2009). While these methods are invaluable for understanding the sedimented components and the volume of the plume that was deposited, they do not include the part of the plume that undergoes long range transport and does not make a detectable layer due to very fine particle sizes and low mass concentration. Because of these limitations, tephra studies do not measure ash in the distal part of plumes, plume edges, and ash from eruptions with small ash volumes (Rose et al., 2000). These dilute plumes still transport fine ash particles that can affect machinery and human health (Horwell and Baxter, 2006; Casadevall, 1994; Przedpelski and Casadevall, 1994). Furthermore, the evidence of processes affecting the size, composition (especially that of aggregates), and shape of ash and other aerosols can be lost once aerosols sediment from the plume. For example, soluble salts can be dissolved during rain events (Delmelle et al., 1997) and aggregated particles may break apart due to sedimentation processes such as wind abrasion or depositional loading (Taddeucci et al., 2011; James et al., 2003; Shoji et al., 1993). The actual processes of sampling and analyzing ash from tephra deposits can alter or destroy aggregate textures which may lead to particle size

distributions and settling rates. An aggregate of fine ash particles will settle at a rate much faster than the settling rates of its constituent particles. But when that aggregate is broken into its individual components, it may seem that smaller particles were removed from the plume much closer to the volcano than those individual grains would have settled according to Stokes' Law (Rose et al., 2000).

Riley et al. (2003) described digital image processing methods for determining the ash particle shape factors from scanning electron microscope (SEM) backscatter images needed as inputs for VATD models. Their methods and results show how to determine useful information for input into VATD models. However, the methods they developed are not appropriate for airborne volcanic ash samples because they required access to specialized equipment and software and they were developed for use on ash samples from tephra deposits, not airborne particulate matter. This paper presents alternate low-cost method for determining comparable shape factors using Energy Dispersive Spectroscopy (EDS) element maps and SEM secondary electron (SE) images of airborne ash sampled at discrete times from volcanic plumes and demonstrate its effectiveness on volcanic plumes from the 2006 eruption of Augustine volcano, Alaska.

The eruption of Augustine volcano in South-Central Alaska (Figure 2.1) provided an excellent opportunity to explore novel methods of airborne volcanic ash collection (Cahill et al., 2010) and explore methods for SEM and EDS aerosol analysis. A DRUM cascade impactor was installed at Homer, AK as the volcano began erupting ash. Favorable winds transported ash erupted during multiple pulses

and during differing phases of activity to the sampling location. Ash erupted on 14 January 2006 was fortuitously sampled just after the eruption and again on 17 January due to entrainment of ash in a low pressure system which brought the ash cloud over the sampling location twice. Analysis of ash from this episode taken at two different times and transport distances gives some insight into aerosol removal rates and processes affecting the ash mass concentration in the plume as it is transported.

2.2 Geologic Setting and Eruptive History

Augustine Volcano (CAVW 1103-01) is a small dome complex, 1252 meters high, which forms Augustine Island in the southwestern portion of Cook Inlet (Figure 2.1). The volcano is located 275 km SW of Anchorage, 110 km west of Homer, 175 km southwest of Soldotna and Kenai, and 185 km north of Kodiak. Before the 2006 eruption, the volcano had seven confirmed historic eruptions (1812, 1883, 1935, 1963-1964, 1971, 1976 and 1986) between Volcanic Explosivity Index 1 and 4 (Siebert and Simkin, 2002-; Newhall and Self, 1982). Previous eruptive activity has included central vent eruptions, gas and ash plumes, dome building, pyroclastic flows, lava flows, and tsunamis caused by sector collapse.

2.3 Augustine 2006 Eruption

Augustine erupted with 13 explosive eruptions over 20 days starting on 11 January 2006 after 20 years of repose (Power et al., 2006). These eruptions were preceded by 8 months of increasing seismicity, deformation, gas emissions, and small

phreatic explosions of steam and rock (Buurman and West, 2010). A principal hazard associated with Augustine eruptions is airborne volcanic ash that can disrupt regional air traffic and affect communities near the volcano as well as thousands of kilometers downwind. During this eruption, air traffic at the Anchorage International Airport and intercontinental flights traversing North Pacific airspace were adversely affected by ash plumes from Augustine. Ash plumes were closely tracked by the Federal Aviation Administration and the National Weather Service and several flights were either cancelled or rerouted due to airborne ash lofted into air traffic corridors across the eastern North Pacific and over Alaska (Neal et al., 2010). The eruption produced measurable ash fall in communities along Cook Inlet (Wallace et al., 2010). Starting on 29 January and lasting through 5 February 2006 the eruptive style became more effusive which produced summit lava domes, pyroclastic flows, and two short blocky lava flows (Vallance et al., 2010).

Aerosol mass from β -gauge and elemental composition from synchrotron x-ray fluorescence (S-XRF) analysis, previously presented in Cahill et al. (2010) show two distinctly different particle size distributions collected from plumes from the two different eruptive styles: 1) explosive, central vent and 2) pyroclastic flow elutriation clouds. The initial eruptive phase (11 to 23 January 2006) was dominated by coarser ash ($35\text{-}1.15\ \mu\text{m}\ \text{O}_A$) associated with the phreatic and phreatomagmatic pulverization of the existing 1996 dome. Virtually no fine ash below $1.15\ \text{O}_A$ was observed over this interval (Figure 2.2). The second phase of the eruption (29 January through 5 February 2006) produced fine ash aerosol ($1.15\text{-}0.09\ \mu\text{m}\ \text{O}_A$) along with coarser ash

(35-1.15 $\mu\text{m } \text{Ø}_A$) (Figure 2.3). The concentration of coarser ash was 2-5 times less during the second eruptive phase than in the initial phase. Fine ash was formed by clast-to-clast milling in the pyroclastic flows (Darteville et al., 2002) that occurred during the open-vent phase of the eruption and was transported in elutriation clouds.

2.4 Sampling and Analytical Techniques

2.4.1 Davis Rotating Unit for Measurement (DRUM) Sampler

Davis Rotating Unit for Measurement (DRUM) samplers, described by Raabe et al. (1988) and Cahill and Wakabayashi (1993), are stand-alone cascade impactors designed to collect time-resolved, size-segregated aerosol (Figure 2.4) over a six-week interval. A vacuum pump draws air into the sampler and aerosol is collected from the air stream by impaction, a type of momentum separation (Reist, 1993). The sampler has several chambers fitted with slotted inlets that accelerate the air and aerosols to specific velocities. These velocities dictate the size fraction collected on a particular stage due to inertial separation influenced by particle aerodynamic diameter. Progressively smaller particles are collected deeper in the instrument. For this study, an 8-stage DRUM was installed on 13 February 2006 at the University of Alaska Field Station at Homer Alaska (Figure 2.5). The size cuts for the sampler were 35.0-5.0, 5.0-2.5, 2.5-1.15, 1.15-0.75, 0.75-0.56, 0.56-0.34, 0.34-0.26, 0.26-0.09 $\mu\text{m } \text{Ø}_A$. Each size cut range is also referred to by its stage number; Stage 1 being the largest size and Stage 8, the smallest. Typically, DRUM samplers are fitted with a

standard $10\ \mu\text{m}\ \text{O}_A$ particle inlet, but for this study a non-standard $35\ \mu\text{m}\ \text{O}_A$ particle inlet was used to collect larger particle sizes.

The impaction substrate is a MylarTM strip attached to metal cylinder, called a drum (Figure 2.6). The MylarTM is coated with a thin film of ultra-pure Apiezon LTM vacuum grease to reduce particle bounce (Lawson, 1980). The drum rotates past the slotted inlet at a constant rate of 4 mm per day. As the drum rotates, blank sampling surface is exposed at the inlet to collect aerosol.

When the sampling interval is completed, the sampler is opened, the drums are removed in clean conditions and placed in sealed containers for shipping. In a clean laboratory, the MylarTM strips are removed from the drum, affixed to a labeled plastic frame with pressure sensitive tape, and the start and end positions are noted. Mass is determined on prepared DRUM samples using β -gauge analysis, a β -particle attenuation technique (Reist, 1993). Elemental composition (28 selected elements between Na and Pb) is determined by S-XRF (Cahill et al., 1999; Cahill, 2003) at the Lawrence Berkeley National Laboratory Advanced Light Source Beam Line 10.3.1 (Cahill et al., 2000).

2.4.2 SEM and EDS Analysis Techniques

Selected stages from the entire 8 stage sample suite (Stages 1, 3, 5, and 7) were analyzed at the Advanced Instrumentation Laboratory (AIL) at the University of Alaska Fairbanks (<http://www.uaf.edu/ail/>) using an ISI-SR-50 scanning electron microscope (SEM) equipped with a Kevex 7000 energy dispersive X-ray

spectrometer (EDS). To prepare the samples for SEM and EDS analysis, each sample was cut into ~2 cm long pieces, affixed to a rigid polystyrene backing, and sputter coated with gold and palladium. The samples were attached to a standard aluminum SEM mount and placed in the SEM chamber. In the chamber, the sample was oriented 25° from horizontal at a working distance of 10 mm.

The SEM and EDS analysis techniques detailed here form the basis for collecting raw images used for automated digital image processing methods for determining volcanic ash particle size distributions and shape descriptors for airborne ash collected during the 2006 eruption of Augustine Volcano. Both secondary SE images (Appendix A) and EDS spectra (Appendix C) were collected on the DRUM samples. For stages 1, 3, and 5, images were made at 200 times resolution; stage 7 was imaged at 400 times resolution due to the smaller particle sizes present. The accelerating voltage was set to 20 kV and the beam was set to the smallest spot size allowed by the instrument for high resolution imaging. During EDS spectra collection and element mapping, the beam spot size was increased to the maximum size available on the instrument to increase x-ray counts to 20,000-30,000 counts per second. Higher counts were found to severely blister and distort the MylarTM, so care was taken to limit sample exposure to 200,000 counts per sample image frame area to avoid damage. EDS element maps (Appendix D) were also prepared with the beam spot size and counts the same as for the EDS spectra. Point dwell times for EDS element map images were set to 6000 μ sec at a 256 kb image resolution. Longer point dwell times caused severe sample blistering and produced poor quality images.

Images and bulk field-of-view spectra were made parallel to the sampling direction from the start of the sampling interval with about 5-10% area overlap between each adjacent image to allow for the construction of image mosaics and to maintain location (and sampling time) within the sample (Figure 2.7). An EDS spectrum of the entire field of view was collected for each frame. When a significant increase in silicon counts was noted, an element map was prepared because the presence of silicon was considered to be an indicator of the presence of volcanic ash. Regardless of silicon count levels, an element map was prepared at regular intervals to show elemental distribution across the field of view during non-volcanic (background) aerosol sampling.

DRUM samples were found to provide excellent images and spectra of particles by Rinkleff et al. (in review), since all the particles are on a smooth surface and the sampling substrate (MylarTM and Apezion LTM) does not contaminate the sample spectra. While the SE images were useful for qualitatively determining particle shapes, EDS element maps were useful for digitally determining particle measurements. Image mosaics of SE images were prepared so that sample distance could be measured (Figure 2.7) and thus, sampling time could be determined. The DRUMs in this study rotated at 4 mm of sampling distance per day so exact particle sampling times could be obtained. The SE images show attractive pictures of the collected aerosols with good resolution for visually determining particle qualities, but they pose several problems for automated image analysis techniques. For example, object edges and rough surfaces are brighter than smooth continuous surfaces in SE

images. Secondary illumination and beam shadowing can also affect SE images. These phenomena can cause automated image processing methods to produce incorrectly estimated particle sizes and shape descriptors (Reed, 2005; Russ, 1990).

2.4.3 Image Analysis Techniques

Silicon EDS maps were used to determine ash shape properties since volcanic ash is chiefly composed of volcanic glass which contains silicon (Heiken and Wohletz, 1985; Fisher and Schminke, 1984). Particle properties including size distribution and shape descriptors such as aspect ratio, roundedness, solidity, perimeter, Feret length and width, Feret angle, circular radius, spherical particle volume, and particle mass (Table 2.1 and Appendix B) were determined by the digital image processing methods described below. These properties are comparable to those described by Riley et al. (2003).

Image J (Ferreria and Rasband, 2011) was used for image processing. This software is an open-source, public-domain, Java-based image processing program developed at the National Institutes of Health (available for download at <http://rsb.info.nih.gov/ij/>). Each element map was inverted (Figure 2.8) to help visually accentuate the element detections, then resized by a four-fold increase to increase the image pixel density to produce smoother particle edges and match the accompanying SE image pixel resolution. Next, each EDS element map was subjected to three thresholding methods included in the Image J package: 1) the default Iso-means of Ridler and Calvard (1978), which is an iterative process that

averages pixel values above and below a threshold, 2) Moments (Tsai, 1985), which attempts to preserve the image moments in the threshold result, and 3) Triangle (Zack et al., 1977), which geometrically determines threshold based on histogram shape. These thresholding methods were chosen because they produced good results for sample images with a range of particle sizes and concentrations. After thresholding, the resultant particles were segmented into smaller particles based on overall particle shape (Figure 2.9). After segmenting, the particles were measured and a table containing the results was produced. After automated processing, each set of images was manually evaluated to determine which thresholding technique produced the result closest to the original element map (Figure 2.10). This decision was made for each element map based on heuristic visual comparison. Those results were retained and the others were discarded.

2.5 Results

2.5.1 Volcanic Ash Aerosol Types

SEM imagery of the Augustine DRUM samples showed three distinct particle types that contained volcanic ash: single grains, non-cored aggregates, and cored aggregates. Background aerosols which consisted of soil particles, sea salts, non-sea salt sulfates, and soot particles from combustion were also collected. Some of these particles were from long-range transport while others came from local sources (Cahill et al., 2010).

2.5.1.1 Single Grain Ash

Single grain ash was observed as individual glass or crystal grains. These particles dominated the aerosol mass over an interval or could coexist with background aerosols (Figure 2.11). These particles were angular, equant, silica-rich, vitric shards. Particle size populations were log normal (Figure 2.12). Rare crystal phases were observed and were much smaller than the glass shards possibly due to their relatively low magmatic volume or faster settling velocities due to their size and/or higher density relative to volcanic glass shards.

2.5.1.2 Ash Aggregates

These aerosols, shown in Figure 2.13, were only observed in Stage 3 (2.5-1.15 $\mu\text{m } \text{O}_A$) from 28 through 31 January and were found either as individual instances within a population of single grain aerosols or in populations dominated by ash aggregate aerosol. They were not present with hybrid aerosols. Non-cored aerosol aggregates consisted almost entirely of glass ash shards with traces of crystal particles. The individual ash grains that comprised the ash aggregates were identical to individual ash grains described above. These particles appeared to be similar to aggregates formed by laboratory simulations by James et al. (2002).

2.5.1.3 Hybrid Aggregates

This class of volcanic ash aerosols includes ash mingled with sea salt and/or non-sea salt sulfate. Hybrid aggregates, shown in Figure 2.14, appeared to have been

disrupted and spread out over larger areas than non-cored aerosols. This may have been due to wet particle droplets impacting the sampling surface and spreading out, then drying due to pressure drops in the DRUM sampler. The resulting sea salt or non-sea salt solid was left behind after the water evaporated. The salt and sulfate could be massive, botryoidal, or cubic particles (Figure 2.15). Non-sea salt sulfate particles occurred as massive, botryoidal, dendritic, or hexagonal forms. Ash associated with the salt or sulfate was often concentrated away from the salt or sulfate particle core within a halo or ring of sulfate or sea salt, but may also have been completely surrounded by sea salt or sulfate. These relationships may be the result of drying processes after sampling occurred. As the solution evaporated, the area of the droplet retracted toward its center and left behind a dry salt or sulfate particle. The shape and size of ash particles in hybrid aggregates was identical to individual ash particle morphology. Rare crystal phases ($\ll 1\%$) were present, similar to the frequencies seen in single grain ash and ash aggregates.

Sea salts were mostly sodium chloride but could occur as calcium chloride, potassium chloride, and other common sea salt types (Lewis and Schwartz, 2004). Non-sea salt sulfate is also a common maritime aerosol (Finlayson-Pitts and Pitts, 1986), but it is possible that some of the sulfate was from the volcano (Rose et al., 2000). Systematic changes in non-sea salt sulfate levels were not observed during eruptive periods from background sulfate levels which may indicate the non-sea salt sulfate is not volcanic. However, identification of sulfate sources would require stable isotope analysis which is beyond the scope of this project.

2.5.2 Volcanic Ash Particle Size Distributions

Particle size distributions determined by image processing methods show log-normal distributions. Most of the particles are small and contain little mass while the fewer larger particles contain most of the mass in the sample. Size distributions for the initial central vent eruptive style sampled on 14 January and again on 17 January 2006 are described below along with the distributions of ash collected from plumes produced by pyroclastic flows on 30 January 2006.

2.5.2.1 Initial Eruption Phase

Ash was observed in the largest DRUM sampler size fractions (35.0-1.15 μm O_A). Below these size cuts, no ash was observed by EDS spectroscopy or by S-XRF. Particle size distributions (Figure 2.12) of ash collected on 14 January are log normal and likely represent the tail end and lower bounds of the overall ash particle distribution produced by explosive fragmentation in the plume. HYSPLIT trajectories (Figure 2.16) (Draxler and Rolph, 2011; Rolph, 2011) showed that the plume sampled on 14 January was entrained in a cyclone which brought the ash plume back to the sampling site on 17 January. Particle distributions (Figure 2.12 A and B) and S-XRF elemental concentrations (Figure 2.2) are higher than those from 14 January. The distributions remained log-normal.

2.5.2.2 Pyroclastic Flow Particles

Ash sampled from pyroclastic flow elutriation plumes was present in measurable amounts in all but the smallest size fraction ($0.26\text{-}0.09\ \mu\text{m}\ \text{Ø}_A$) (Figure 2.17). SEM and EDS analysis also showed the presence of ash from $35.0\text{-}0.26\ \mu\text{m}\ \text{Ø}_A$. Particle size distributions (Figure 2.17) were log-normal, but the size distribution for the $0.34\text{-}0.26\ \mu\text{m}\ \text{Ø}_A$ stage (Figure 2.17 D) showed a distinct decrease and possible dual mode. This is interpreted to be the result of image artifacts which produced noise that was measured as the smallest particles. The mode centered on $0.2\ \mu\text{m}^2$ may represent the tail end of particle sizes that were present in the elutriation cloud.

2.6 Discussion

Volcanic ash undergoes physical and chemical changes as soon as it is erupted into the atmosphere (Mather et al., 2003). As it is transported, larger particles preferentially fall out near the vent while finer grains settle slower and travel farther before sedimenting (Fisher, 1964). As the particles travel, they evolve from simple pyroclasts into complex particles that are part volcanic and part atmospheric. Their forms depend on their transport time, the contents of the eruptive cloud, and composition of the atmosphere where they transport (e.g. Rose et al., 2000). Several processes may occur during transport which may affect aggregation processes (Mather et al., 2003). For example, an ash particle may collide with, adhere to, or abrade other particles in the plume (Darteville et al., 2002; James et al., 2002; Sorem 1982). Ash also may be scavenged by water droplets or provide a surface where

chemical reactions can take place (Delmelle et al., 2007; Simpson et al., 2000). Lastly, ash can provide a nucleation site for water condensation (Folch et al., 2010). When ash combines with other particles during transport, it ceases to be an exclusively volcanic particle and its aerodynamic properties and thus settling rate change (Rose et al., 2000).

2.6.1 Potential Aggregation Processes

The three ash types collected by the DRUM sampler from the 2006 Augustine plume (individual grains, ash aggregates, and hybrid aggregates) indicate different post-eruptive aerosol formation processes. Individual grains could exist when the particle has had a relatively short time for transport or the particle number density is sufficiently low to inhibit a high rate of particle-particle collisions or electrostatic attraction (James et al., 2002; Fuchs, 1964). Another scenario may involve a relatively dry plume or atmosphere preventing droplet nucleation or scavenging. Several formation processes for ash aggregates have been discussed by various authors. Ice hydrometeor aggregation analogous to the formation of hailstones has been proposed by Durant and Rose (2009) and Durant et al. (2009; 2008). Wet aggregation of ash by water droplets has been modeled by Folch et al. (2010) and Vietch and Woods (2001). The ice particles and or water droplets containing ash in either of these instances evaporate before the particle sediments (Rose et al., 2000). James et al. (2002) produced dry aggregates in controlled laboratory conditions from fracto-emission particle charging and subsequent aggregation of oppositely charged

particles. Particles could also build electric charge as they collide and grind together in the pyroclastic flow (Darteville et al., 2002). This milling process has been cited as a means for generating both fine ash and particle charge. Any one of these processes, or a combination could explain the presence of ash aggregates. The formation of ash aggregates sampled from Augustine plumes produced by pyroclastic flows is interpreted to be the result of ash milling and electrostatic charging.

Hybrid aggregates likely form when ash is scavenged by water droplets by collision and/or electrostatic attraction (Rose and Durant, 2009). The presence of mud rain has been commonly observed during large eruptions (Textor et al., 2006), but the aerosols collected from Augustine ($35\text{-}0.01\ \mu\text{m}\ \text{Ø}_A$) were not so large as to constitute a raindrop ($>0.5\ \text{mm}$ in diameter) (Marshall and Palmer, 1948). Maritime water droplets commonly contain salts from sea spray (Lewis and Schwartz, 2004). As these droplets mix upward from the moist marine boundary layer into the atmosphere, ash particles mixing downward from a dispersing ash cloud could be scavenged by them (Durant and Rose, 2009; Durant et al., 2009). Subsequent droplet evaporation could form a dry particle before sampling, or pressure drops in the sampler could cause wet droplets to dry and leave behind a salt/ash deposit on the sampling surface. A droplet that dried while suspended may appear as a salt crystal with ash coating its surface while a droplet that impacted and dried could show a halo of ash and a core of salt. The latter seems to more completely describe the observed cored aggregates sampled from the Augustine plumes. This indicates that these particles were wet when they were sampled.

2.6.2 Implications of Ash Aggregation Processes for Transport Models and Satellite Detection Methods

There are two major implications of observing how volcanic aerosol changes from single grains to complex aggregates while being transported in a dispersing plume: 1) Model results derived from aggregation related fallout rates determined from tephra studies may underestimate fine-grained ash transport distances and 2) satellite detection methods dependent on 10-12 μm wavelengths may be more sensitive to particles larger than those which undergo long range transport (Prata, 1989). Aggregation has been cited often in the literature as the main process for ash removal from the plume at rates faster than those for the constituent ash grains (Pinto et al., 1989). Analysis of ash from Augustine volcano shows that ash aggregation occurs by several processes, at different efficiencies, and at different rates within a plume. Not all ash particles form aggregates; some fine ash remains suspended while other ash forms aggregates and falls to the ground. Models which assume that all ash falls out of the plume as aggregates will underestimate the concentration of fine ash that does not aggregate and undergoes long range transport.

Satellite detection of volcanic ash relies heavily on the Brightness Temperature Difference (BTD) method of Prata (1989). The BTD is dependent on particles being near the Thermal Infrared (TIR) wavelengths ($\sim 10\text{-}12 \mu\text{m}$) used by the method. This sampling shows that a portion of a plume consists of particles much smaller than the sensitivity of TIR wavelengths (Rose et al., 2000). These particles ($<$

1 μm in diameter) are smaller than the wavelengths used in the BTM so they do not react strongly with the 10-12 μm radiation. Therefore when the plume is diffuse enough, it does not produce an ash signal in the split window, meaning that diffuse fine volcanic ash is below the detection limit of current techniques in standard use for volcanic ash detection.

Since diffuse fine ash is essentially invisible to satellite detection, it is crucial to employ models to forecast and track fine ash. Cahill et al. (2010) showed that PUFF (Searcy et al., 1989) and HYSPLIT (Draxler and Rolph, 2011; Rolph, 2011) models were a good first-order approximation for ash transport and dispersal, but inputs to more complex models such as WRF-Chem may require a more complete understanding of plume aerosol processes to properly model the fall-out rates and long-range transport of volcanic ash (Mastin et al., 2009).

2.7 Acknowledgements

We would like to acknowledge the extensive assistance we received from the University of Alaska Advanced Instrumentation Laboratory for developing an imaging method for DRUM samples by SEM and EDS spectroscopy. we would also like to extend our gratitude to the Alaska Volcano Observatory for hosting the placement of the DRUM sampler at the Homer Field Station. This work was supported by Army Research Laboratory contract W911NF-07-1-0346 and by the Alaska Volcano Observatory (AVO) through U.S. Geological Survey cooperative agreements 03HQAG0032 and 03HQAG0059. AVO is a cooperative tri-partite

program supported by the U.S. Geological Survey, the University of Alaska Fairbanks Geological Institute, and the Alaska Division of Geological and Geophysical Surveys.

2.8 References

Baxter, P., 2000. Impacts of Eruptions on Human Health. In: Sigurdsson, H., Houghton, B., McNutt, R.R., Stix, J. (Eds.), *Encyclopedia of Volcanoes*. Academic Press, New York, NY, pp. 1035-1043.

Blong, R.J., 1984. *Volcanic Hazards: A sourcebook on the effects of eruptions*. Academic Press, Sidney, Australia.

Buurman, H., West, M.E., 2010. Seismic precursors to volcanic explosions during the 2006 eruption of Augustine Volcano. In: Power, J.A., Coombs, M.L., Freymueller, J.T. (Eds.), *The 2006 eruption of Augustine Volcano, Alaska*. U.S. Geological Survey Professional Paper 1769, pp. 41–57.

Cahill, C.F., 2003. Asian aerosol transport to Alaska during ACE-Asia. *Journal of Geophysical Research*. 108, 8664-8872.

Cahill, C.F., Rinkleff, P., Dehn, J., Webley, P., Cahill, T., Barnes, D., 2010. Aerosol measurement from a recent Alaskan volcanic eruption: Implications for volcanic ash transport predictions. *Journal of Volcanology and Geothermal Research*. 198, 76-80.

Cahill, T.A., Wakabayashi, P., 1993. Compositional analysis of size-segregated aerosol samples. In: Newman, L. (Ed.), *Measurement Challenges in Atmospheric Chemistry*, American Chemical Society, pp. 211-228.

Cahill, T.A., Cliff, S.S., Perry, K.D., Jimenez-Cruz, M., Kelly, P.B., Shackelford, J., McHugo, S.A., Thompson, A., 2000. S-XRF and atmospheric aerosols: Health, visibility, and climate change. *Advanced Light Source Compendium of User Abstracts*, Lawrence Berkeley National Laboratory. <http://www.als.lbl.gov/als/compendium> (last accessed on 10 March 2012).

Cahill, T., Cliff, S., Perry, K., Jimenez-Cruz, M., McHugo, S., 1999. Size and time resolved anthropogenic components of aerosols via synchrotron x-ray fluorescence: Application to Asian aerosol transport. Abstracts, American Geophysical Union 1999 Fall Meeting, December. San Francisco, California, pp. 13-17.

Casadevall, T.J., 1994. The 1989–1990 eruption of Redoubt Volcano Alaska: Impacts on aircraft operations. *Journal of Volcanology and Geothermal Research*. 62, 301-316.

Darteville, S., Ernst, G.J., Stix, J., Bernard, A., 2002. Origin of the Mount Pinatubo climactic eruption cloud: Implications for volcanic hazards and atmospheric impacts. *Geology*. 30, 663-666.

- Delmelle, P., Lambert, M., Dufrêne, Y., Gerin, P., Óskarsson, N., 2007. Gas/aerosol–ash interaction in volcanic plumes: New insights from surface analyses of fine ash particles. *Earth and Planetary Science Letters*. 259, 159–170.
- Draxler, R.R., Rolph, G.D., 2011. HYSPLIT (HYbrid Single-Particle Lagrangian Integrated Trajectory). NOAA Air Resources Laboratory, Silver Spring, MD. Model access via NOAA ARL READY Website: <http://ready.arl.noaa.gov/HYSPLIT.php> (last accessed on 10 March 2012).
- Durant, A.J., Rose, W.I., 2009. Sedimentological constraints on hydrometeor-enhanced particle deposition: 1992 eruptions of Crater Peak, Alaska. *Journal of Volcanology and Geothermal Research*. 186, 40–59.
- Durant, A.J., Rose, W.I., Sarna-Wojcicki, A.M., Carey, S., Volentik, A.C.M., 2009. Hydrometeor-enhanced tephra sedimentation: Constraints from the 18 May 1980 eruption of Mount St. Helens. *Journal of Geophysical Research*. 114, 1-28.
- Durant, A.J., Shaw, R.A., Rose, W.I., Mi, Y., Ernst, G.G.J., 2008. Ice nucleation and overseeding of ice in volcanic clouds. *Journal of Geophysical Research*. 113, 1-13.
- Ferreria, T., Rasband, W., 2011. Image J user guide. <http://imagej.nih.gov/ij/docs/user-guide.pdf> (last accessed on 10 March 2012).
- Finlayson-Pitts, B.J., Pitts J.N., 1986. *Atmospheric Chemistry: Fundamentals and Experimental Techniques*. Wiley-Interscience, New York, NY.
- Fisher, R.V., 1964. Maximum size, median diameter, and sorting of tephra. *Journal of Geophysical Research*. 69, 341-355.
- Fisher, R.V., Schminke, H.-U., 1984. *Pyroclastic Rocks*. Springer-Verlag, New York, NY.
- Folch, A., Costa, A., Durant, A., Macedonio, G., 2010. A model for wet aggregation of ash particles in volcanic plumes and clouds: 2. Model application. *Journal of Geophysical Research*. 115, 148-227.
- Fuchs, N.A., 1964. *The Mechanics of Aerosols*. Dover Publications, New York, NY.
- Grainger, R.G., Highwood, E.J., 2003. Changes in stratospheric composition, chemistry, radiation, and climate caused by volcanic eruptions. In: Oppenheimer, C., Pyle, D.M., Barclay, J. (Eds.), *Volcanic Degassing*. Geological Society, London, Special Publications 213, pp. 329-347.

Heiken, G., Wohletz, K., 1985. *Volcanic Ash*. University of California Press, Berkeley, CA.

Hobbs, P.V., Radke, L.F., Lyons, J.H., Ferek, R.J., Coffman, D.J., 1991. Airborne measurements of particles and gas emissions from the 1990 volcanic eruptions of Mount Redoubt. *Journal of Geophysical Research*. 96, 18,735-18,752.

Hobbs, P.V., Tuell, J.P., Hegg, D.A., Radke, L.F., Eltgroth, M.K., 1982. Particles and gases in the emissions from the 1980-1981 volcanic eruptions of Mt. St. Helens. *Journal of Geophysical Research*. 87, 11,062-11,086.

Horwell, C.J., Baxter, P.J., 2006. The respiratory health hazards of volcanic ash: A review for volcanic risk mitigation. *Bulletin of Volcanology*. 69, 1-24.

Hunton, D.E., Viggiano, A.A., Miller, T.M., Ballenthin, J.O., Reeves, J.M., Wilson, J.C., Lee, S.-H., Anderson, B.E., Brune, W.H., Harder, H., Simpas, J.B., Oskarsson, N., 2005. In-situ aircraft observations of the 2000 Mt. Hekla volcanic cloud: Composition and chemical evolution in the Arctic lower stratosphere. *Journal of Volcanology and Geothermal Research*. 145, 23–34.

James, M.R., Lane, S.J., Gilbert, J.S., 2003. Density, construction, and drag coefficient of electrostatic volcanic ash aggregates. *Journal of Geophysical Research*. 108, 1-12.

James, M.R., Gilbert, J.S., Lane, S.J., 2002. Experimental investigation of volcanic particle aggregation in the absence of a liquid phase. *Journal of Geophysical Research*. 107, 148-227.

Langman, B., Zasek, K., Hort, M., 2010. Atmospheric distribution and removal of volcanic ash after the eruption of Kasatochi volcano: A regional model study. *Journal of Geophysical Research*. 115, 1-10.

Lawson, D., 1980. Impaction surface coatings intercomparison and measurements with cascade impactors. *Atmospheric Environment*. 14, 195-199.

Leifer, R., Hinchliffe, L., Fisenne, I., Franklin, H., Knutson, E., Olden, M., Sedlacek, W., Mroz, E., Cahill, T., 1981. Measurements of the stratospheric plume from the Mount St. Helens eruption: Radioactivity and chemical composition. *Science*. 20, 904 – 907.

Lewis, E.R., Schwartz, S.E., 2004. *Sea Salt Production: Mechanisms, Methods, Measurements and Models*. Geophysical Monograph 152. American Geophysical Union. Washington, D.C.

Marshall, J.S., Palmer W.M., 1948. The distribution of raindrops with size. *Journal of Meteorology*. 5, 165-166.

Mastin, L.G., Guffanti, M., Servranckx, R., Webley, P.W., Barsotti, S., Dean, K., Durant, A., Ewert, J.W., Neri, A., Rose, W.I., Schneider, D.J., Siebert, L., Stunder, B., Swanson, G., Tupper, A., Volentik, A., Waythomas, C.F., 2009. A multidisciplinary effort to assign realistic source parameters to model of volcanic ash-cloud transport and dispersion during eruptions. In: Mastin, L.G., Webley, P.W. (Eds.), *Journal of Volcanology and Geothermal Research: Special Issue on Volcanic Ash Clouds*. 186, 10–21.

Mather, T.A., Pyle, D.M., Oppenheimer, C., 2003. Tropospheric Volcanic Aerosol. In: Robock, A., Oppenheimer, C. (Eds.), *Volcanism and the Earth's Atmosphere*. American Geophysical Union, Washington D.C., pp. 189-212.

Neal, C.A., Murray, T.L., Power, J.A., Adleman, J.N., Whitmore, P.M., Osiensky, J.M., 2010. Hazard information management, interagency coordination, and impacts of the 2005–2006 eruption of Augustine Volcano. In: Power, J.A., Coombs, M.L., Freymueller, J.T. (Eds.), *The 2006 eruption of Augustine Volcano, Alaska*. U.S. Geological Survey Professional Paper 1769, pp. 645–667.

Newhall, C.G., Self, S., 1982. The Volcanic Explosivity Index (VEI): An estimate of explosive magnitude for historical volcanism. *Journal of Geophysical Research*. 87, 1231-1238.

Óskarsson, N., 1980. The interaction between volcanic gases and tephra, fluorine adhering to tephra of the 1970 Hekla eruption. *Journal of Volcanology and Geothermal Research*. 8, 251–266.

Pinto, J.P., Turco, R.P., Toon, O.B., 1989. Self-limiting physical and chemical effects in volcanic eruption clouds. *Journal of Geophysical Research*. 94, 11,165-11,174.

Power, J.A., Nye, C.J., Coombs, M.L., Wessels, R.L., Cervelli, P.F., Dehn, J., Wallace, K.L., Freymueller, J.T., Doukas, M.P., 2006. The reawakening of Alaska's Augustine volcano. *EOS*. 87, 373-377.

Prata, A.J., 1989. Observations of volcanic ash clouds in the 10-12 μm window using AVHRR/2 data, *International Journal of Remote Sensing*. 10, 751-761.

- Przedpelski, Z.J., Casadevall, T.J., 1994. Impact of volcanic ash from 15 December 1989 Redoubt volcano eruption on GE CF6-80C2 turbofan engines. In: Casadevall, T.J. (Ed.), *Volcanic Ash and Aviation Safety: Proceedings of the First International Symposium on Volcanic Ash and Aviation Safety*. U.S. Geological Survey Bulletin 2047, pp. 129-135.
- Raabe, O.G., Braaten, D.A., Axelbaum, R.L., Teague, S.V., Cahill, T.A., 1988. Calibration studies of the DRUM impactor. *Journal of Aerosol Science*. 19, 183-195.
- Reed, S., 2005. *Electron Microprobe Analysis and Scanning Electron Microscopy in Geology*. Cambridge University Press, New York, NY.
- Reist, P.C., 1993. *Aerosol Science and Technology, Second Edition*. McGraw-Hill, New York, NY.
- Ridler, T.W., Calvard, S., 1978. Picture thresholding using an iterative selection method. *IEEE Transactions on Systems, Man, and Cybernetics*. 8, 630-632.
- Riley, C.M., Rose, W.I., Bluth, G.J.S., 2003. Quantitative shape measurements of distal volcanic ash. *Journal of Geophysical Research*. 108, 2504-2519.
- Rinkleff, P.G., Cahill, C.F., Stichick, M., Characterization of airborne ash collected during the 2009 Redoubt volcano eruption. *Journal of Volcanology and Geothermal Research* (in review).
- Rolph, G.D., 2011. Real-time Environmental Applications and Display sYstem (READY). NOAA Air Resources Laboratory, Silver Spring, MD. <http://ready.arl.noaa.gov> (last accessed on 10 March 2012).
- Rose, W.I., Durant, A.J., 2009. Fine ash content of explosive eruptions. *Journal of Volcanology and Geothermal Research*. 186, 32-39.
- Rose, W.I., Bluth, G.J.S., Ernst, G.G.J., 2000. Integrating retrievals of volcanic cloud characteristics from satellite remote sensors: A summary. *Philosophical Transactions of the Royal Society of London*. 358, 1585-1606.
- Russ, J., 1990. *Computer Assisted Microscopy: The Measurement and Analysis of Images*. Plenum Press, New York, NY.
- Searcy, C., Dean, K., Stringer, W., 1998. PUFF: A high-resolution volcanic ash tracking model. *Journal of Volcanology and Geothermal Research*. 80, 1-16.

- Shoji, S., Nanzyo, M., Dahlgren, R., 1993. *Volcanic Ash Soils: Genesis, Properties and Utilization*. Elsevier, New York, NY.
- Siebert, L., Simkin, T., 2002-. *Volcanoes of the World: An Illustrated Catalog of Holocene Volcanoes and their Eruptions*. Smithsonian Institution, Global Volcanism Program, Digital Information Series, GVP-3. <http://www.volcano.si.edu/world/> (last accessed on 10 March 2012).
- Simpson, J.J., Hufford, G., Pieri, D., Berg, J., 2000. Failures in detecting ash from a satellite-based technique. *Remote Sensing of the Environment*. 72, 191-217.
- Sorem, D.K., 1982. Volcanic ash clusters: Tephra rafts and scavengers. *Journal of Volcanology and Geothermal Research*. 13, 63-71.
- Taddeucci, J., Scarlato, P., Montanaro, C., Cimarelli, C., Del Bello, E., Freda, C., Andronico, D., Gudmundsson, M.T., Dingwell, D.B., 2011. Aggregation-dominated ash settling from the Eyjafjallajökull volcanic cloud illuminated by field and laboratory high-speed imaging. *Geology*. 39, 891-894.
- Textor, C., Graf, H.F., Herzog, M., Oberhuber, J.M., Rose, W.I., Ernst, G.G.J., 2006. Volcanic particle aggregation in explosive eruption columns. Part I: Parameterization of the microphysics of hydrometeors and ash. *Journal of Volcanology and Geothermal Research*. 150, 359-377.
- Tsai, W., 1985. Moment-preserving thresholding: A new approach. *Computer Vision, Graphics, and Image Processing*. 29, 377-393.
- Vallance, J.W., Bull, K.F., Coombs, M.L., 2010. Pyroclastic flows, lahars, and mixed avalanches generated during the 2006 eruption of Augustine Volcano. In: Power, J.A., Coombs, M.L., Freymueller, J.T. (Eds.), *The 2006 eruption of Augustine Volcano, Alaska*: U.S. Geological Survey Professional Paper 1769, pp. 219–267.
- Vietch, G., Woods, A.W., 2001. Particle aggregation in volcanic plumes. *Journal of Geophysical Research*. 106, 26,425-26,441.
- Wallace, K.L., Neal, C.A., McGimsey, R.G., 2010. Timing, distribution, and character of tephra fall from the 2005-2006 eruption of Augustine Volcano. In: Power, J.A., Coombs, M.L., Freymueller, J.T. (Eds.), *The 2006 eruption of Augustine Volcano, Alaska*: U.S. Geological Survey Professional Paper 1769, pp. 187–217.
- Zack, G., Rogers, W., Latt, S., 1977. Automatic measurement of sister chromatid exchange frequency. *Journal of Histochemistry and Cytochemistry*. 25, 741–53.

2.9. Figures

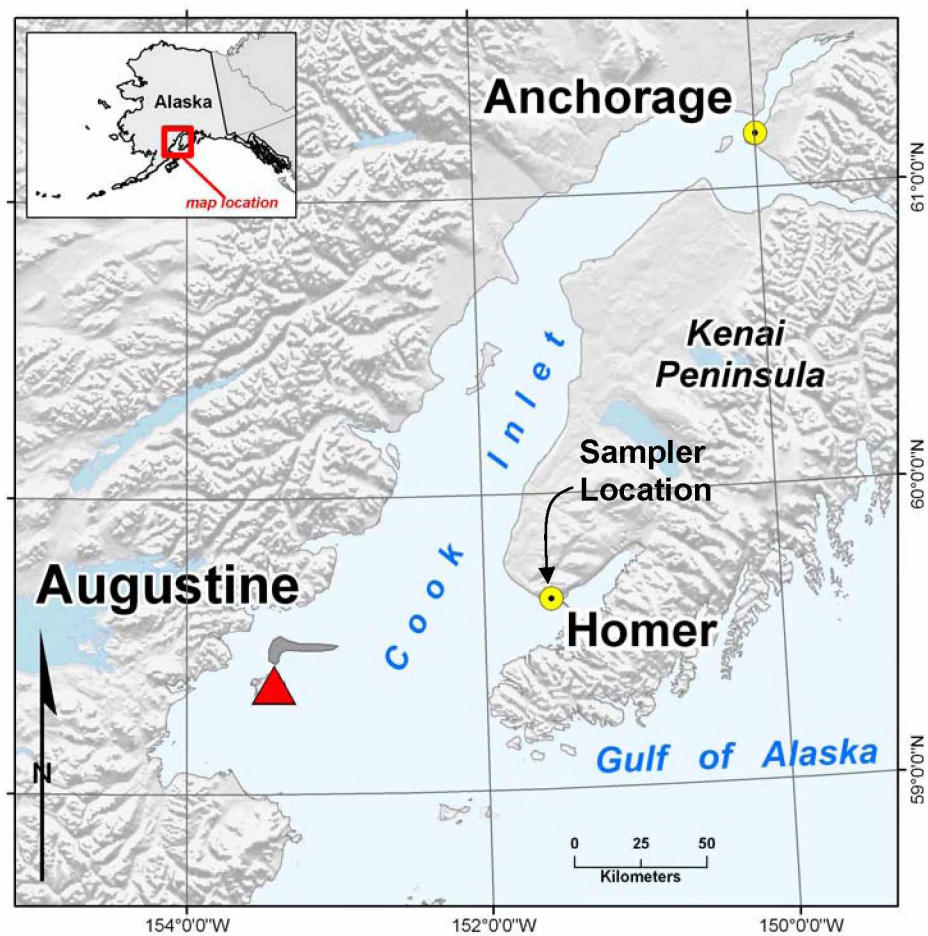


Figure 2.1. Location map of Augustine Volcano and the sampling location near Homer, Alaska. Augustine is located in Cook Inlet 275 km west-southwest of Anchorage and 110 km west of Homer.

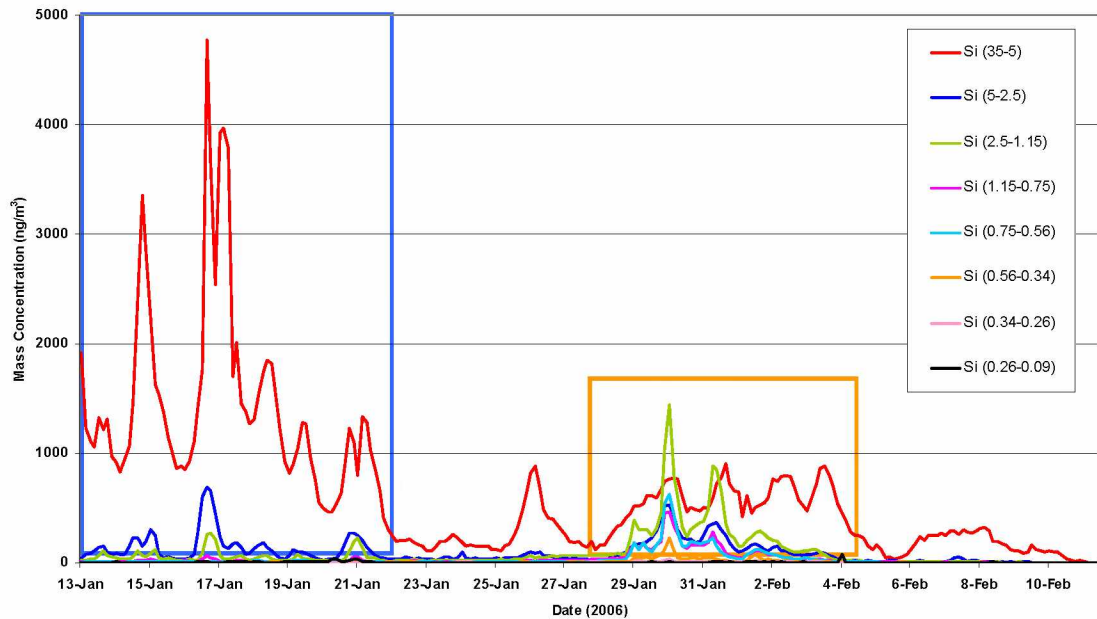


Figure 2.2. Silicon mass concentration relative to time. The initial eruptive phase from 13 to 22 January (blue box) is dominated by larger aerosols ($35.0\text{-}1.15\ \mu\text{m}\ \text{O}_A$). Smaller size fractions have essentially no silicon present. The eruptive style for the period starting on 28 January through 5 February (orange box) was dominated by pyroclastic flows. While significant ash mass concentrations were present in the larger size fractions, significant ash mass concentrations were also present in smaller size fractions ($1.15\text{-}0.26\ \mu\text{m}\ \text{O}_A$).

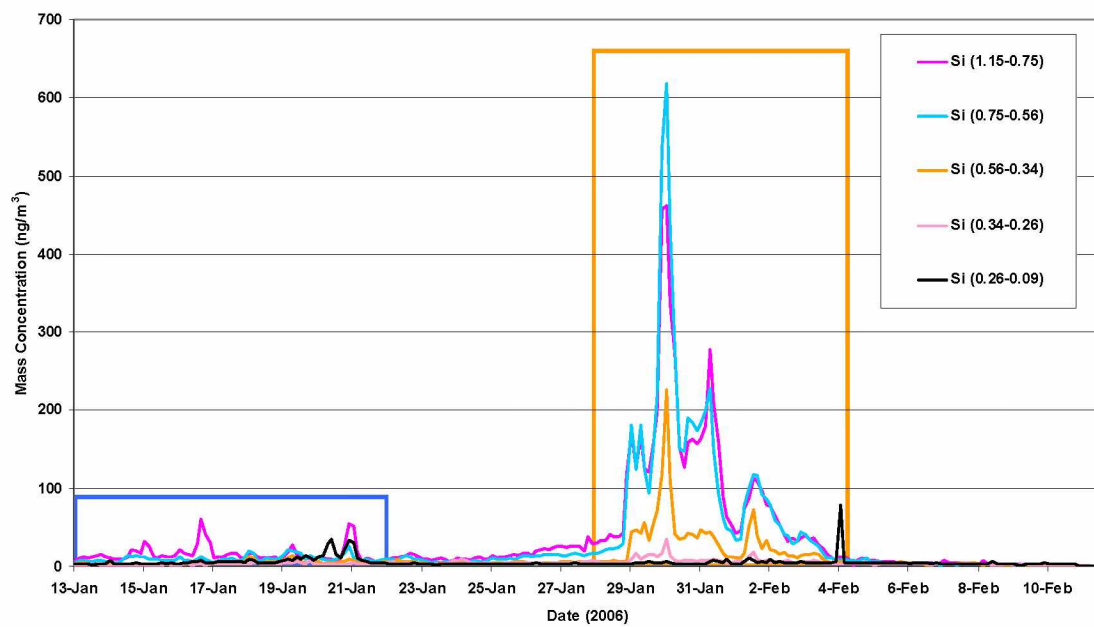


Figure 2.3. Silicon mass concentration relative to time (1.15-0.09 $\mu\text{m } \text{O}_A$). The initial eruptive phase indicated by the blue box had very little ash present due to the explosive ash-forming processes that occurred during this phase. Over the pyroclastic flow-dominated phase (orange box) clast-to-clast milling produced fine ash 1.15-0.26 $\mu\text{m } \text{O}_A$.

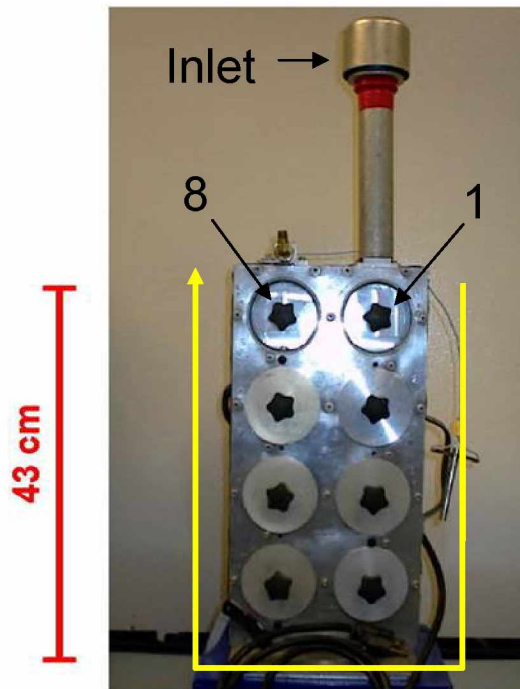


Figure 2.4. An 8-stage DRUM cascade impactor. Arrows indicate the flow direction. The inlet pictured is a standard $10\ \mu\text{m}\ \text{O}_A$ configuration. The inlet, Stage 1 (inlet to $5.0\ \mu\text{m}\ \text{O}_A$) and Stage 8 ($0.26\text{-}0.09\ \mu\text{m}\ \text{O}_A$) are indicated by arrows. The inlet shown here imparts a $10\ \mu\text{m}\ \text{O}_A$ initial size cut. The yellow arrow indicates the flow direction through the sampler. Image courtesy of T. Cahill and the Delta Group, University of California, Davis.



Figure 2.5. The 8-stage DRUM impactor installed at the University of Alaska Homer, AK Field Station. The sampler was inverted from its normal deployment configuration and was fitted with a special inlet (white pipe) for collecting $35.0 \mu\text{m}$ O_A and smaller aerosol.



Figure 2.6. An example drum with collected aerosol. This drum (not from this study) has been used to collect aerosol over an extended period. The dark lines are likely heavy industrial pollutants and carbon soot. The lines on the drum surface result from the internal slotted orifice directing aerosols to impact on the drum surface over a discrete time interval.

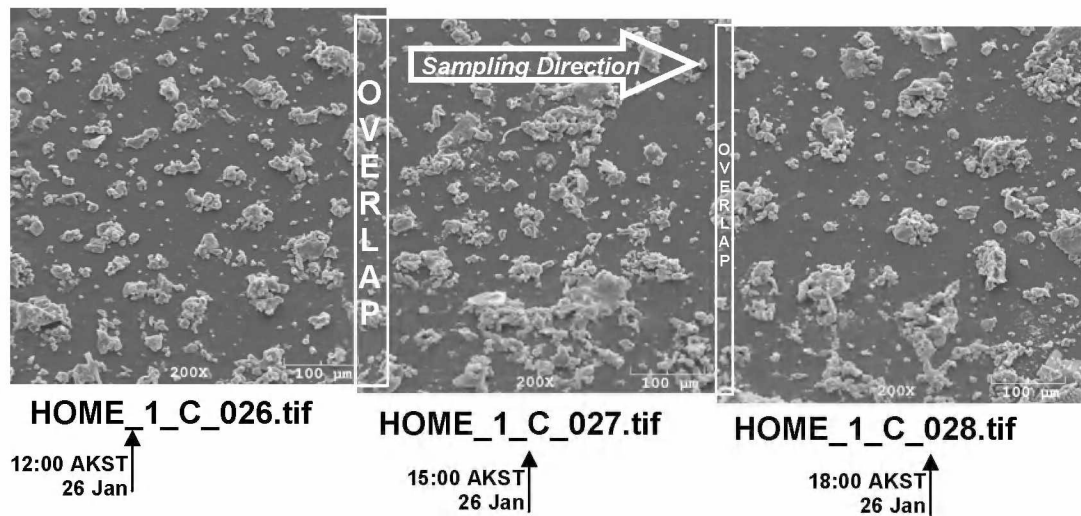


Figure 2.7. SEM DRUM sample image mosaic. The large particles are hybrid aggregates or ash comingled with non-sea salt sulfates and sea salts; smaller particles are individual ash grains and sea salt particles. Each individual image represents 3 hours of sampling time based on a drum rotation rate of 4 mm/day. The entire mosaic represents about 8.5 hours of sampling time taking image overlaps into account.

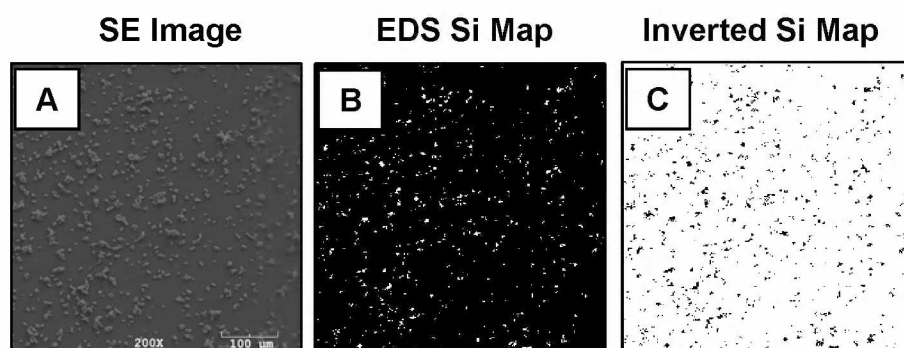


Figure 2.8. EDS element map image pre-processing steps. The corresponding secondary electron image (A) is analyzed by EDS for Si element composition (B). The resulting element map is inverted to more clearly show EDS X-ray detects.

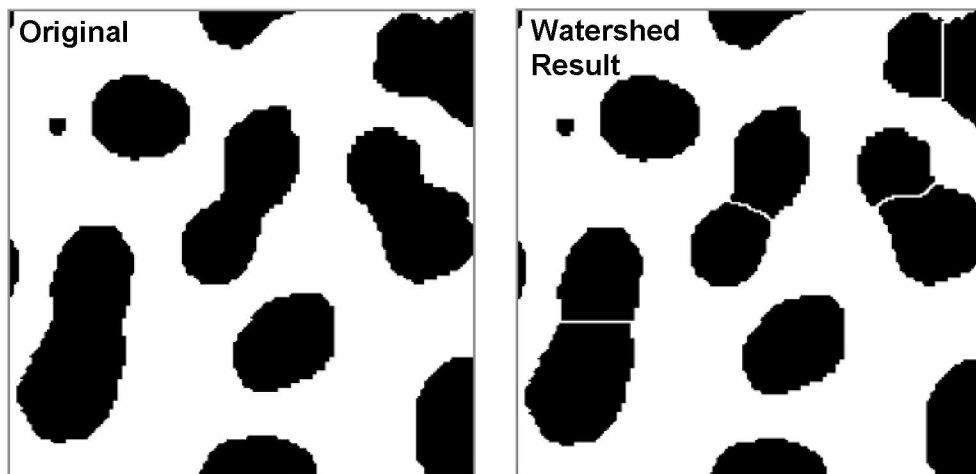


Figure 2.9. Particles digitally segmented by the ‘watershed’ method. Some particles were segmented while others retained their original dimensions. Figures are from Ferreria and Rasband (2011).

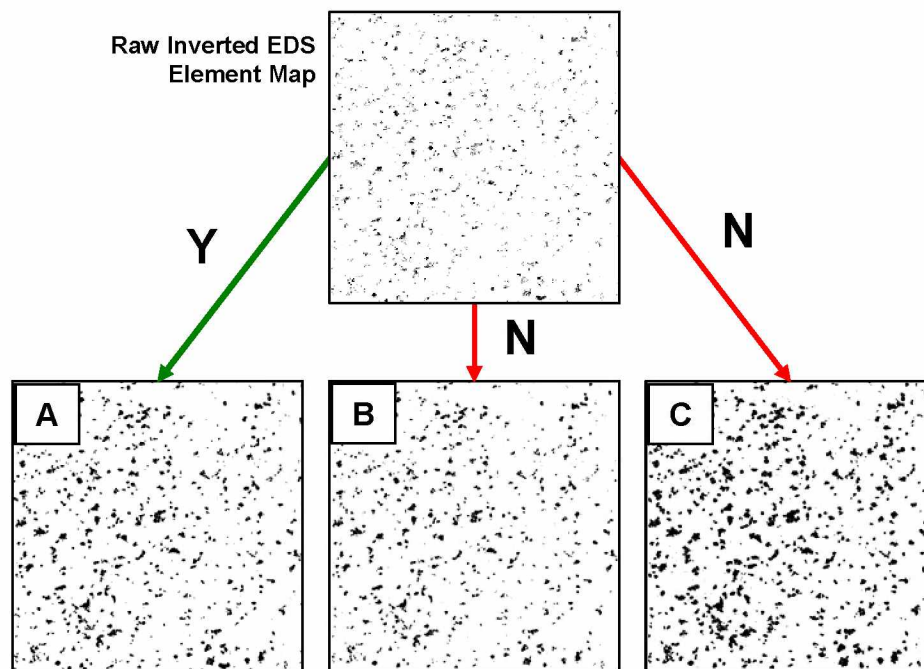


Figure 2.10. Post thresholding image selection. After the inverted element map is thresholded by the three methods indicated in the text and segmented, manual review of the threshold results is conducted. The original inverted element map is visually compared to the threshold results and the result most closely matching the inverted image (A) is retained. The other two images (B & C) are discarded.

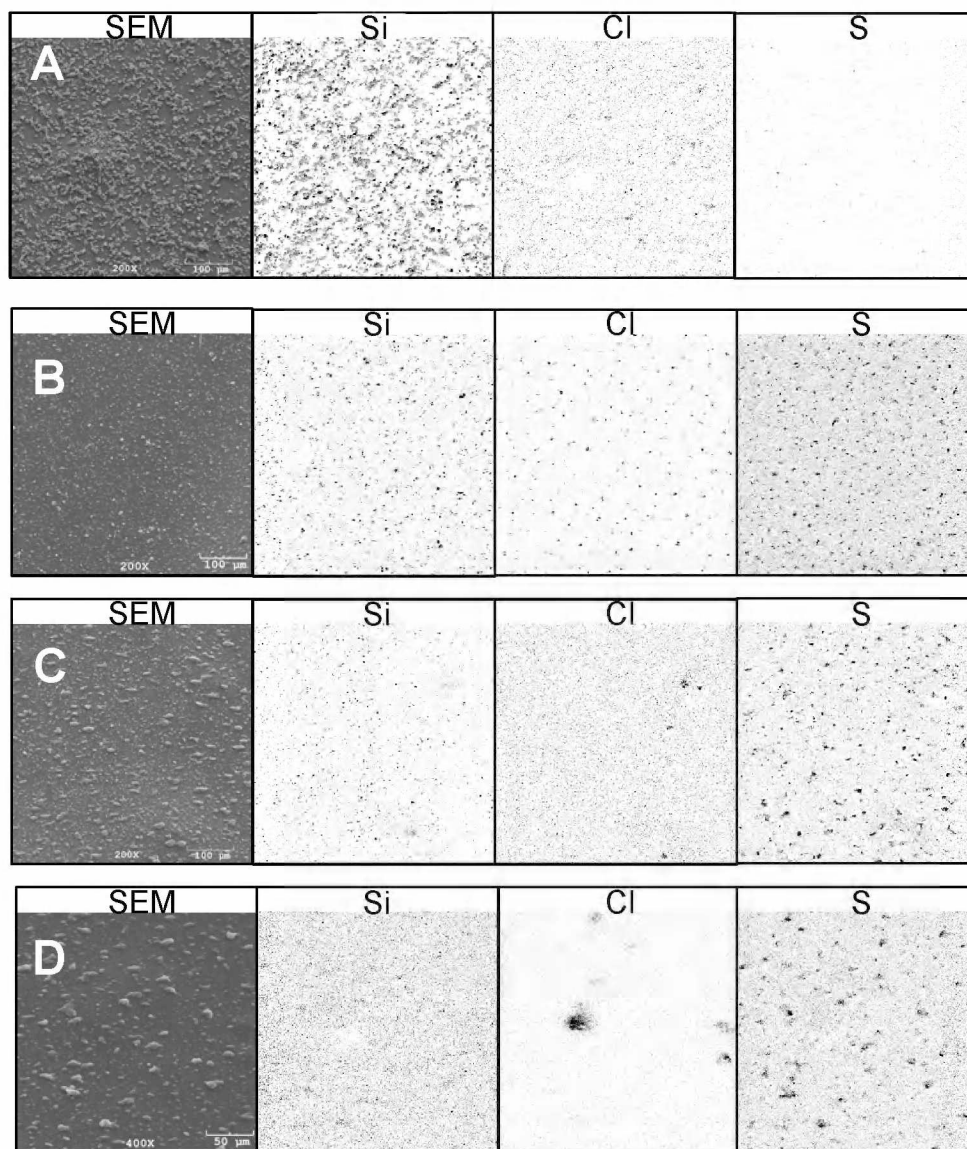


Figure 2.11. Single ash SEM images. These images (A and B) show the general features of individual glassy ash grains. These images were obtained from DRUM samples collected on 30 January 2006. The images from Stage 5 and 7 (C and D) are included to show the lack of ash present. The particles present in these stages are non-sea salt sulfate aerosol.

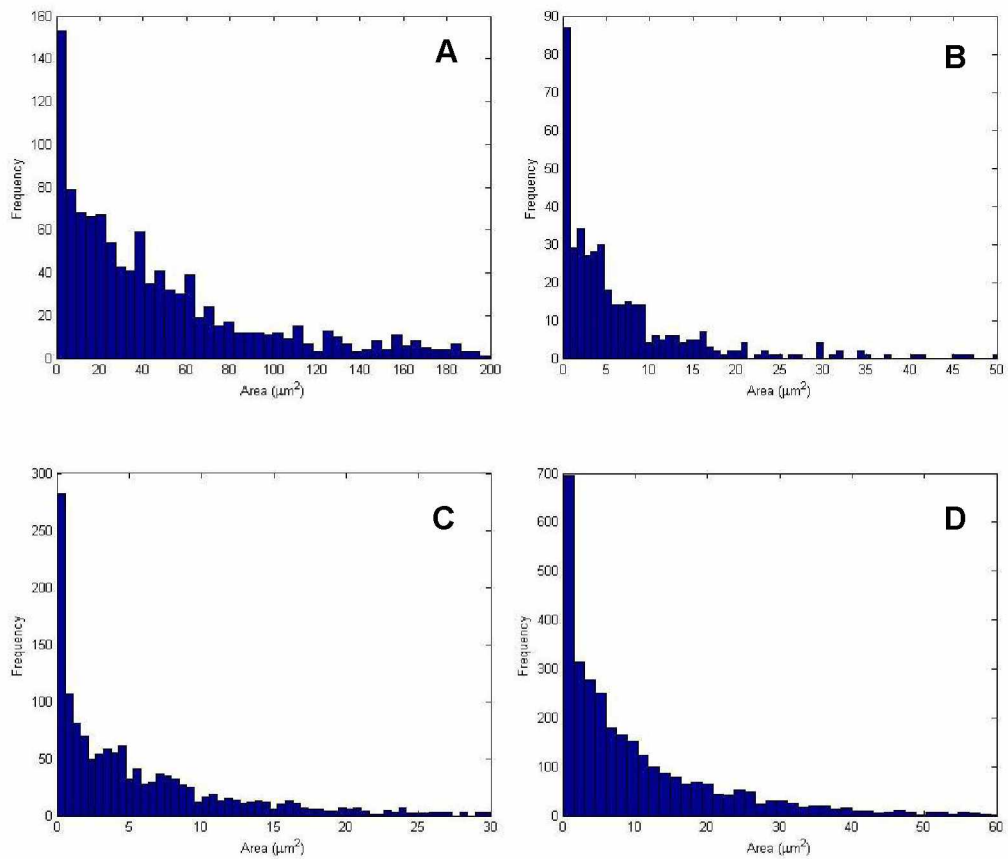


Figure 2.12. Particle size distribution for single grain ash. Single grain ash particle size distributions for ash collected on 14 (A and B) and 17 January 2006 (C and D) shown here are log-normal. The plume sampled on 14 January was sampled again on 17 January due to favorable weather conditions. Comparison of early plume and late plume distributions show enrichment in larger particles possibly due to either particle aggregation or the plume settling low enough to be sampled at a higher mass concentration near the ground level.

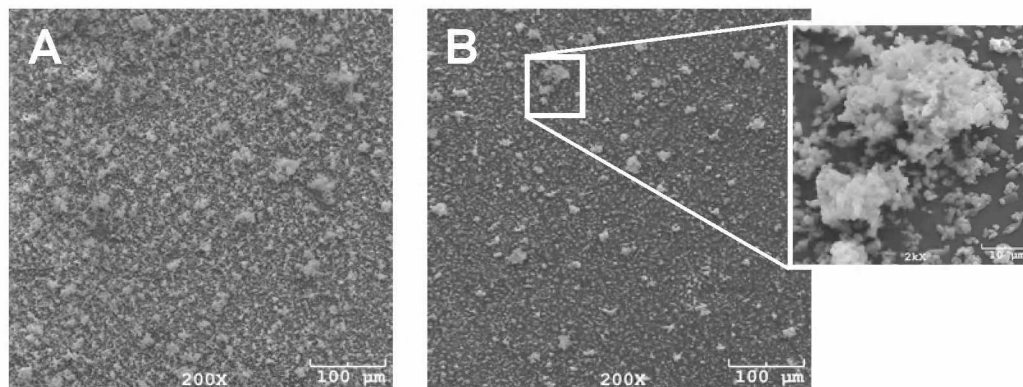


Figure 2.13. Ash aggregate images. Ash aggregates were only observed in the 2.5-1.15 μm O_A Stage 3 aerosols collected from plumes from pyroclastic flows. These images are of samples collected during 30 January 2006 and show ash aggregates present with individual ash grains.

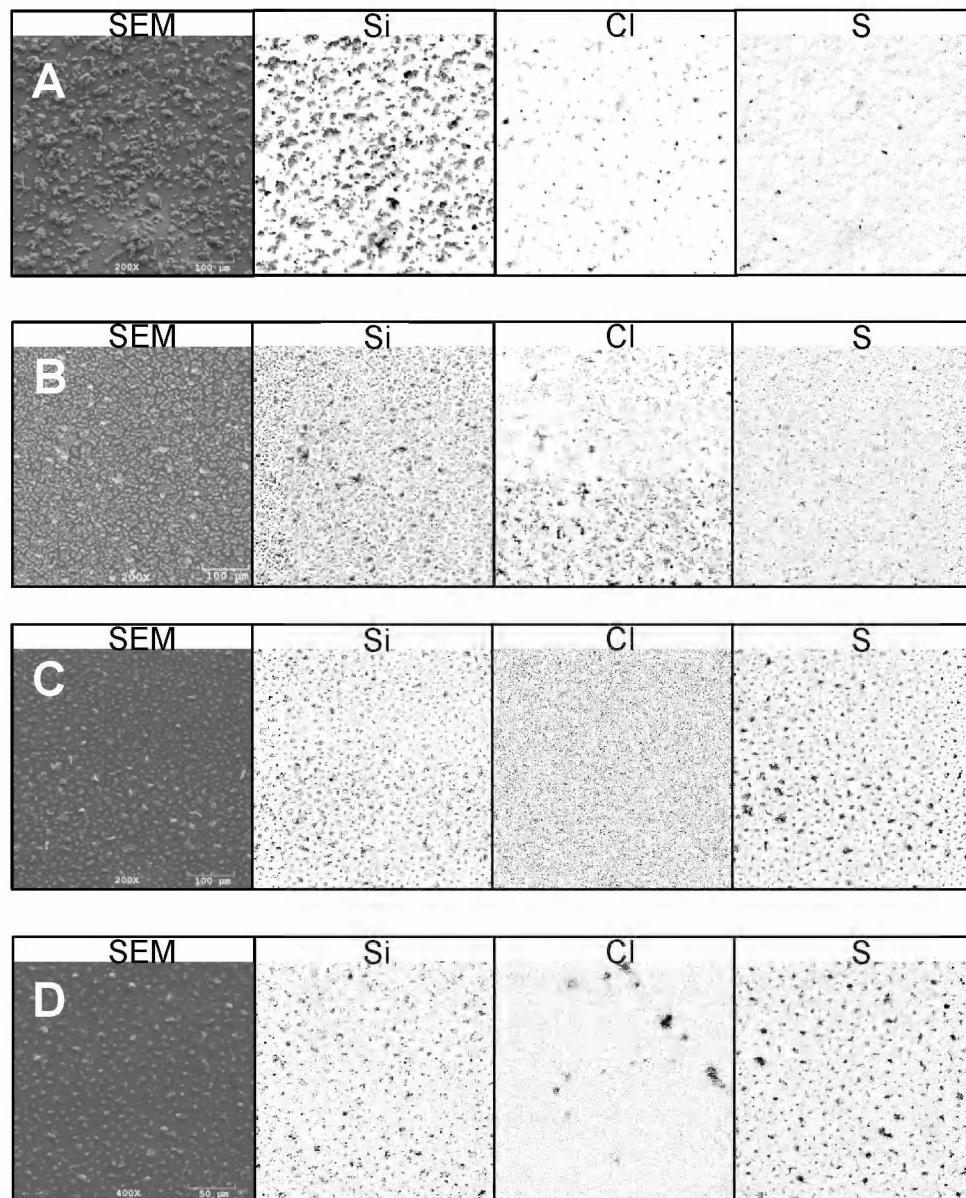


Figure 2.14. Hybrid ash aggregate images. Hybrid ash aggregates were found in all stages. Ash imaged in A was collected in Stage 1 on 14 January 2006, B was collected in Stage 3 on 31 January 2006, C was collected in Stage 5 on 3 February 2006, and D was collected by Stage 7 on 30 January 2006. In the larger sizes ($35.0\text{-}1.15\ \mu\text{m}\ \text{Ø}_A$) the dominant aerosol was sea salt that had mingled with ash. Smaller size fractions were mostly non-sea salt sulfate that had combined with volcanic ash.

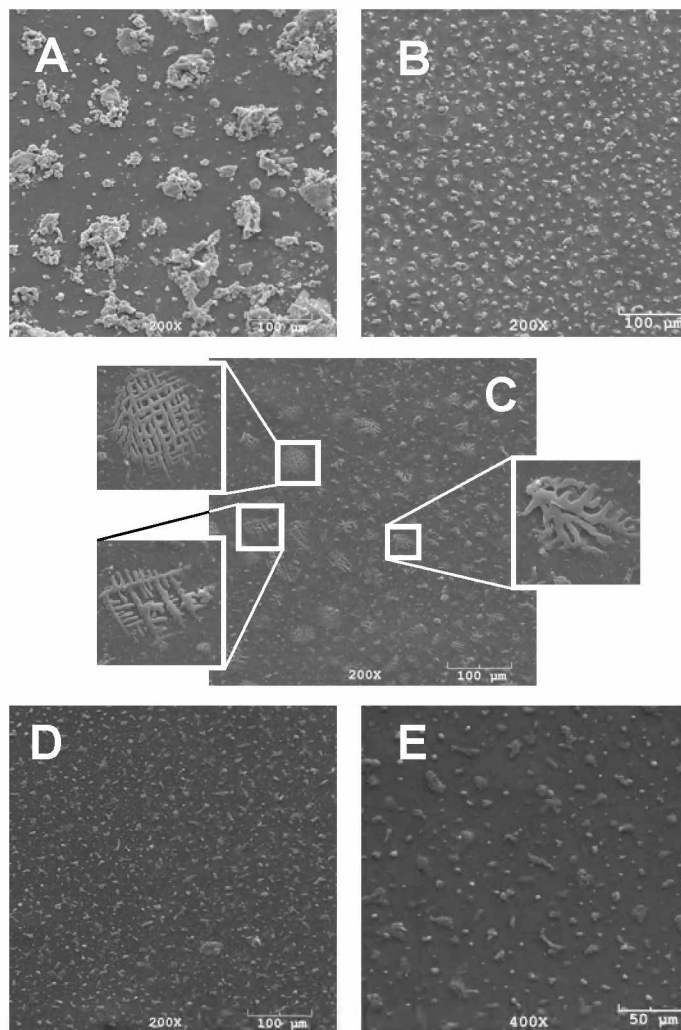


Figure 2.15. Non-ash aerosols collected by DRUM sampler. The aerosols, shown in A and B were collected on 26 January 2006 in Stage 1 and 5 respectively, are mostly sea salt with minor amounts of non-sea salt sulfate. Aerosols shown in C and D were collected in Stage 5 on 16 January and 23 January 2006 respectively. Aerosols shown in E were collected in Stage 7 on 26 January 2006. Images C, D, and E show non-sea salt sulfates. It is interpreted that the dendritic forms shown in C were the result of a wet sulfate droplet drying on the sample surface after being sampled.

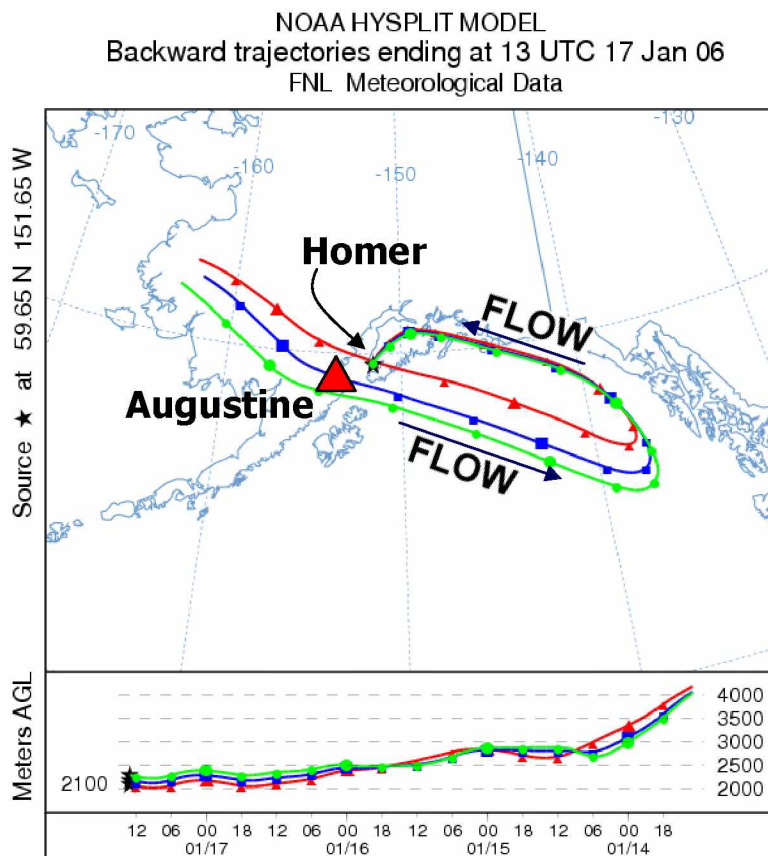


Figure 2.16. HYSPLIT back trajectory showing the path of the plume sampled first on 14 January and again on 17 January 2006. Note how the altitude of the plume descends over the transport path. This is due to modeled air parcel isentropic movement, not by HYSPLIT modeling ash settling rates.

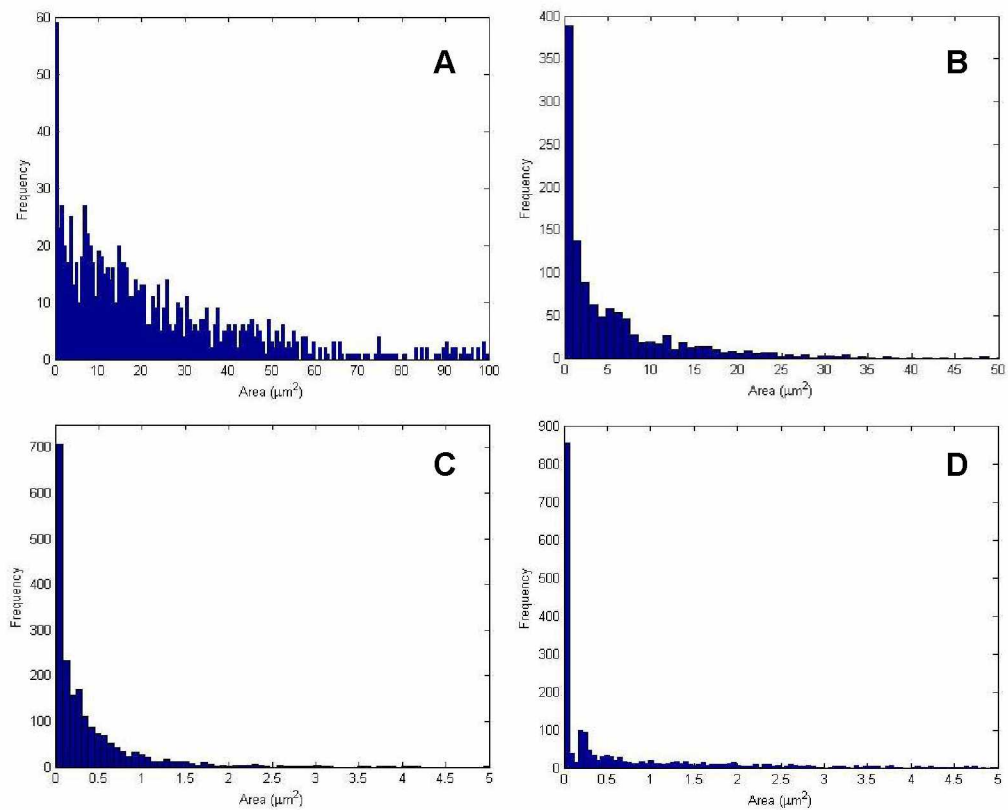


Figure 2.17. Pyroclastic flow elutriation plume particle size distributions. Ash was present in Stages 1-7. The particle size distributions shown here are from Stages 1, 3, 5 and 7. The total distribution in log-normal as are those from Stages 1-5. Stage 7 shows a bimodal distribution possibly due to the smallest particle sizes ($\leq 0.01 \mu\text{m}^2$) being the result of image noise. The second mode centered at $0.02 \mu\text{m}^2$ may represent the very fine end of the particle size distribution for the elutriation plume.

2.10. Tables

Table 2.1. Shape Descriptors

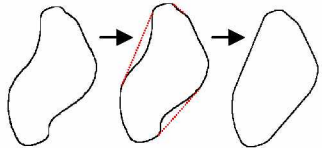


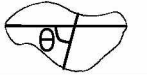
Shape and Size Parameters	Definition
Area	Sum of the pixels of a particle.
Perimeter	Length of the outside boundary of a particle.
Convex Area 	Convex area is the area encompassed by a perimeter that touches only convex parts of the particle boundary much the same way a tightly wrapped rubber band would define the area of a complex object.
Maximum Feret 	The longest distance between any two points described by parallel tangents along the particle perimeter. Also called caliper distance.
Minimum Feret 	The shortest distance along the particle perimeter described by two points with parallel tangents.
Feret Angle 	The angle (θ) between the Maximum Feret and the Minimum Feret..
Major Axis	The primary axis of a best fitting ellipse.
Minor Axis	The secondary axis of a best fitting ellipse.
Aspect Ratio	The ratio of the particle major axis and minor axis. Particles with an aspect ratio of 1 are circular; greater values indicate increasing elongation.
Roundedness	Inverse of the Aspect Ratio. Calculated by: $4 \times ([Area]) / (\pi \times [Major\ axis]^2)$
Solidity	$[Area] / [Convex\ Area]$
Circularity	The degree of elongation of the particle. Calculated by: $4\pi \times ([Area]) / ([Perimeter]^2)$. 1 indicates a perfect circle; as the value approaches zero, the particle becomes more elongate.

Table after Riley et al. (2003). Definitions from Ferreira and Rasband (2011).

Chapter 3 Daily Variations in PM_{2.5} Volcanic Ash Concentration Reaching Sand Point, AK From the 2007 Eruption of Pavlof Volcano¹

Abstract

Pavlof Volcano, located on the Alaska Peninsula southwest of Anchorage, Alaska, erupted from 14 August to 13 September, 2007 and sent ash plumes into the North Pacific Ocean which disrupted regional air traffic and produced ash fall in nearby communities. The early phase eruption activity occurred as low altitude ash plumes and lahars. The waning phase was dominated by low altitude and low concentration ash emissions. A DRUM cascade impactor was installed at the village of Sand Point, AK during the waning phase of the eruption to sample airborne fine ash (2.5 - 0.1 μm in aerodynamic diameter or O_A) erupted by the volcano. Aerosol samples were analyzed for mass by β -gauge and elemental composition by synchrotron x-ray fluorescence. Scanning electron microscopy (SEM) was used to image individual ash particles and background aerosols. Energy-dispersive x-ray spectroscopy was used during SEM analysis to qualitatively determine the chemistry of individual aerosol particles. Aerosol samples collected during the waning phase of the eruption from 27 August through 2 September 2007 show strong diurnal cycles in

¹ Rinkleff, PG., in prep. Daily Variations in PM_{2.5} Volcanic ash concentration reaching Sand Point, AK from the 2007 eruption of Pavlof Volcano. Prepared for submission to the Journal of Volcanology and Geothermal Research.

the concentration of ash reaching sampling locations; ash concentrations were highest in the morning and lowest in the early afternoon. Backward tracking trajectories determined by the HYSPLIT atmospheric transport model confirmed the transport of ash from Pavlof Volcano to Sand Point during this interval and showed that stable meteorological conditions allowed for the downward mixing of volcanic aerosols to the sampling site. Although no visible ash fallout was observed during aerosol sampling, these results demonstrate that volcanic ash was present in respirable ($\leq 2.5 \mu\text{m } \text{O}_A$ or $\text{PM}_{2.5}$) size fractions downwind of the volcano even during periods of low ash emissions.

3.1 Introduction

Every year some 20-30 volcanoes erupt worldwide (Siebert and Simkin, 2002-). While the large eruptions capture headlines and public attention, smaller eruptions are far more common and can have significant impacts on a local and regional scale (Neal et al., 1997; Kenedi et al., 2000). Current models used for forecasting volcanic ash dispersion and satellite ash detection and tracking methods are essential tools for emergency management personnel in affected communities downwind of erupting volcanoes. Volcanic ash satellite detection methods and atmospheric volcanic ash transport and dispersion (VATD) model validation require quantitative measurements of individual ash particles and the atmosphere into which they are erupted (Webley et al., 2010; Mastin et al., 2009; Webley and Mastin, 2009). This information may help refine satellite detection methods and VATD models by providing in-situ data for satellite threshold determinations and comparisons with model predictions to evaluate the effectiveness of the model. These refinements will help scientists evaluate satellite images and improve model predictions to give decision makers improved ash forecasts on which to base their hazard warnings to mitigate the effects of volcanic ash emissions on aircraft, property, and human health (Neal et al., 2010; Mastin et al., 2009). Improved volcanic ash and gas model input parameters would also improve the understanding of the influence volcanic ash has on the natural environment and climate (Langman et al., 2010). Unfortunately, few direct measurements of airborne volcanic ash size, composition, concentration, morphology, and particle-atmosphere interactions exist. Mather et al. (2003) and Rose et al. (2000) review the limited

number of tropospheric volcanic ash measurements reported in the literature. Most airborne ash studies referenced are of limited duration (hours to days) and contain limited compositional information. The Mt. St. Helens, Redoubt, and Masaya volcano studies presented in Leifer et al. (1981), Hobbs et al. (1991; 1982), and Mather et al. (2003) provide four of the best records of volcanic aerosols but none provide the needed information for model validation or detection method validation.

3.2 Satellite Ash Detection Methods

Infrared bands in the 10-12 μm spectral region have been successfully used to detect volcanic ash (Schneider et al., 1995; Wen and Rose, 1994). Prata (1989a; 1989b) developed a radiative transfer model to simulate spectral differences in temperature for a volcanic ash cloud viewed from space. This difference is due to the much stronger scattering nature of silicate minerals compared to water and ice particles in meteorological clouds (Yu et al., 2002). This is the basis for the Brightness Temperature Difference (BTD) algorithm of Prata (1989a), used to detect ash by satellite observations. This is the chief method used by volcano observatories to detect ash clouds (e.g., Dean et al., 2004; Schneider et al., 1995). Several satellite sensors, listed in Table 1, provide suitable data for ash detection by the BTD method. Volcanic clouds have negative BTD (e.g., AVHRR band 4 minus band 5) (Prata, 1989a; Schneider et al., 1995; Wen and Rose, 1994), while meteorological clouds generally have positive BTD (Yamanouchi et al., 1987). The BTD does not detect opaque clouds because it uses thermal transmittance and commonly produces false

positives and negatives (Prata et al., 2001; Rose et al., 2001; Simpson et al., 2000 as examples) due to a variety of atmospheric conditions such as air inversions and variable background landcover. A temperature inversion causes a false positive BTDR signal since the majority of radiation in the 11.9 μm wavelength (AVHRR and GOES Band 5, MODIS Band 32, and MTSAT IR Band 2) emanates from a higher altitude at a higher temperature due to differential absorption (Simpson et al., 2000). Variable land cover may also cause a loss of ash signal when a dispersing cloud moves over open water. When the upwelling radiation from land is cooler than that over open water, the ash signal can diminish due to differential absorption causing radiation in the $\sim 10.7 \mu\text{m}$ wavelength (AVHRR and GOES Band 4, MODIS Band 31, and MTSAT IR Band 1) to emanate at warmer temperatures than the 11.9 μm wavelength. Water and ice can also mask the presence of ash since water and ice have a positive ΔT which increases with increasing water content (Simpson et al., 2000; Prata, 1989b). Furthermore, detection limits of the BTDR technique and BTDR values for specific atmospheric ash mass concentrations have not been established due to the lack of in-situ measurements of ash in volcanic clouds (Rose et al., 2000).

3.3 Tephra Studies

Traditional tephra studies are conducted on fall deposits (Sparks et al., 1997; Fisher and Schminke, 1984). While these methods are invaluable for understanding what portion and volume of the plume was deposited, they do not sample the part of the plume that undergoes long range transport and does not deposit a detectable ash

layer due to very fine particle sizes and low concentrations. Furthermore, the evidence of processes affecting the size, composition, and shape of ash and other aerosol aggregates can be lost once aerosols sediment from the plume. Soluble salts can be altered or leached from sedimented ash (Delmelle et al., 2007). Weakly aggregated particles may break apart or collapse upon landing (James et al., 2003) or disintegrate due to aeolian processes, precipitation events, depositional loading, bioturbation, and pedogenesis (Ping, 2000; Shoji et al., 1993; Jenny, 1941). Indeed, only two types of aggregated ash particles are found in deposits: accretionary lapilli and cored lapilli (Schumacher and Schminke, 1991; Fisher and Schminke, 1984) which range from several mm to several cm in diameter. Tephra studies may miss small eruptions and plumes with low ash concentrations as well as the very distal edges of plumes where significant fallout has removed larger pyroclasts and aggregated particles. These dilute plumes, although not found in the geologic record, still transport fine ash particles which can affect machinery and human health (Horwell and Baxter, 2006; Baxter, 2000; Kenedi et al., 2000; Neal et al., 1997).

The 2006 eruption of Augustine Volcano was the first occasion where a DRUM cascade impactor was used to collect fine airborne volcanic ash (Cahill et al., 2010). This technique showed the effectiveness of DRUM impactors for collecting time, size, and compositionally-resolved aerosols downwind and at a safe distance from erupting volcanoes. The August, 2007 eruption of Pavlof Volcano, Alaska, offered an opportunity to use a DRUM sampler to collect a long-term, size and time-

resolved, volcanic aerosol composition and concentration time series for use in validating satellite detection methods and VATD models.

3.4 Eruptive Chronology and Geologic Setting

Pavlof Volcano ended an 11 year period of repose on 14 August 2007 with Strombolian activity (Volcanic Explosive Index 2-3) which lasted 31 days until 13 September 2007 (Waythomas et al., 2008; Siebert and Simkin, 2002-; Newhall and Self, 1982). The eruption was preceded by a minor increase in seismicity the previous day and was characterized by nearly continuous lava fountaining, explosions, and lahars. Incandescence on the edifice and light ash fall was reported by residents of the nearby village of Sand Point, Alaska some 100 km to the east (Figure 3.1). Explosions produced low-altitude (5-6 km ASL) diffuse ash plumes that were too low to have affected local or regional air travel but did bring ash to communities downwind of the volcano. While this eruption did not produce ash plumes that entered commercial airspace, commercial air traffic in the North Pacific was disrupted due to volcanic ash advisories, advisory NOTAMs (NOTice To AirMen) and SIGMETs (SIGnificant METeological hazard) issued by the Federal Aviation Administration and the National Weather Service that caused flights to be diverted around the area near the volcano (T. Neal and J. Adleman, written communication, 2007)

The volcano (CAVW # 1102-03) is located at 55.42 N 161.88 W (Siebert and Simkin, 2002-) and described by Waythomas et al. (2008) as a symmetrical snow and

ice-covered stratovolcano, 2519 m high, located near the Izembek National Wildlife Refuge, 60 km northeast of the village of Cold Bay, 50 km northeast of the village of King Cove, 90 km west of the village of Sand Point, and 75 km southwest of the village of Nelson Lagoon (Figure 3.1). It is considered one of the most active volcanoes in North America and has erupted some 70 times since 1762. Typical eruptions of Pavlof have produced moderate Strombolian eruptions (VEI 2 to 3) with lava fountaining, spatter-fed lava flows, lahars and minor ash production. Explosive activity has occurred during several historic eruptions including those in 1906, 1950, 1973, 1975, 1980, 1981, 1983, 1986, 1990, and 1996 and has produced ash plumes that reached altitudes of up to 15 km and ash fall deposits up to 1 cm thick in nearby communities. The volcano has been seismically monitored since 1973. Current seismic monitoring is currently supplemented by satellite monitoring techniques, local observations, and periodic field studies (Waythomas et al., 2008; Siebert and Simkin, 2002-).

3.5 Aerosol Collection

A 3-stage Davis Rotating-drum Unit for Measurement (DRUM) cascade impactor sampler (Figure 3.2 A) was placed at the Aleutians East Borough office in Sand Point, Alaska (55.34 N 160.48 W) on 27 August 2007 at 13:15 AKDT and operated until 14:00 AKDT on 3 October 2007 to collect aerosol in air masses in transit from the volcano and surrounding area (Figure 3.2 C).

The DRUM impactor is a stand-alone sampler designed to collect time-resolved, size-segregated aerosol. Cahill et al. (2010) showed that DRUM impactors are effective instruments for collecting volcanic aerosol during eruptions both at proximal and distal locations. The operating principles of DRUM cascade impactors are described in Raabe et al. (1988) and Cahill and Wakabayashi (1993). Aerosol is collected by particle impaction on an Apiezon-LTM coated MylarTM strip affixed to a rotating cylinder called a drum (Figure 3.2 A). The Apiezon-LTM coating aids in particle adhesion and reduces particle bounce (Lawson, 1980). The drum rotates past a slotted orifice at a controlled speed which allows for sample collection to be time-resolved. Impaction size ranges are dictated by particle mass and air flow velocity that are controlled by the slot orifice size and air flow rate (Reist, 1993). Larger particles are inertially removed at lower velocities while smaller particles remain suspended in the air stream. At the higher air stream velocities produced by narrower slotted inlets, smaller particles impact.

The sampler is typically fitted with a shrouded inlet and cyclone to impart an initial size cut. For the Pavlof eruption sampling, the sampler was fitted with an inlet which imparted an initial size cut of 10 μm (in aerodynamic diameter $\text{\textcircled{A}}$) and a cyclone which made another size cut of 2.5 μm $\text{\textcircled{A}}$ before aerosol entered the sampler. The sampling size cuts were set at 2.5-1.15, 1.15-0.34, and 0.34-0.1 μm $\text{\textcircled{A}}$. Smaller aerosols were not collected and were allowed to vent from the sampler. The sampling interval was 6 weeks which gave the drums a rotation rate 4 mm/day and a time resolution of 3 hours.

When the sampling interval was completed, the sampler was opened and the sampling media were removed in a clean laboratory. The Mylar™ strips were removed from the sampling drum, affixed to a labeled plastic frame with pressure sensitive tape, and start and end positions were noted. Mass was determined on prepared DRUM samples by β -gauge, a particle attenuation technique (Reist, 1993), and elemental composition (28 selected elements between Na and Pb) was determined by Synchrotron X-Ray Fluorescence (S-XRF) (Cahill, 2003; Cahill et al., 1999) at the Lawrence Berkeley National Laboratory Advanced Light Source Beam Line 10.3.1 (Cahill et al., 2000).

3.6 SEM and EDS Spectroscopy

Samples were analyzed at the Advanced Instrumentation Laboratory at the University of Alaska, Fairbanks (<http://www.uaf.edu/ail/>) with an ISI-SR-50 scanning electron microscope (SEM) equipped with a Kevex 7000 energy dispersive X-ray spectrometer (EDS). Each sample was cut into ~2 cm long pieces, affixed to a rigid polystyrene backing, and sputter coated with gold and palladium. The samples were attached to a standard aluminum SEM mount and placed in the SEM chamber. In the chamber, the sample was oriented 25° from horizontal at a working distance of 10 mm.

The accelerating voltage was set to 20 kV and the beam was set to the smallest spot size allowed by the instrument for high resolution imaging. During EDS spectra collection and element mapping, the beam spot size was increased to the

maximum size available on the instrument to increase x-ray counts to 20,000-30,000 counts per second. Higher counts were found to severely blister and distort the MylarTM, so care was taken to limit sample exposure to 200,000 counts per sample image frame area to avoid damage. EDS element maps were also prepared with the beam spot size and counts the same as for the EDS spectra. Point dwell times for EDS element map images were set to 6000 μ sec at a 256 kb image resolution. Longer point dwell times caused severe sample blistering and produced poor images.

Images and bulk field-of-view spectra were made parallel to the sampling direction from the start of the sampling interval with about 5-10% area overlap between each adjacent image to allow for the construction of image mosaics and to maintain location (and sampling time) within the sample (Figure 3.3 and Appendix E). An EDS spectrum of the entire field of view was collected for each frame (Appendix G). When a significant increase in silicon counts was noted, an element map (Appendix H) was prepared because the presence of silicon was considered to be an indicator of the presence of volcanic ash. Regardless of silicon count levels, an element map was prepared at regular intervals to show elemental distribution across the field of view during non-volcanic (background) aerosol sampling.

DRUM samples were found to provide excellent SEM images and EDS spectra of particles since all the particles reside on a smooth surface and the sampling substrate (MylarTM and Apezion LTM) does not contaminate the sample spectra.

3.7 HYSPLIT Air Mass Tracking Method

The HYSPLIT (Hybrid Single Particle Lagrangian Integrated Trajectory Model) (Rolph, 2011; Draxler and Rolph, 2011) atmospheric transport model was used to track air parcels and determine aerosol sources impacting the site during the sampled interval. HYSPLIT plots parcel trajectories either forward or backwards in time. Since the location of the volcano and time of the eruption was known, it was possible to cross-check each model run against the sample data to determine if aerosol at the sampler was from an eruption or another source.

3.8 Results

3.8.1 Identification and Description of Ash

Interpretation of elemental concentrations acquired by S-XRF for the Sand Point DRUM samples from 27 August through 3 October 2007 showed that the sampled aerosol mass was dominated by volcanic ash from Pavlof Volcano from the start of sampling until 2 September 2007. Aerosols collected during the first seven days of sampling are dominated by high concentrations of crustal elements Si, Al, Ca, Fe, Mg, K, and Ti, consistent with the general composition of calc-alkaline volcanic ash (Figure 3.4) (Heiken and Wohletz, 1985). These aerosols are interpreted to be volcanic ash based on HYSPLIT back trajectories that show air masses being transported from Pavlof Volcano to Sand Point from 27 August to 2 September (Figure 3.5). No long-range transport sources for crustal element aerosols such as the Gobi Desert (Cahill, 2003) were indicated by HYSPLIT trajectories during this time

period. The source for aerosols collected after 2 September was predominantly maritime. The silicon data (Figure 3.6) showed that a strong diurnal cycle brought ash to the sampling site from 27 August to 2 September. Ash aerosol mass concentrations are highest in the morning (~07:15 AKDT) and lowest in the early afternoon (~15:15 AKDT). This is consistent with air undergoing radiative cooling at night and sinking in the atmosphere, bringing the plume to ground level. As the day progressed, air parcels in the plume warmed and became more buoyant, so ash was mostly transported at altitudes higher than the sampling site. The remainder of the sampling period was dominated by sea salt and non-sea salt sulfate aerosols and showed no systematic variability.

SEM analysis and accompanying EDS spectroscopy, shown in Figure 3.7 A-F, support this interpretation. Angular, equant, Si-rich particles were observed in all 3 stages especially in the morning samples taken during this period. The relative abundance of Si-rich particles varied in a manner consistent with the timing shown in the β -gauge mass and S-XRF elemental data over the same sampling period. Si-rich particles were interpreted to be volcanic ash due to their chemical composition and particle shape (Heiken and Wohletz, 1985), as well as their collection time. Furthermore, HYSPLIT runs showed that air masses traveled from the volcano to the sampling site during the period from the start of sampling until 2 September 2007.

The major proportion of ash particles are glass shards. Phenocrysts are extremely rare and comprise less than 1% of the overall sample. Phenocrysts are generally too small to identify in secondary electron SEM images, but may be

identified by strong concentrations of specific elements in a small area of the element map. Although it is difficult to tell exactly what phases are present, some elements may indicate but not definitively identify the presence of common igneous rock-forming minerals. Fe and Ti together may indicate ilmenite or magnetite, Ca, Fe, and Mg together may indicate pyroxene or amphibole, Al together with Ca or Na may indicate feldspars, and P may indicate apatite (Deer et al., 1992).

3.8.2 Sulfur and Sea Salt in Maritime Aerosols

Na and Cl rich particles were present in the 2.5-1.15 $\mu\text{m } \text{O}_A$ stage along with a few S-rich particles. In the 1.15-0.34 and 0.34-0.1 $\mu\text{m } \text{O}_A$ stages abundant S-rich particles were present with few Cl and Na-rich particles. The Na and Cl-rich particles were commonly cubic but also appeared as amorphous particles. S-rich particles did not exhibit a characteristic shape. The Na and Cl rich particles were interpreted to be sea salt, and the S-rich particles were interpreted to be non-sea salt sulfate; both common families of maritime aerosols. Elemental concentrations after 2 September to the end of the sampling period (3 October 2007) were dominated by Cl, S, and Ca due to a shift in regional wind patterns from generally northwesterly (from the direction of Pavlof) to southeasterly winds from the Gulf of Alaska and Pacific Ocean. Tables 2 and 3 show that these elements are common constituents in sea salts and non-sea salt sulfates.

Sea salt is composed of mainly NaCl with minor amounts of K, Mg, Br, Ca, and sulfate with traces of other elements (Table 2). Sea salt aerosols are produced by

wave action and break-up of the upper-most layer of the ocean surface. According to Finlayson-Pitts and Pitts (1986), sulfur compounds are emitted into the atmosphere from sources such as sea spray, volcanic eruptions, and biogenic processes. Volcanic sulfur is emitted as SO_2 with smaller amounts of H_2S (Symonds et al., 1994). Sea spray contains sulfate, also called non-sea salt sulfate, from biogenic sources of reduced sulfur compounds which oxidize in the atmosphere (Table 3).

SO_2 oxidizes to sulfate in the atmosphere by two main reactions, either homogeneous reactions taking place in the gas phase or heterogeneous processes taking place in cloud, fog, or aerosol droplets (Seinfeld and Pandis, 2006; Finlayson-Pitts and Pitts, 1986). SO_2 is a highly water soluble gas and will strongly partition into the solution phase. The oxidation rate of SO_2 to sulfate is influenced by solar flux and has a diurnal, latitudinal, and seasonal dependence (Stockwell and Calvert, 1983).

Conversion of SO_2 to sulfate by heterogeneous aqueous conversion may have provided a means to convert whatever SO_2 may have been erupted, but it is unclear from the SEM images and element maps if sulfate is actually associated with ash. Since the eruption was in its waning phases, the erupting magma may have been degassed and too low in water, SO_2 , and other magmatic volatiles (Symonds et al., 1994; Francis, 1993) to have provided sufficient interparticle friction to produce significant electrostatic charges on ash particles to encourage particle attraction (James et al., 2003; Sparks et al., 1997). In any event, background sea salt and non-sea salt sulfate aerosols did not appear to form particle aggregates with the volcanic ash.

Volcanic and maritime aerosols were sampled in air masses at the sampling site from 27 August – 2 September 2007 as individual ash aerosols. It is possible that the sea salt and non-sea salt sulfate aerosols were initially liquid droplets, but since they are not mingled with volcanic ash it is proposed that the ash did not have enough atmospheric residence time or electrostatic charge, or was too diffuse to form hybrid aerosol before sampling. Another possibility is that wet aerosol droplets containing sulfate and/or sea salts could have dried before encountering airborne volcanic ash. Sparks et al. (1997) concluded that volcanic ash needs sufficient electrostatic charge, humidity, or meteoric water for aggregates formation.

Some EDS element maps showed a possible weak signal for sulfur associated with some of the volcanic ash particles. It is possible the ash was coated with sulfate formed from the conversion of SO_2 to sulfate (Seinfeld and Pandis, 2006; Finlayson-Pitts and Pitts, 1986) from the eruption or other sources. Another possibility may be that the sulfur detections were the result of misinterpretation of x-ray production near other x-ray peaks, specifically the Au $\text{M}\alpha_1$ peak (2,122.9 eV) near the S $\text{K}\alpha_1$ (2,307.84 eV), $\text{K}\alpha_2$ (2,306.64 eV), and $\text{K}\beta_1$ (2,464.04 eV) lines (Thompson et al., 2009). The full width-half maximum spread of the Au $\text{M}\alpha_1$ energy may contribute counts to the S $\text{K}\alpha_1$, $\text{K}\alpha_2$, and $\text{K}\beta_1$ lines where S is not present in the sample (Reed, 1995). Interference from Au $\text{M}\alpha_1$ x-rays was assumed to be the cause of the weak sulfur signal. This assumption was based on the relatively strong sulfur signal associated with sulfate aerosol relative to background sulfur detections present when spectra were taken on blank gold and palladium coated MylarTM.

3.8.3 Meteorological Influences

Weather data shown in Figure 3.8, obtained from unofficial National Weather Service data from the Sand Point (PASD) station accessed from Weather Underground (weatherunderground.com), showed that the weather conditions during the eruption sampling were unusually calm. These unusually calm conditions may have influenced the ash mass concentrations and the particle types sampled from air masses at Sand Point. Generally, weather conditions in this region are dominated by frequent storms with high winds and heavy precipitation (National Climate Data Center, www.ncdc.noaa.gov, accessed on 15/02/2011). From the start of the sampling period on 27 August, wind speeds rarely exceed 20 km/h until 2 September and were usually below 16 km/h over this period. Wind direction was generally northerly. Winds increased to 32-48 km/h with gusts after 2 September 2007. Wind direction after 2 September was variable, but typically from the south to southeast. Precipitation (not shown in Figure 3.8) was low during the entire sampling interval, either > 0.06 inches, trace, or none with the exception of 1 October when 1.31 inches was recorded over a 24 hour period. Temperatures recorded from 27 August to 2 September show a diurnal variation of 6 to 10° C. Temperatures were highest in the mid-afternoon (~15:00 AKDT) and lowest in the mid morning (~7:00 AM AKDT). After 2 September, temperatures hovered near the average high temperature for the region and exhibited no significant daily variation.

Plumes detected by the BTD algorithm (28 – 31 August) exhibited a generally weak ash signal and were observed to be propagating to the south-southeast from the

volcano (Figure 3.9). Photographs of the eruption taken during this period show that the plume was low, diffuse, and bent over and likely contained a low ash concentration (Figure 3.10). These observations agree with expectations based on the eruptive rate, weather observations described above, and HYSPLIT model runs. The low wind speeds over 27 August to 2 September may have minimized dilution of the plume with the surrounding atmosphere. The low relative humidity over the same interval may have allowed for wet droplets to dry before encountering ash or for droplets containing ash to dry while suspended. The daily temperature variations observed from 27 August to 2 September coincide with diurnal variations in ash mass concentration variations in air masses sampled at Sand Point.

3.9 Conclusions

Ash was observed in DRUM samples collected during the first week of sampling (27 August - 2 September 2007), even though no substantial ash fall was recorded at Sand Point. Local residents reported having itchy eyes, raspy throats, and minor breathing difficulties during the eruption. These conditions are common symptoms of exposure to respirable airborne volcanic ash (Baxter, 2000) and show that ash mass concentrations were high enough to cause minor health effects in populations downwind of Pavlof Volcano.

Ash concentrations at Sand Point during the waning phase of the eruption were driven largely by the relative buoyancy of advected air masses influenced by diurnal heating and cooling. Ash concentrations were high in the morning and low in

the afternoon. Particles larger than $PM_{2.5}$, if present in appreciable concentrations, would have settled out of the plume and made some visible accumulation, but none was noted at Sand Point, indicating the volcano was producing mostly fine ash aerosol. This is consistent with the lack of split-window satellite ash detections which would indicate the presence of larger ash particles during the sampling interval. Also, SO_2 levels were likely low because the eruption had expended its volatiles (Symonds et al., 1994; Francis, 1993), so limited SO_2 to sulfate conversion was expected due to limited SO_2 presence. The relatively short transport distance and time would not have allowed for substantial conversion of volcanic SO_2 to sulfate.

3.10 Acknowledgements

I wish to thank the members of the Alaska Volcano Observatory and the staff of the University of Alaska Fairbanks Advanced Instrumentation Laboratory for logistical and technical support with this project. I also thank the Aleutians East Borough, especially Ms. Tina Anderson, the Borough Clerk, for generously hosting the placement of a DRUM sampler at the Borough office in Sand Point, Alaska. This work was supported by Army Research Laboratory contract W911NF-07-1-0346.

3.11 References

Baxter, P., 2000. Impacts of Eruptions on Human Health. In: Sigurdsson, H., Houghton, B., McNutt, R.R., Stix, J. (Eds.), *Encyclopedia of Volcanoes*. Academic Press, New York, NY, pp. 1035-1043.

Cahill, C.F., 2003. Asian aerosol transport to Alaska during ACE-Asia. *Journal of Geophysical Research*. 108, 8664-8872.

Cahill, C.F., Rinkleff, P., Dehn, J., Webley, P., Cahill, T., Barnes, D., 2010. Aerosol measurement from a recent Alaskan volcanic eruption: Implications for volcanic ash transport predictions. *Journal of Volcanology and Geothermal Research*. 198, 76-80.

Cahill, T.A., Wakabayashi, P., 1993. Compositional analysis of size-segregated aerosol samples. In: Newman, L. (Ed.), *Measurement Challenges in Atmospheric Chemistry*, American Chemical Society, pp. 211-228.

Cahill, T.A., Cliff, S.S., Perry, K.D., Jimenez-Cruz, M., Kelly, P.B., Shackelford, J., McHugo, S.A., Thompson, A., 2000. S-XRF and atmospheric aerosols: Health, visibility, and climate change. *Advanced Light Source Compendium of User Abstracts*, Lawrence Berkeley National Laboratory. <http://www.als.lbl.gov/als/compendium> (last accessed on 10 March 2012).

Cahill, T., Cliff, S., Perry, K., Jimenez-Cruz, M., McHugo, S., 1999. Size and time resolved anthropogenic components of aerosols via synchrotron x-ray fluorescence: Application to Asian aerosol transport. *Abstracts, American Geophysical Union 1999 Fall Meeting, December*. San Francisco, California, pp. 13-17.

Dean, K., Dehn, J., Papp, K., Smith, S., Izbekov, P., Peterson, R., Kearney, C., Steffke, A., 2004. Integrated observations of the 2001 eruption of Mt. Cleveland, Alaska. *Journal of Volcanology and Geothermal Research*. 135, 51-73.

Deer, W.A., Howie, R.A., Zussman, J., 1992. *The Rock-Forming Minerals*, 2nd Edition. Addison Wesley Longman Limited, Essex, England.

Delmelle, P., Lambert, M., Dufrêne, Y., Gerin, P., Óskarsson, N., 2007. Gas/aerosol-ash interaction in volcanic plumes: New insights from surface analyses of fine ash particles. *Earth and Planetary Science Letters*. 259, 159-170.

Draxler, R.R., Rolph, G.D., 2011. HYSPLIT (HYbrid Single-Particle Lagrangian Integrated Trajectory) NOAA ARL READY NOAA Air Resources Laboratory, Silver Spring, MD. <http://www.arl.noaa.gov/ready/hysplit4.html> (last accessed on 10 March 2012).

- Finlayson-Pitts, B.J., Pitts, J.N., 1986. *Atmospheric Chemistry*. Wiley, New York, NY.
- Fisher, R.V., Schminke, H.-U., 1984. *Pyroclastic Rocks*. Springer-Verlag, New York, NY.
- Francis, P., 1993. *Volcanoes: A Planetary Perspective*. Oxford University Press, New York, NY.
- Heiken, G., Wohletz, K., 1985. *Volcanic Ash*. University of California Press, Berkeley, CA.
- Hobbs, P.V., Radke, L.F., Lyons, J.H., Ferek, R.J., Coffman, D.J., 1991. Airborne measurements of particles and gas emissions from the 1990 volcanic eruptions of Mount Redoubt. *Journal of Geophysical Research*. 96, 18,735-18,752.
- Hobbs, P.V., Tuell, J.P., Hegg, D.A., Radke, L.F., Eltgroth, M.K., 1982. Particles and gases in the emissions from the 1980-1981 volcanic eruptions of Mt. St. Helens. *Journal of Geophysical Research*. 87, 11,062-11,086.
- Horwell, C.J., Baxter, P.J., 2006. The respiratory health hazards of volcanic ash: A review for volcanic risk mitigation. *Bulletin of Volcanology*. 69, 1-24.
- James, M.R., Lane, S.J., Gilbert, J., 2003. Density, construction, and drag coefficient of electrostatic volcanic ash aggregates. *Journal of Geophysical Research*. 108, 1-12.
- Jenny, H., 1941. *Factors of Soil Formation, A System of Quantitative Pedology*. Dover, New York, NY.
- Kenedi, C., Brantley, S., Hendley, J., Stauffer, P., 2000. Volcanic ash fall - a "hard rain" of abrasive particles. U.S. Geological Survey Fact Sheet FS 027-00, 2 p.
- Langman, B., Zasek, K., Hort., M., 2010. Atmospheric distribution and removal of volcanic ash after the eruption of Kasatochi volcano: A regional model study. *Journal of Geophysical Research*. 115, 1-10.
- Lawson, D., 1980. Impaction surface coatings intercomparison and measurements with cascade impactors. *Atmospheric Environment*. 14, 195-199.
- Lewis, E.R., Schwartz, S.E., 2004. *Sea Salt Production: Mechanisms, Methods, Measurements and Models*. Geophysical Monograph 152. American Geophysical Union. Washington, D.C.

Leifer, R., Hinchliffe, L., Fisenne, I., Franklin, H., Knutson, E., Olden, M., Sedlacek, W., Mroz, E., Cahill, T., 1981. Measurements of the stratospheric plume from the Mount St. Helens eruption: Radioactivity and chemical composition. *Science*. 214, 904–907.

Mastin, L.G., Guffanti, M., Servranckx, R., Webley, P.W., Barsotti, S., Dean, K., Durant, A., Ewert, J.W., Neri, A., Rose, W.I., Schneider, D.J., Siebert, L., Stunder, B., Swanson, G., Tupper, A., Volentik, A., Waythomas, C.F., 2009. A multidisciplinary effort to assign realistic source parameters to model of volcanic ash-cloud transport and dispersion during eruptions. In: Mastin, L.G., Webley, P.W. (Eds.), *Journal of Volcanology and Geothermal Research: Special Issue on Volcanic Ash Clouds*. 186, pp. 10–21.

Mather, T.A., Pyle, D.M., Oppenheimer, C., 2003. Tropospheric Volcanic Aerosol. In: Robock, A., Oppenheimer, C. (Eds.), *Volcanism and the Earth's Atmosphere*. American Geophysical Union, Washington D.C., pp. 189-212.

Neal, C.A., Murray, T.L., Power, J.A., Adleman, J.N., Whitmore, P.M., Osiensky, J.M., 2010. Hazard information management, interagency coordination, and impacts of the 2005–2006 eruption of Augustine Volcano. In: Power, J.A., Coombs, M.L., Freymueller, J.T. (Eds.), *The 2006 eruption of Augustine Volcano, Alaska*. U.S. Geological Survey Professional Paper 1769, pp. 645–667.

Neal, C., Casadevall, T., Miller, T., Hendley, J., Stauffer, P., 1997. Volcanic ash - Danger to aircraft in the North Pacific. U.S. Geological Survey Fact Sheet FS 30-0097, 2 p.

Newhall, C.G., Self, S., 1982. The Volcanic Explosivity Index (VEI): An estimate of explosive magnitude for historical volcanism. *Journal of Geophysical Research*. 87, 1231-1238.

Ping, C., 2000. Volcanic soils. In: Sigurdsson, H., Houghton, B., McNutt, S., Stix, J. (Eds.), *Encyclopedia of Volcanoes*. Academic Press, New York, NY. pp.1035-1071.

Prata, A.J., 1989a. Observations of volcanic ash clouds in the 10-12 μm window using AVHRR/2 data. *International Journal of Remote Sensing*. 10, 751-761.

Prata, A.J., 1989b. Infrared radiative transfer calculations for volcanic ash clouds. *Geophysical Research Letters*. 16, 1293-1296.

Prata, A.J., Bluth, G., Rose, W., Schneider, D., Tupper, A., 2001 Comments on "Failures in detecting volcanic ash from a satellite-based technique". *Remote Sensing of Environment*. 78, 341-346.

- Raabe, O.G., Braaten, D.A., Axelbaum, R.L., Teague, S.V., Cahill, T.A., 1988. Calibration studies of the DRUM impactor, *Journal of Aerosol Science*. 19, 183-195.
- Reed, S., 2005. *Electron Microprobe Analysis and Scanning Electron Microscopy in Geology*. Cambridge University Press, New York, NY.
- Reist, P.C., 1993. *Aerosol Science and Technology*, Second Edition. McGraw-Hill, New York, NY.
- Rolph, G.D., 2011. Real-time Environmental Applications and Display sYstem (READY) NOAA Air Resources Laboratory, Silver Spring, MD. <http://ready.arl.noaa.gov> (last accessed on 10 March 2012).
- Rose, W., Bluth, G., Schneider, D., Ernst, G., Riley, C., Henderson, L., McGimsey, R., 2001. Observations of volcanic clouds in their first few days of atmospheric residence: The 1992 eruptions of Crater Peak, Mount Spurr Volcano, Alaska. *Journal of Geology*. 109, 677-694.
- Rose, W.I., Bluth, G.J.S., Ernst, G.G.J., 2000. Integrating retrievals of volcanic cloud characteristics from satellite remote sensors: A summary. *Philosophical Transactions of the Royal Society of London*. 358, 1585-1606.
- Schneider, D., Rose, W., Kelley, L., 1995. Tracking of 1992 eruption clouds from Crater Peak vent of Mount Spurr Volcano, Alaska, using AVHRR. In: Keith, T.E.C. (Ed.), *The 1992 eruptions of Crater Peak vent, Mount Spurr Volcano, Alaska*, U.S. Geological Survey Bulletin B 2139, pp. 27-36.
- Schumacher, R., Schminke, H.-U., 1991. Internal structure and occurrence of accretionary lapilli-a case study at Laacher See volcano. *Bulletin of Volcanology*. 53, 612-634.
- Seinfeld, J.H., Pandis, S.N., 2006. *Atmospheric Chemistry and Physics*. Wiley, Hoboken, NJ.
- Shoji, S., Nanzyo, M., Dahlgren, R., 1993. *Volcanic Ash Soils: Genesis, Properties and Utilization*. Elsevier, New York, NY.
- Siebert, L., Simkin, T., 2002-. *Volcanoes of the World: An Illustrated Catalog of Holocene Volcanoes and their Eruptions*. Smithsonian Institution, Global Volcanism Program, Digital Information Series, GVP-3. <http://www.volcano.si.edu/world/> (last accessed on 10 March 2012).

- Simpson, J., Hufford, G., Pieri, D., Berg, D., 2000. Failures to detect volcanic ash from a satellite-based technique. *Remote Sensing of the Environment*. 72, 191-217.
- Sparks, R.S.J., Bursik, M.I., Carey, S.N., Gilbert, J.S., Glaze, L.S., Sigurdsson, H., Woods, A.W., 1997. *Volcanic Plumes*. John Wiley, Hoboken, N.J.
- Stockwell, W.R., Calvert, J.G., 1983. The mechanism of the HO-SO₂ reaction. *Atmospheric Environment*. 17, 2231-2235.
- Symonds, R., Rose, W., Bluth, G., Gerlach, T., 1994. Volcanic gas studies: Methods, results, and applications. In: Carroll, M.R., and Holloway, J.R. (Eds.), *Volatiles in Magmas*. Mineralogical Society of America Reviews in Mineralogy, Volume 30, pp. 1-66.
- Thompson, A.C., Kirz, J., Attwood, D.T., Gullickson, E.M., Howells, M.R., Kortwright, J.B., Liu, Y., Robinson, A.L., Underwood, J.H., Lindau, I., Pianetta, P., Winick, H., Williams, G.P., Scofield, J.H., 2009. *X-Ray Data Booklet*. Third Edition Thompson, A.C. (Ed.), Lawrence Berkeley National Laboratory. University of California, Berkeley, California. LBNL/PUB-490 Rev. 3. <http://xdb.lbl.gov> (last accessed on 10 March 2012).
- Waythomas, C., Prejean, S., McNutt, S., 2008. Alaska's Pavlof volcano ends 11-year repose. *Eos*. 89, 209-211.
- Webley, P., Mastin, L., 2009. Improved prediction and tracking of volcanic ash clouds. *Journal of Volcanology and Geothermal Research*. 186, 1-9.
- Webley, P.W., Dean, K.G., Dehn, J., Bailey, J.E., Peterson, R., 2010. Volcanic-ash dispersion modeling of the 2006 eruption of Augustine volcano using the Puff Model. In: Power, J.A., Coombs, M.L., and Freymueller, J.T. (Eds.), *The 2006 eruption of Augustine Volcano, Alaska*. U.S. Geological Survey Professional Paper 1769, pp. 482-501.
- Wen, S., Rose, W., 1994. Retrieval of sizes and total masses of particles in volcanic clouds using AVHRR band 4 and 5. *Journal of Geophysical Research*. 99, 5421-5431.
- Yamanouchi, T., Suzuki, K., Kawaguchi, S., 1987. Detection of clouds in Antarctica from infrared multispectral data of AVHRR. *Journal of the Meteorological Society of Japan*. 65, 949-962.
- Yu, T., Rose, W., Prata, A., 2002. Atmospheric correction for satellite-based volcanic ash mapping and retrievals using "split window" IR data from GOES and AVHRR. *Journal of Geophysical Research*. 107, 4311-4335.

3.12 Figures

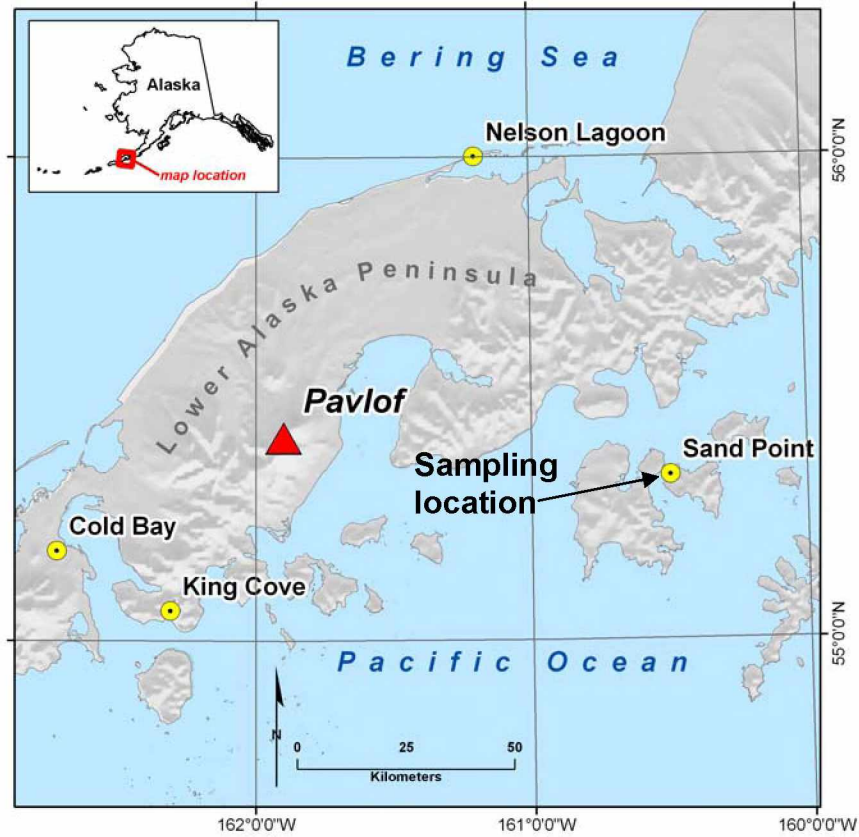


Figure 3.1. Location map of Pavlof Volcano and the sampling location in Sand Point, Alaska. Pavlof is located on the Lower Alaska Peninsula between the Pacific Ocean and the Bering Sea 90 km west of Sand Point.

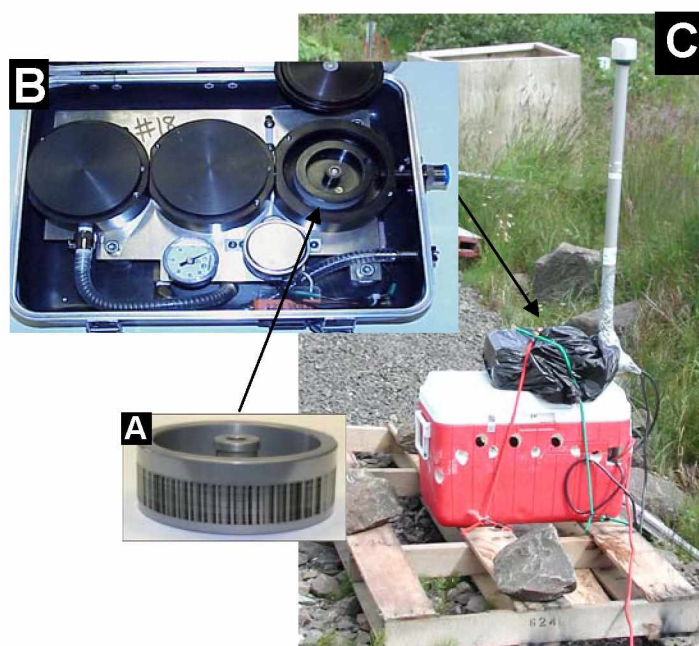


Figure 3.2. Three stage DRUM sampler, sample drum, and installation at Sand Point, Alaska. The dark lines on the sample drum (A) pictured here (not from this study) are likely heavy industrial pollutants and carbon soot. Three sample drums fit in the chambers in the DRUM sampler (B). For installation at Sand Point (C), the sampler was wrapped in a plastic bag and attached to the red cooler which contained the vacuum pump. The plastic bag gave a measure of weather resistance to the sampler. Holes in the cooler allowed air circulation necessary for keeping the pump cool. The entire sampler assembly was attached with bungee cords to a wooden pallet weighted with rocks to give the sampler set-up some stability. The sampler was connected to local AC power and operated unattended for 6 weeks. The entire sampler assembly was transported in the red cooler.

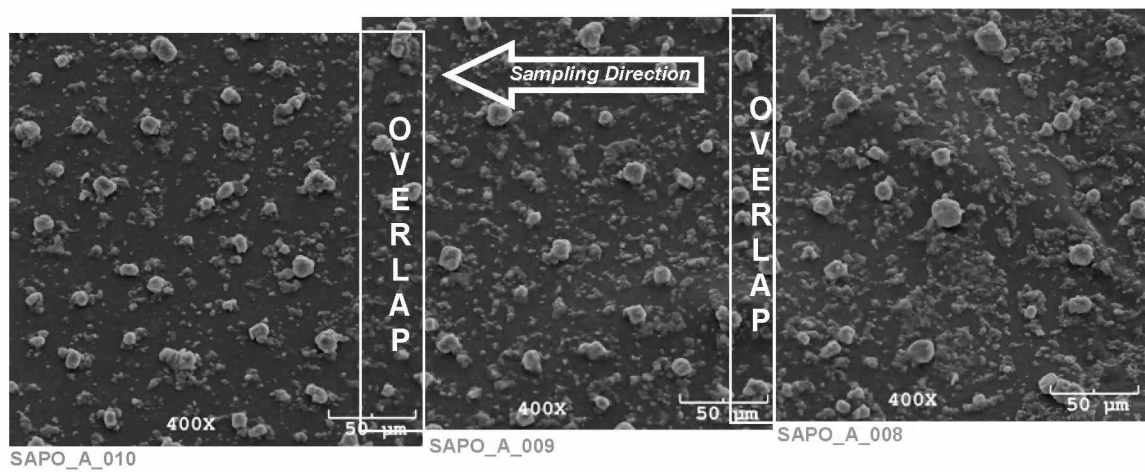


Figure 3.3. SEM DRUM sample image mosaic. The large particles are sea salts; smaller particles are volcanic ash. Each individual image represents 1.4 hours of sampling time based on a rotation rate of 4 mm/day. The entire mosaic represents 4 hours of sampling time taking the image overlaps into account.

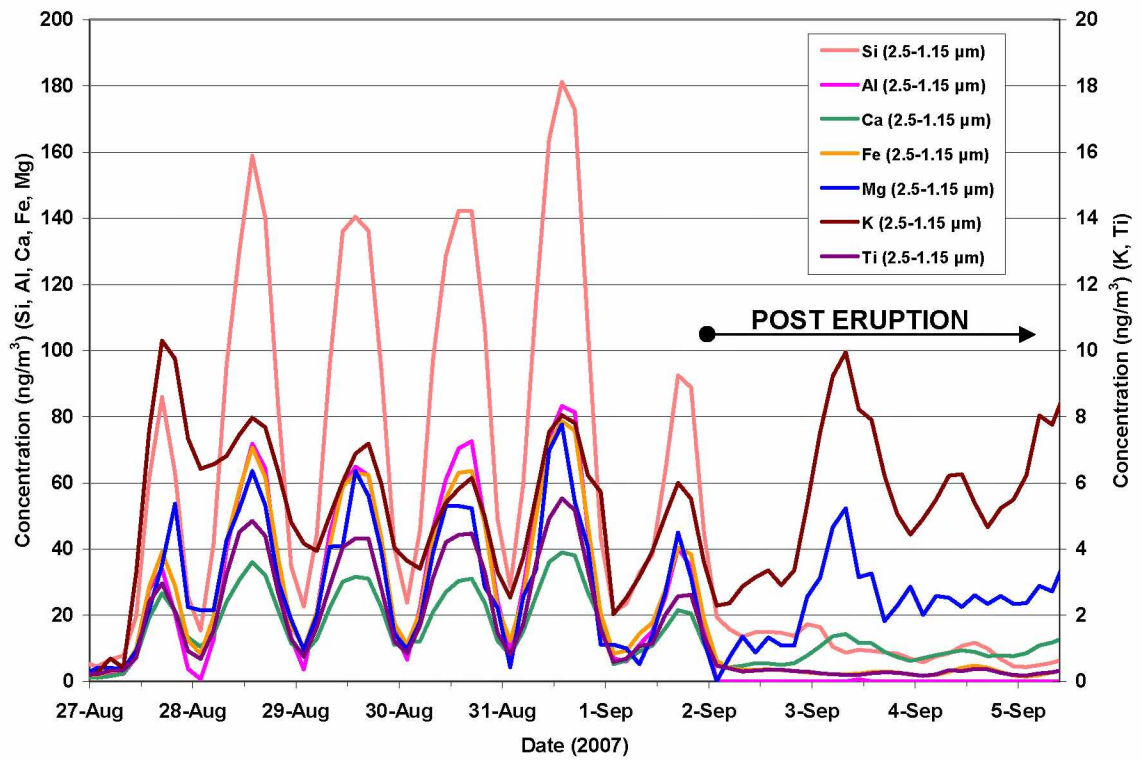


Figure 3.4. Si, Al, Ca, Fe, Mg, K, and Ti concentration versus time (2.5-1.15 μm O_A) showing diurnal variation.

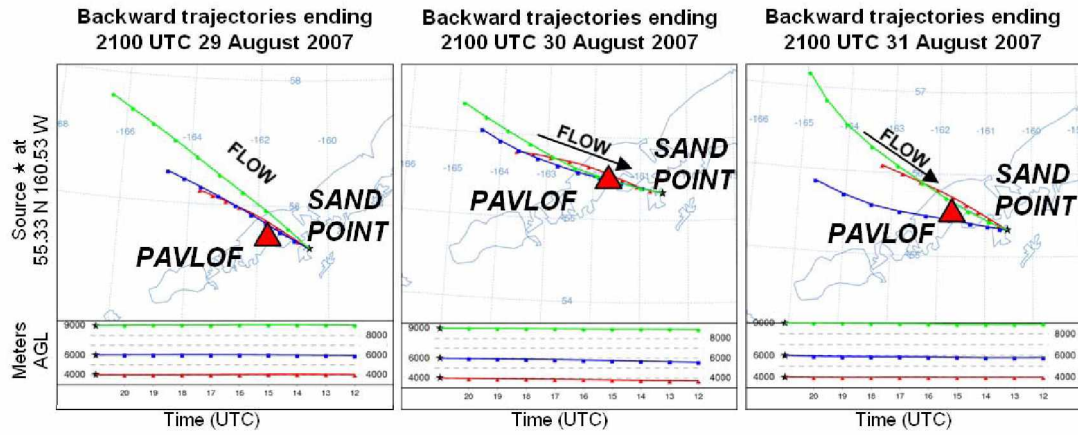


Figure 3.5. HYSPLIT back trajectories for 29-31 August 2007 over Sand Point, Alaska.

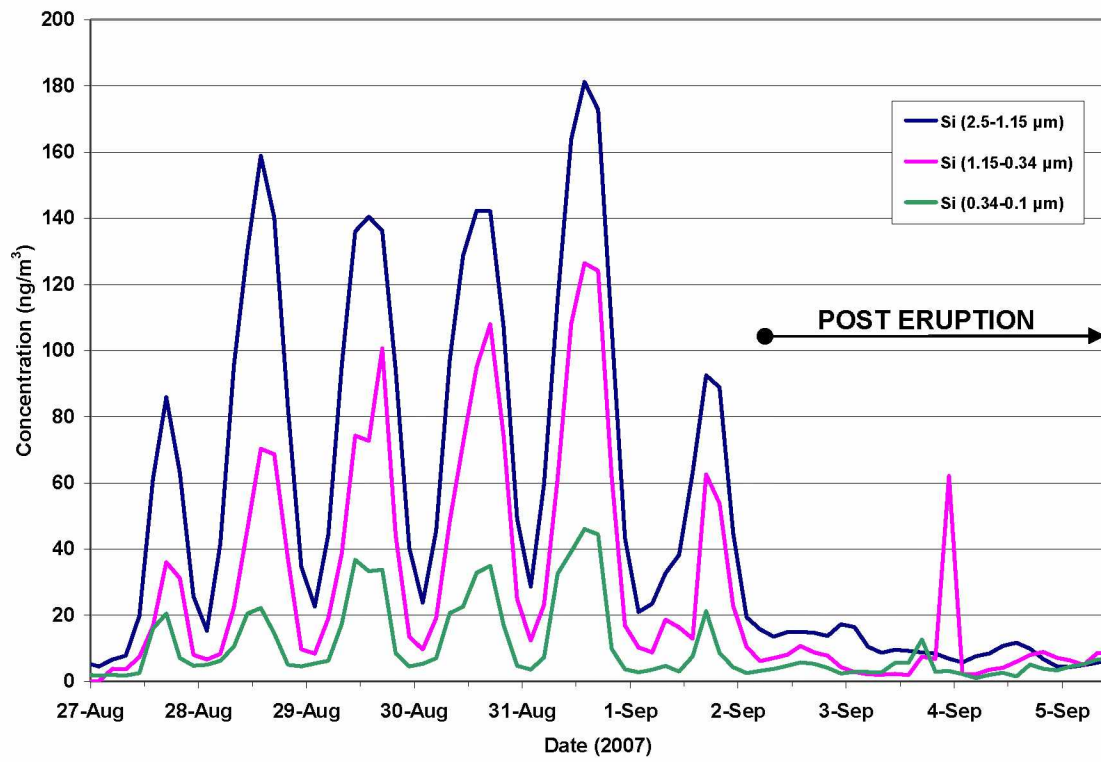


Figure 3.6. Silicon concentration versus time for all stages showing diurnal variation.

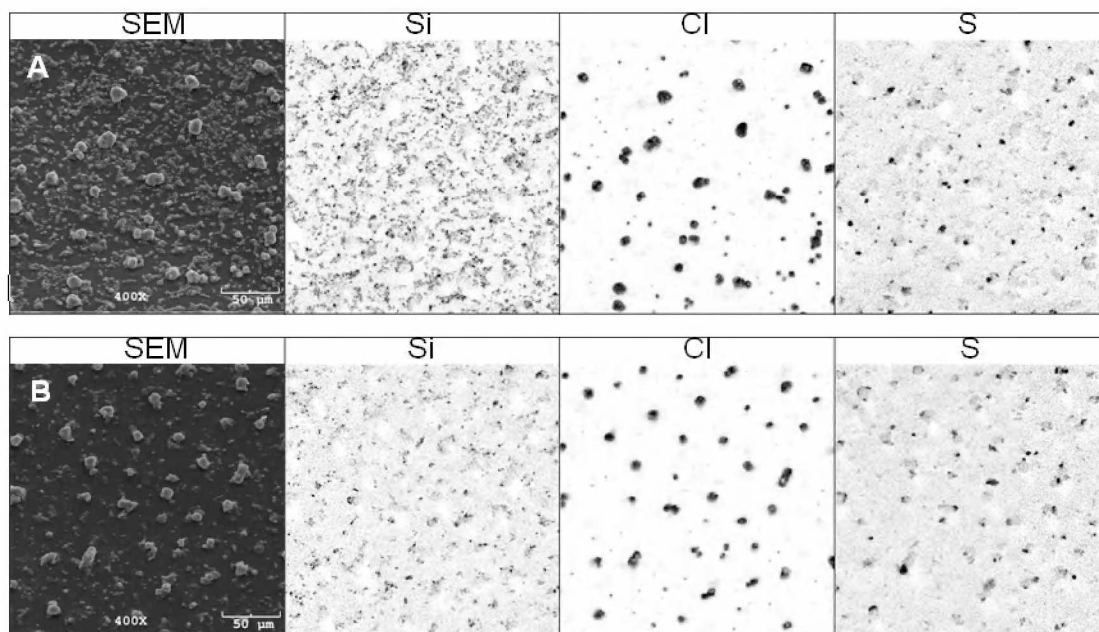


Figure 3.7 A and B. SEM Images and EDS maps from Stage 1 ($2.5-1.15 \mu\text{m } \text{Ø}_A$). A, collected at 17:00 AKDT on 27 August 2007, shows abundant volcanic ash along with large sea salt particles. B, collected at 23:00 AKDT on 27 August 2007, shows infrequent ash particles along with abundant sea salt particles. Both images have minor sulfate aerosols.

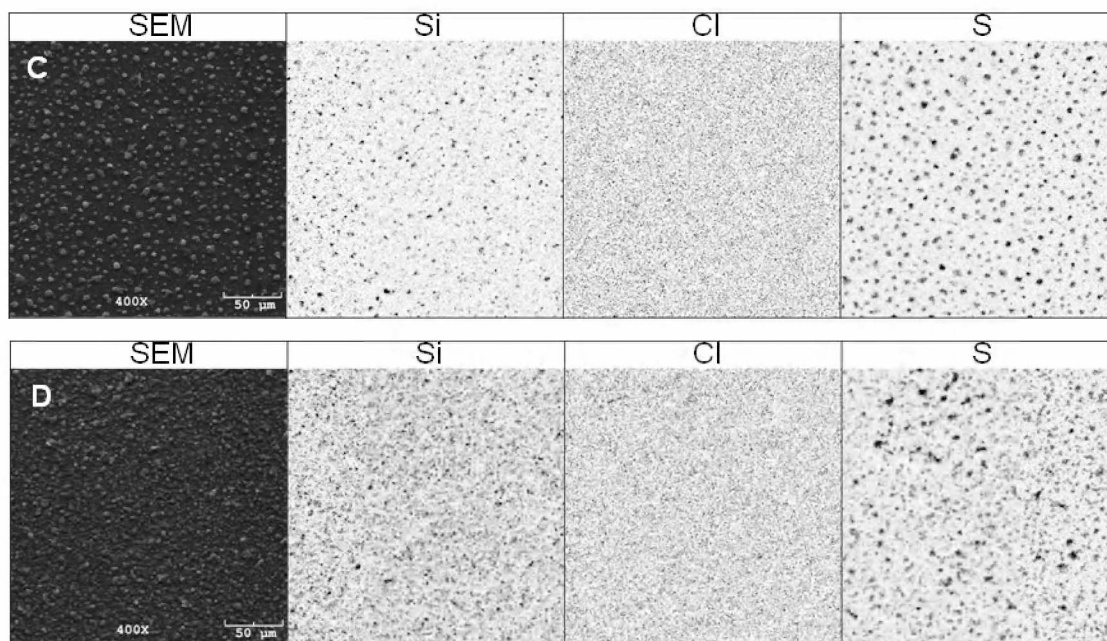


Figure 3.7 C and D. SEM images and EDS maps from Stage 2 (1.15-0.34 μm O_A). C was collected at 18:00 AKDT on 30 August 2007 and shows sparse volcanic ash along with abundant sulfate. D was collected at 02:00 AKDT on 31 August 2007 and shows abundant volcanic ash and sulfate. Both images show little sea salt.

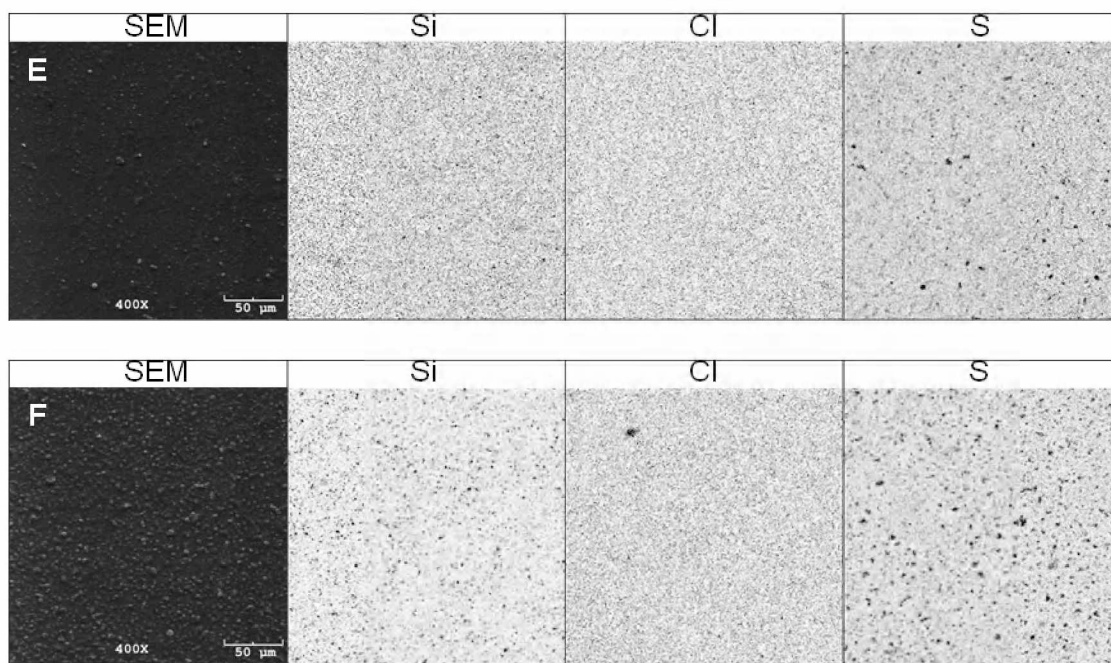


Figure 3.7 E and F. SEM images and EDS maps from Stage 3 ($0.34\text{-}0.1\ \mu\text{m}\ \text{O}_A$). E was collected at 18:00 AKDT on 30 August 2007 and shows sparse volcanic ash along with occasional sulfate. F was collected at 05:00 AKDT on 31 August 2007.

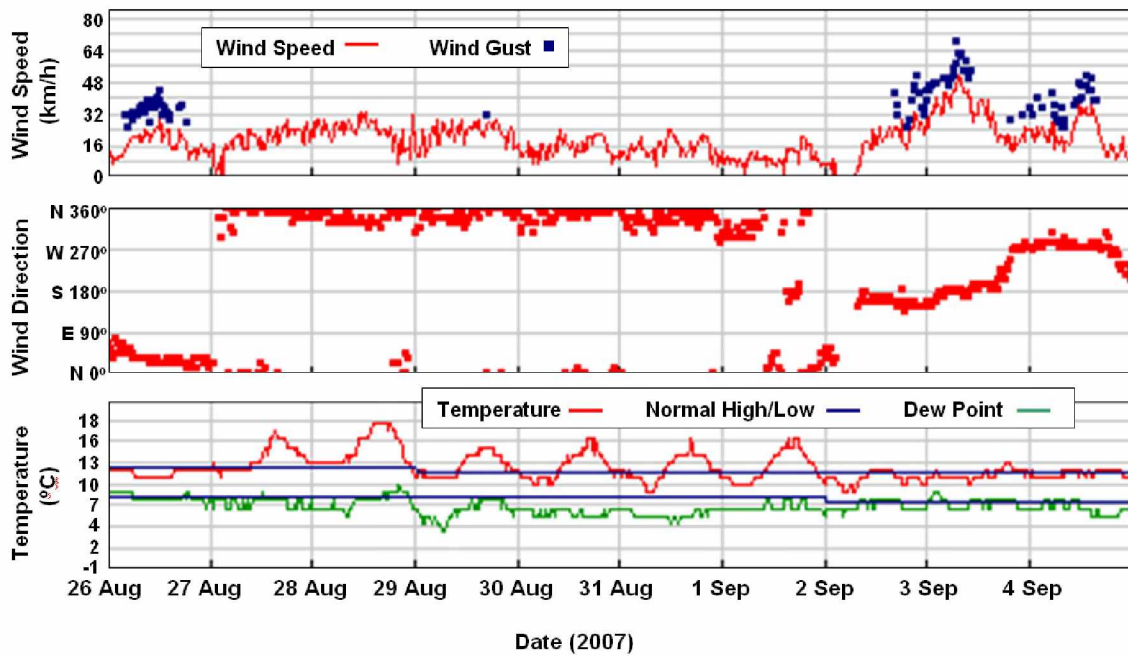


Figure 3.8. Wind direction and speed data from Cold Bay, AK from 26 August – 8 September 2007. Source: Weather Underground www.wunderground.com accessed on 13 May 2011, based on unofficial National Weather Service station Sand Point PASD weather data. The nearest official data are available from the Cold Bay PACD station which show similar conditions over these intervals.

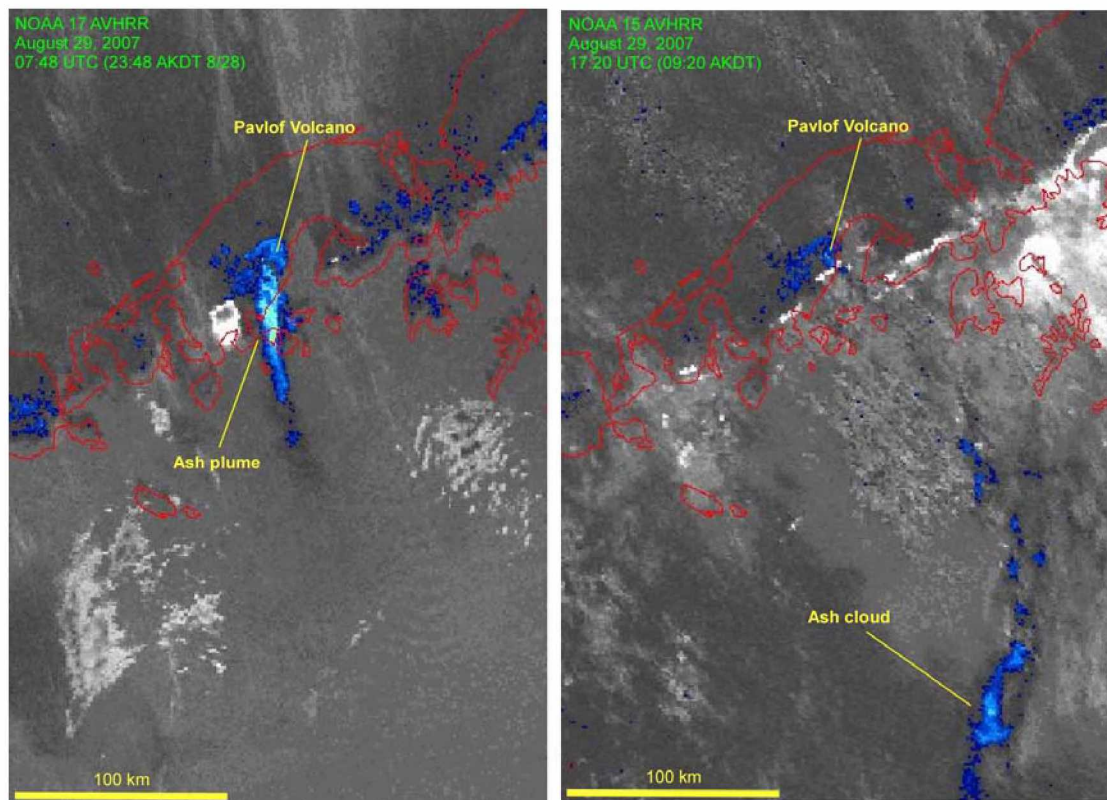


Figure 3.9. AVHRR BT-D split-window images showing ash clouds at Pavlof Volcano. The left image was taken on 28 August 2007 at 11:48PM AKDT (29 August 07:48 UTC) and the right image was taken almost ten hours later on 29 August at 09:20 AKDT (17:20 UTC). Areas that may contain ash are colored blue through light green. The earlier image shows the ash plume during an explosive phase of the eruption. The later image show the remnants of that earlier plume as detached ash clouds. Other blue areas scattered along the peninsula are algorithm artifacts not related to ash. Image and caption credit: Rick Wessels. Image courtesy of AVO/USGS.



Figure 3.10. Photo of steam and ash erupting from Pavlof volcano on 29 August 2007, from 13:10-13:15, AKDT. This image was taken from the northwest. The plume is weak and bent over. Steam is evident near the summit, but only diffuse ash is visible downwind of the volcano. Image credit: Guy Tytgat. Image courtesy of AVO/USGS.

3.13. Tables

Table 3.1. Satellite Sensors Used for Brightness Temperature Difference Ash Detection.

Satellite		Bands Used for BTD Algorithm	
AVHRR ¹	Advanced Very High Resolution Radiometer	Band 4 (10.30 - 11.30 μm)	Band 5 (11.50 - 12.50 μm)
GOES ¹	Geostationary Operational Environmental Satellite	Band 4 (10.7 μm)	Band 5 (12.0 μm)
MODIS ²	Moderate Resolution Imaging Spectroradiometer	Band 31 (10.78-11.28 μm)	Band 32 (11.77-12.27 μm)
MTSAT ³	Multi-Functional Transport Satellite	IR Band 1 (10.8 μm)	IR Band 2 (12.0 μm)

1) US, NOAA 2) US NASA 3) Japan JAXA

Table 3.2. Composition of Sea Salt Particles in Clean Atmospheres

Species	Percent by Weight
Al	$4.6 \times 10^4 - 5.5 \times 10^3$
Ba	1.4×10^4
Br	1.9×10^1
C (non-carbonate)	$3.5 \times 10^3 - 8.7 \times 10^3$
Ca	1.16
Cl	5.504×10^1
Cu	-
Fe	$5.0 \times 10^5 - 5.0 \times 10^4$
I	1.4×10^4
K	1.1
Mg	3.69
Mn	$2.5 \times 10^6 - 2.5 \times 10^5$
Na	3.061×10^2
NH ₄ ⁺	$1.4 \times 10^6 - 1.4 \times 10^5$
NO ₃ ⁻	$3.0 \times 10^6 - 2.0 \times 10^3$
Pb	$1.2 \times 10^5 - 1.4 \times 10^5$
Si	$1.4 \times 10^4 - 9.4 \times 10^3$
SO ₄ ²⁻	7.86
V	9.0×10^7
Zn	$1.4 \times 10^5 - 4.0 \times 10^5$

Based on the assumption that the composition is the same as that of seawater. Source: Lewis and Schwartz (2004).

Table 3.3. Atmospheric Sulfur Aerosols.

Name	Formula	Usual Atmospheric State
Sulfur Dioxide	$\text{SO}_2 \cdot \text{H}_2\text{O}$	Aqueous
Bisulfate ion	HSO_3^-	Aqueous
Sulfite ion	SO_3^{2-}	Aqueous
Sulfuric acid	H_2SO_4	Gas/aqueous, aerosol
Bisulfate ion	HSO_4^-	Aqueous/aerosol
Sulfate ion	SO_4^{2-}	Aerosol
Methane sulfonic acid (MSA)	$\text{CH}_3\text{SO}_3\text{H}$	Gas/aqueous
Hydroxymethane sulfonic acid (HMSA)	$\text{HOCH}_2\text{SO}_3\text{H}$	Aqueous

Source: Seinfeld and Pandis (2006).

Chapter 4 Characterization of Airborne Volcanic Ash Aerosols Collected During the 2009 Redoubt Volcano Eruption²

Abstract

Airborne fine volcanic ash erupted by Redoubt Volcano during March and April, 2009 was continuously sampled at several locations downwind of the volcano using Beta Attenuation Mass monitors (BAM-1020), Environmental Beta Attenuation Monitors (EBAMs), and Davis Rotating Unit for Measurement (DRUM) aerosol samplers to examine atmospheric processes influencing ash transport. The BAM-1020s collected particulate matter $\leq 10 \mu\text{m}$ in aerodynamic diameter (O_A) and smaller (PM_{10}) or particulate matter $\leq 2.5 \mu\text{m}$ O_A ($\text{PM}_{2.5}$). The EBAMs collected PM_{10} and DRUM samplers collected $\text{PM}_{2.5}$ aerosols. The real-time hourly mass concentration data reported by the EBAMs and BAM-1020s is presented here along with ex-post facto elemental composition data from the DRUM sampler. The analysis of DRUM, EBAM, and BAM-1020 samples by scanning electron microscope (SEM) and energy dispersive spectroscopy (EDS) is also presented here. During the initial eruption of Redoubt on 23 March 2009, PM_{10} ash was present in air masses in Anchorage and Soldotna, but no $\text{PM}_{2.5}$ ash was observed over the same interval. As the plume was

¹ Rinkleff, P.G., Cahill, C.F., Stichick, M., in review. Characterization of airborne volcanic ash aerosols collected during the 2009 Redoubt Volcano eruption. Submitted to Journal of Volcanology and Geothermal Research.

transported to the northeast, $PM_{2.5}$ ash was collected at Denali National Park and Preserve. Larger particles (PM_{10}) were falling out at faster rates closer to the volcano while finer particles ($PM_{2.5}$) were falling out at farther transport distances. The EBAM and BAM-1020 are ideal for reporting real-time mass concentrations, while the DRUM sampler is good at providing samples suitable for detailed mass concentrations, chemistry, and particle morphology measurements after the sampling period has concluded. A combination of collocated EBAMs or BAM-1020s and DRUM samplers accompanied by other sampling methods such as standard tephra collection is recommended for future volcanic aerosol studies and eruption response activities to provide real-time mass concentration data, detailed post-eruptive ash chemistry, and particle morphology analysis for volcanic ash transport and dispersion model inputs.

4.1 Introduction

Airborne volcanic ash is a well known hazard to aircraft (Casadevall, 1994) and human health (Horwell and Baxter, 2006; Baxter, 2000). Knowledge about how volcanic ash is transported for volcanic ash transport and dispersion (VATD) models is important for protecting aircraft and human health (Mastin et al., 2009). Recent studies focus on the information needed to assess physical processes affecting the transport of ash and potential hazards from airborne ash have been conducted by Riley et al. (2003), Durant and Rose (2009), and Gislason et al. (2011). These studies propose methods for measuring the shape and size distribution of volcanic ash by digital image processing techniques. The methods used in these studies relied on large sample volumes collected from fall deposits which were analyzed with specialized equipment and costly proprietary image processing software to produce measurements of a large number of particles. These studies and other work using more common microscopy techniques (e.g. Heiken and Wohletz, 1985; Fisher and Schminke, 1984) show that volcanic ash particle shapes are typically complex elongate shards. VATD models assume that all particles are spherical due to the complexity of modeling the settling velocities of non-spherical particles (Rose and Durant, 2009; Brown and Lawler, 2003). The settling velocities of spherical particles are relatively easy to calculate using Stokes' Law, but as particle shape becomes more complex, calculating the settling velocity becomes an arduous task (Reist, 1993, Fuchs, 1964). Laboratory analogues and computer models have shown that particle shape has a significant influence on the settling velocity and particle aggregation rates

(Folch et al., 2010; James et al., 2002; Carey and Sigurdsson, 1982). Future VATD models will require data describing the shape and size distribution of volcanic ash in the atmosphere to refine model algorithms (Mastin et al., 2009; Webley and Mastin, 2009). Along with findings about volcanic ash fate and transport, this study details two methods for sampling airborne ash for microbeam analysis.

The collection methods used for this study include direct sampling of airborne ash by Environmental Beta Attenuation Monitors (EBAMs) (MetOne, 2009), Beta Attenuation Mass Monitors (BAM-1020) (Alaska Department of Environmental Conservation, 2009a), and Davis Rotating Unit for Measurement (DRUM) inertial cascade impactors (Cahill and Wakabayashi, 1993; Raabe et al., 1988). Ash samples were imaged by scanning electron microscope (SEM) and energy dispersive spectroscopy (EDS) (Reed, 2005; Russ, 1990). The comparison of these two collection methods and particle analysis techniques as applied to the 2009 eruption of Redoubt Volcano are discussed here.

4.1.1 Geologic Setting and Eruptive History

Redoubt Volcano (CAVW 1103-03) is a 3801 m high stratovolcano located on the western shore of Alaska's Cook Inlet at 60.48°N 152.74°W, 170 km southwest of Anchorage (Figure 4.1) (Siebert and Simkin, 2002-). It is the most active Holocene volcano on Cook Inlet and has produced Volcanic Explosivity Index 3 level activity including ash plumes, mud flows, pyroclastic flows, and lava domes (Siebert and Simkin, 2002-; Newhall and Self, 1982). During the 1989 eruption, significant

damage occurred at the Drift River oil terminal near Redoubt due to lahar inundation. During the same eruptive period, a KLM 747 passenger jet entered an ash cloud, experienced total engine failure and suffered extensive damage, but safely landed after the crew was able to restart some engines and direct the aircraft to Anchorage International Airport (Casadevall, 1994). Prior to the 1989 eruption, Redoubt erupted during 1967, 1966, and 1902 (Siebert and Simkin, 2002-). Possible eruptions occurred in 1933 and 1819. The volcano is currently monitored with a permanent geodetic and seismic network and by satellite observation techniques (Power et al., in review; Webley et al., in review).

4.1.2 Redoubt Volcano 2009 Eruption

Redoubt began erupting after a period of increased seismicity that ended 20 years of repose. The eruption began on 23 March 2009, produced ash plumes, lava flows, lahars, and pyroclastic flows, and built several lava domes (Bull and Buurman, in review; Siebert and Simkin, 2002-). Ash from this eruption entered commercial airspace and disrupted air traffic in the North Pacific Ocean, prompted the closure of Anchorage International Airport, and caused the cancellation or diversion of several flights originating in Asia, Europe, the North-American west coast, and flights originating in Alaska (L. Demer, Airport opens, residents clean up ash. Anchorage Daily News, 29 March 2009). Ash fell on communities on the Kenai Peninsula, the City of Anchorage, communities along Alaska's Parks Highway, and as far north as Fairbanks (G. Bryson, Redoubt quiets after sending ash north. Anchorage Daily

News, 23 March 2009). The eruption also prompted Chevron to suspend production at several oil and gas wells operating in Cook Inlet and halt operations at the Drift River oil terminal near Redoubt Volcano due to safety concerns related to the eruption (R. Mauer, Drift River terminal may resume shipping; platforms start up. Anchorage Daily News, 13 July 2009).

4.1.3 Sampling Sites

This eruption presented an excellent opportunity to collect volcanic ash at several locations with a variety of methods including BAM-1020s, EBAMs, DRUM cascade impactors, and traditional tephra sampling. The Municipality of Anchorage (MOA) and the Alaska Department of Environmental Conservation operate several BAM-1020s in Anchorage, Palmer and Wasilla, Alaska, as part of an ongoing Environmental Protection Agency mandated particulate monitoring program (Municipality of Anchorage, 2009; Alaska Department of Environmental Conservation, 2009a). In addition, an EBAM operated by the U.S. Fish and Wildlife Service was operating in Soldotna, Alaska, in anticipation of an eruption. A year-long DEC study was underway at the time of the eruption to monitor regional air quality in the vicinity of Denali National Park and Preserve (Cahill et al., 2009). This study used DRUM samplers located at the Denali National Park and Preserve Headquarters (DNP&P HQ) and other locations near the park and preserve for aerosol collection. In addition to these samplers, another DRUM sampler was installed at Ninilchik on the Kenai Peninsula in anticipation of the eruption. The location of

these samplers is shown in Figure 4.1. Tephra samples were also collected at various times and locations during and after eruption pulses. Results from the tephra work are presented elsewhere in this volume³ by Wallace et al. (in review) and Mastin et al. (in review).

The location of the ash samplers provided an opportunity to observe changes in particle size distributions and fallout processes at several locations downwind of the erupting volcano. Previous studies on plume dynamics rely on modeling (e.g. Mastin et al., 2009; Peterson and Dean, 2007; Vietch and Woods, 2001; Sparks et al., 1997), post-eruption tephra collection (e.g. Gislason et al., 2011; Delmelle et al., 2007; Riley et al., 2003; McGimsey et al., 2002; Carey and Sigurdsson, 1982) or time-limited, single-location aerosol collection (e.g. Hunton et al., 2005; Galindo et al., 1998; Hobbs et al., 1991; Woods and Chuan, 1983; Chuan et al., 1981; Stith et al., 1977). In this study, we analyzed ash collected by DRUM samplers located at the DNP&P HQ and Ninilchik, Alaska, for particle shape and chemistry. Samples collected by EBAMs and BAM-1020s were determined to be unsuitable for EDS analysis and were not used for particle shape and size distribution analysis. However, the range of collection techniques employed to collect ash from Redoubt Volcano provides a broad perspective on the strengths and weaknesses inherent in each technique which may help to develop a comprehensive methodology for collecting

² This chapter has been submitted for publication to the Journal of Volcanology and Geothermal Research Special Volume on the Redoubt 2009 Eruption.

volcanic ash for real-time aerosol hazard monitoring and post eruptive ash aerosol analysis.

4.2 Sample Collection Techniques

4.2.1 Environmental Beta Attenuation Monitors (EBAMs) and Beta Attenuation Mass Monitors (BAM-1020s)

Environmental Beta Attenuation Monitors (EBAMs) (MetOne, 2009) (Figure 4.2) and Beta Attenuation Mass Monitors (BAM-1020s) (Alaska Department of Environmental Conservation, 2009a; 2009b), manufactured by Met One Instruments, Inc. (www.metone.com) are continuous particulate monitors commonly used in the United States for monitoring fine particulate matter. Particulate matter $\leq 10 \mu\text{m}$ (in aerodynamic diameter or Ø_A) is referred to as PM_{10} while $\text{PM}_{2.5}$ refers to particulate matter $\leq 2.5 \mu\text{m } \text{Ø}_A$. The BAM-1020 is a U.S. Federal Equivalent Method for monitoring particulate matter. The EBAM is a portable particulate monitor that makes measurements which are traceable to U.S. Environmental Protection Agency requirements for automated PM_{10} and $\text{PM}_{2.5}$ measurements. EBAMs and BAM-1020s operate unattended for up to 60 days and can report real-time aerosol mass concentration data by a variety of communication links. Air is drawn into these samplers by a vacuum pump and aerosols are collected on a continuous glass fiber filter strip (Figures 4.3 and 4.4 A-C). Size-selective concentration measurements are made using standard sampling inlets including total suspended particulate (TSP), PM_{10} , $\text{PM}_{2.5}$, or PM_1 inlets. TSP refers to the total suspended particulate load ≤ 100

$\mu\text{m } \varnothing_A$. Flow-dependent cut points in the size selective inlets are maintained using an integral flow meter, a pressure sensor, and an ambient temperature sensor. The PM_{10} inlet removes particles larger than $10 \mu\text{m}$ and is not affected by wind speed and wind direction. For $\text{PM}_{2.5}$ or PM_1 , secondary size selection is made using a downstream inlet. The collected aerosol mass is measured by the attenuation of a ^{14}C β -particle source. The BAM-1020s located in Anchorage, Palmer, and Wasilla were configured to collect PM_{10} and $\text{PM}_{2.5}$. The Soldotna EBAM was configured to collect PM_{10} .

4.2.2 Davis Rotating Unit for Measurement (DRUM) Sampler

Davis Rotating Unit for Measurement or DRUM samplers, described by Raabe et al. (1988) and Cahill and Wakabayashi (1993), are stand-alone samplers designed to collect time-resolved, size-segregated aerosol (Figure 4.5 A) over a six-week interval. Air is drawn into the sampler by a vacuum pump and aerosol is collected from the air stream by impaction, a type of momentum separation (Reist, 1993). Impaction causes dense aerosol suspended in an accelerated air stream directed normal to the sampling surface to stick to the surface when the air stream is diverted, while lighter particles remain suspended in the air stream. The sampler has several chambers fitted with slotted inlets that accelerate the air and aerosols to specific velocities. These velocities dictate the size fraction collected on a particular stage due to inertial separation influenced by particle aerodynamic diameter. Progressively smaller particles are collected deeper in the instrument. For this study, 3-stage DRUMs were used. The size cuts for the samplers were 2.5-1.15, 1.15-0.34,

and $0.34\text{-}0.1\ \mu\text{m}\ \text{Ø}_A$. The sampler may be fitted with a final filter to collect any remaining aerosols that did not impact, but this has not been done in volcanic sampling campaigns due to possible sampler clogging during times of high aerosol concentrations. The sampler may be fitted with a variety of inlets to achieve an initial size cut. Typically, the sampler is fitted with a PM_{10} initial inlet attached to a $\text{PM}_{2.5}$ cyclone. Other configurations are possible, but for this study, DRUM samplers were configured to collect $\text{PM}_{2.5}$.

The impaction substrate is a MylarTM strip attached to metal cylinder, called a drum (Figure 4.5 B). The MylarTM is coated with a thin film of ultra-pure Apiezon LTM vacuum grease to reduce particle bounce (Lawson, 1980). When the sampler is activated, the drum rotates past the slotted inlet at a rate of 4 mm per day. As the drum rotates, fresh sampling surface is exposed under the inlet to collect aerosol.

When the sampling interval is completed, the sampler is opened, the drums are removed in clean conditions and placed in sealed containers for shipping. In a clean laboratory, the MylarTM strips are removed from the drum, affixed to a labeled plastic frame with pressure sensitive tape, and the start and end positions are noted. Mass is determined on prepared DRUM samples using β -gauge analysis, a particle attenuation technique (Reist, 1993). Elemental composition (28 selected elements between Na and Pb) is determined by Synchrotron X-Ray Fluorescence (S-XRF) (Cahill, 2003; Cahill et al., 1999) at the Lawrence Berkeley National Laboratory Advanced Light Source Beam Line 10.3.1 (Cahill et al., 2000).

4.2.3 Tephra Sampling

Tephra samples were also collected during this eruption (Wallace et al., in review; Mastin et al., in review). Fresh tephra samples may be collected by a variety of methods including collecting ash from a measured area and over a specific time, collecting a sample of snow, melting it and retaining the solid fraction, or collecting ash on a plastic sheet, metal pan, or other surface (e.g. Gislason et al., 2011; Delmelle et al., 2007; Riley et al., 2003; McGimsey et al., 2002; Carey and Sigurdsson, 1982). Depending on the specific study, tephra collection methods can be quite ordered including specific measurements of area and discrete collection time interval or may merely involve collecting a grab sample of tephra from an unmeasured area. In all cases, tephra sampling occurs after pyroclastic materials have sedimented from the plume or dispersing ash cloud.

4.3. SEM Sample Analysis

4.3.1 DRUM Sample Analysis

Samples were analyzed at the Advanced Instrumentation Laboratory (AIL) at the University of Alaska Fairbanks (<http://www.uaf.edu/ail/>) with a ISI-SR-50 scanning electron microscope (SEM) equipped with a Kevex 7000 energy dispersive X-ray spectrometer (EDS). Each sample was cut into ~2 cm long pieces which were affixed to a rigid polystyrene backing, and sputter-coated with gold and palladium. The samples were attached to a standard aluminum SEM stub grounded with metal tape, and placed in the SEM chamber. In the chamber, the sample was oriented 25°

from horizontal at a working distance of 10 mm. The accelerating voltage was set to 20 kV and the beam was set to its smallest spot size for imaging. During EDS spectra collection and element mapping, the beam spot size was increased to its maximum size to increase x-ray counts.

Images and bulk field-of-view spectra were made parallel to the sampling direction from the start of the sampling interval with about 5-10% area overlap from image to image to allow for the construction of image mosaics and to maintain location (and sampling time) within the sample (Figure 4.6). The EDS spectrum of the entire field of view was collected for each frame to indicate the overall composition of the particles in the field of view. Depending on the spectra, an element map of the frame was prepared. In general, when volcanic aerosols, indicated by high Si counts were observed, an element map was prepared. But periodically an element map was prepared to show elemental distribution across the entire sampling interval to describe the background, non-volcanic aerosols.

4.3.2 EBAM and BAM-1020 Sample Analysis

Glass fiber filter tapes were retrieved from the EBAM in Soldotna which was collecting PM_{10} and BAM-1020s in Anchorage which were collecting PM_{10} and $PM_{2.5}$. Sample spots on the tapes were indicated by dark quartered spots spaced at regular intervals (Figures 4.3 and 4.4 A and B). Since no automatic marking was made on the filter tape by the EBAM, the tapes were manually marked at intervals during the monitoring period to give some time indexing to the filter tape. Filter

tapes are several meters long (enough for 60 days of continuous monitoring), so indexing was needed to determine either the sampling time of a specific spot or the spot location when mass loads were low or when light-colored aerosols were sampled. Also, when a sampling or instrument error is detected, such as instrument saturation or communication dropout, the filter tape automatically advances to a clean spot to continue monitoring, so a 24-hour period could contain more than 24 sample spots. After the tape was manually indexed for time, a small portion (1/4) of the 1 cm diameter sample spot was cut from the filter tape and fixed to a 3 x 2 cm polystyrene sheet with double-sided tape. The sample quarter was labeled and another sample quarter was attached adjacent to it until the plastic sheet was filled (about 12-14 sample points total). The sample mounts were then sputter coated and placed in the SEM chamber in an identical manner to the DRUM samples described above. The configuration (beam current, working distance, etc.) of the SEM was intentionally made identical to that of the DRUM samples to allow for a more direct comparison of results.

Four to five areas per sample were imaged and spot spectra of individual particles were collected with the EDS. Area spectra of the type made on the DRUM samples were not collected on EBAM samples because the glass fiber filter media produced a strong background of silicon, calcium, and aluminum (Figure 4.7). For this reason, only single point and small area spectra were collected for particles apparent on the filter surface. Even with small areas and point spectra collection, the filter media contaminated the spectra (Figure 4.8) and the heat produced by the

electron beam interacting with the sample fused the particles on the filter media and partially fused the filter media itself (Figure 4.9). The PM_{10} aerosols were generally found on the filter surface, but the $PM_{2.5}$ aerosols were embedded deep in the filter media making the imaging difficult (Figure 4.10). For these reasons, samples on glass fiber filter tape were deemed unsuitable for SEM imaging and EDS analysis.

4.4 SEM and EDS Analysis Techniques

Both secondary electron (SE) images and element maps were collected on the DRUM samples. DRUM samples were found to provide excellent images and spectra of particles since all the particles are on a smooth surface and the sampling substrate (MylarTM and Apezion LTM film) did not contaminate the sample spectra. Secondary electron images were useful for qualitatively determining particle shapes. Image mosaics of SE images were prepared so that sample distance could be measured (Figure 4.6), and thus, sampling time could be determined. The DRUMs in this study rotated at 4 mm of sampling distance per day so exact particle sampling times could be obtained. Although SE images provide attractive images of particles in DRUM samples, these images pose several problems for automated image analysis such as beam shadowing, secondary illumination, and edge effects (Reed, 2005; Russ, 1990). The SEM and EDS analysis techniques detailed here form the basis for collecting raw images for automated digital image processing to determine volcanic ash particle size distributions and shape descriptors for airborne ash collected during the 2006 eruption of Augustine Volcano, as detailed in Chapter 2.

4.5 Discussion

The EBAM and BAM-1020 real-time data from Soldotna and Anchorage, reported during the initial eruption pulses on 23 March 2009 show a distinct increase of PM_{10} but have no accompanying increase in $PM_{2.5}$ (Figure 4.11 A-B). No significant increases in PM_{10} or $PM_{2.5}$ were observed in the real-time data from either Palmer or Wasilla over the same period (Figure 4.11 C-D, and Figure 4.12). During this eruption, the HYSPLIT (Draxler and Rolph, 2003; Rolph, 2003) VATD model was used to provide forward and backward trajectories for ash cloud transport. This model has been shown by Cahill et al. (2010) to provide a good first order representation of fine volcanic particle transport. HYSPLIT trajectories indicate that air masses traveled from the vicinity of Redoubt during the eruptive period on 23 March and passed over Soldotna, Anchorage, Palmer, and Wasilla (Figure 4.13); however, the forcing of air masses over topographic features could have raised the ash to higher altitudes than the sampling locations in Wasilla and Palmer. Also, the work done at Pavlof Volcano (described in Chapter 3) has shown that daily mass concentration variations in volcanic ash transport can occur due to diurnal variations in heating and radiative cooling of air masses. The combination of these effects could explain why ash was observed in Soldotna and Anchorage but not in Wasilla and Palmer.

Analysis of S-XRF (Figure 4.14) and SEM/EDS data (Figure 4.15 A and B) show that volcanic ash was present in the $PM_{2.5}$ size fraction at DNP&P HQ during the initial eruption and subsequent eruptive pulses from Redoubt (Figure 4.16). Mass

concentration events evident in the DRUM data after 31 March 2009 were caused by aerosol from the north and northeast of the sampling location. Ash was detected in the largest DRUM stages (2.5-1.15 and 1.15-0.34 μm). The third stage had only trace amounts of ash present. It was difficult to separate the silicon found in the 0.34-0.1 μm size fraction EDS images during the time of eruption from that of background aerosols. Particles in the 1.15-0.34 and 0.34-0.1 μm size fraction SE images (Figure 4.15 B) do not readily show characteristic volcanic shapes, such as shards and bubble wall morphology, because they are too small to clearly image.

Eruptive style has a significant influence on the particle size range produced. Central vent eruptions produce coarser ash while pyroclastic flows produce significant fine ash due to in-flow clast-to-clast milling (Darteville et al., 2002). The difference in particle size distribution relative to eruptive style was clearly seen in DRUM sampling conducted during the Augustine 2006 eruption (Cahill et al., 2010). Since the initial eruptive style of Redoubt was characterized as explosive central vent-type eruptions, the ash produced was coarser than ash produced by pyroclastic flows. This may explain the absence of ash in the smallest DRUM size fraction. The ash sampled at the DNP&P HQ may represent the fine, tail end of the particle distribution that was present in the plume ~12 hours after the initial eruption event.

Chlorine-rich particles were observed in DRUM samples from Ninilchik and more rarely at DNP&P HQ (Figure 4.15 C-D) as cubes, spheres, and rods in the 2.5-1.15 and 1.15-0.34 μm O_A stages and was present at intervals in the overall aerosol mass during eruptive and non-eruptive periods. EDS analysis confirmed that sea salt

particles are composed of Cl, Na, Ca, Mg, and K, all common sea salt constituents (Lewis and Schwartz, 2004). Samples from Ninilchik contained much higher amounts of sea salt than those from DNP&P HQ, likely due to Ninilchik being adjacent to Cook Inlet. Sea salts sampled in DNP&P HQ were likely transported to the sampling site in air masses originating in a maritime environment.

Sulfate aerosol was present in DRUM samples from both locations. Sulfate was observed in all three stages, but was most common in the 1.15-0.34 μm O_A stage. Sulfate composition was confirmed by EDS spectroscopy. Sulfate found on samples from Ninilchik often exhibited crystal habit but also occurred as massive forms. Sulfate contained in DNP&P HQ commonly exhibited massive forms with rare crystalline shapes. The sulfate sampled at Ninilchik is interpreted to be chiefly composed of non-sea salt sulfate from maritime sources with minor amounts of high-temperature source sulfate, while the sulfate sampled at DNP&P HQ to be primarily from local high-temperature combustion sources with minor contributions of non-sea salt sulfate. The strong presence of sulfate during non-eruptive periods indicates that the sulfate does not have a significant volcanic source.

4.6 Conclusion

Several sampling and reporting methods are necessary for providing real-time mass-concentration data during an eruption and post eruption detailed analysis. The BAM-1020 and EBAM monitors provide real-time mass concentration data while DRUM samplers provide suitable samples for post-eruption aerosol analysis. Co-

location of these and other instruments at several locations, especially near population centers, combined with standard tephra sampling is necessary to satisfy real-time mass concentration reporting requirements and post-eruptive analysis needs. SEM and EDS provide good-quality images and spectra of particles in DRUM samples which are suitable for digital image processing methods. EBAM and BAM-1020 filter samples are not suitable for high quality post sampling analysis due to sample degradation during EDS analysis and unacceptable contamination from the filter media.

The analysis of airborne volcanic ash sampled during the 2009 Redoubt eruption demonstrates how particle size, local conditions, and topography may influence mass concentrations of volcanic ash at locations downwind of an erupting volcano. Sulfate aerosol sampled during non-volcanic and volcanic episodes did not significantly vary in concentration or morphology relative to the presence or absence of volcanic ash which indicated the sulfate may not have had a significant volcanic contribution. The abundance and morphology of background sulfate aerosol may help determine the source of sulfate in some volcanic clouds.

4.7 Acknowledgements

I would like to thank the Municipality of Anchorage Air Quality Monitoring Program for providing BAM-1020 filter tapes and data, the Soldotna office of the U.S. Fish and Wildlife Service for the use of their EBAM, providing live EBAMs data and filter tapes, the Ninilchick School and the Kenai Borough School District for

facilitating the placement of a DRUM sampler at their facility, and the Alaska Department of Environmental Conservation Air Quality Division for providing DRUM samples and data from a regional air quality study. This work was made possible with the generous encouragement and technical support of the staff of the Advanced Instrumentation Laboratory at the University of Alaska Fairbanks. This work was supported by Army Research Laboratory contract W911NF-07-1-0346.

4.8 References

Alaska Department of Environmental Conservation, Division of Air Quality, Air Monitoring and Quality Assurance Section, 2009a. Alaska's 2009 Air Monitoring Network Plan. www.dec.state.ak.us/air/am/am_airmonplan.htm (last accessed on 10 March 2012).

Alaska Department of Environmental Conservation, Division of Air Quality, Air Monitoring and Quality Assurance Section, 2009b. MetOne Instruments Beta Attenuation Mass (BAM) Monitor Model 1020. www.dec.state.ak.us/air/am/am_sops1.htm (last accessed on 10 March 2012).

Baxter, P., 2000. Impacts of Eruptions on Human Health. In: Sigurdsson, H., Houghton, B., McNutt, R.R., Stix, J. (Eds.), *Encyclopedia of Volcanoes*. Academic Press, New York, NY, pp. 1035-1043.

Brown, P., Lawler D., 2003. Sphere drag and settling velocity revisited. *Journal of Environmental Engineering*. 129, 222-231.

Bryson, G., 23 March 2009. Redoubt quiets after sending ash north. *Anchorage Daily News*. <http://www.adn.com> (last accessed on 10 March 2012).

Bull, K.F., Buurnam, H., in review. An overview of the 2009 eruption of Redoubt Volcano. *Journal of Volcanology and Geothermal Research*, Special Issue on the 2009 Redoubt Eruption.

Cahill, C.F., 2003. Asian aerosol transport to Alaska during ACE-Asia. *Journal of Geophysical Research*. 108, 8664-8872.

Cahill C.F., Rinkleff, P., Dehn, J., Webley, P., Cahill, T., Barnes, D., 2010. Aerosol measurement from a recent Alaskan volcanic eruption: Implications for volcanic ash transport predictions. *Journal of Volcanology and Geothermal Research*. 198, 76-80.

Cahill, C.F., Wallace, A.N., Cahill, T.A., Barnes, D.E., 2009. The impact of transported aerosols on visibility in Denali National Park and Preserve, Alaska. Abstracts, American Association for Aerosol Research 28th Annual Conference October 2009, Minneapolis, Minnesota, abstract #1119.

Cahill, T.A., Wakabayashi, P., 1993. Compositional analysis of size-segregated aerosol samples. In: Newman, L. (Ed.), *Measurement Challenges in Atmospheric Chemistry*, American Chemical Society, pp. 211-228.

Cahill, T.A., Cliff, S.S., Perry, K.D., Jimenez-Cruz, M., Kelly, P.B., Shackelford, J., McHugo, S.A., Thompson, A., 2000. S-XRF and atmospheric aerosols: Health, visibility, and climate change. Advanced Light Source Compendium of User Abstracts, Lawrence Berkeley National Laboratory. <http://www.als.lbl.gov/als/compendium> (last accessed on 10 March 2012).

Cahill, T.A., Cliff, S., Perry, K., Jimenez-Cruz, M., McHugo, S., 1999. Size and time resolved anthropogenic components of aerosols via synchrotron x-ray fluorescence: Application to Asian aerosol transport. Abstracts, American Geophysical Union 1999 Fall Meeting, December. San Francisco, California, pp. 13-17.

Carey, S.N., Sigurdsson, H., 1982. Influence of particle aggregation on deposition of distal tephra from the May 18, 1980, eruption of Mount St. Helens volcano. *Journal of Geophysical Research*. 87, 7061-7072.

Casadevall, T.J., 1994. The 1989–1990 eruption of Redoubt Volcano Alaska: Impacts on aircraft operations. *Journal of Volcanology and Geothermal Research*. 62, 301-316.

Chuan, R.L., Woods, D.C., McCormick, M.P., 1981. Characterization of aerosols from eruptions of Mount St. Helens. *Science*. 211, 830-832.

Darteville, S., Ernst, G.J., Stix, J., Bernard, A., 2002. Origin of the Mount Pinatubo climactic eruption cloud: Implications for volcanic hazards and atmospheric impacts. *Geology*. 30, 663-666.

Delmelle, P., Lambert, M., Dufrêne, Y., Gerin, P., Óskarsson, N., 2007. Gas/aerosol–ash interaction in volcanic plumes: New insights from surface analyses of fine ash particles. *Earth and Planetary Science Letters*. 259, 159–170.

Demer, L., 29 March, 2009. Airport opens, residents clean up ash. Anchorage Daily News. <http://www.adn.com> (last accessed on 10 March 2012).

Draxler, R.R., Rolph, G.D., 2011. HYSPLIT (HYbrid Single-Particle Lagrangian Integrated Trajectory) NOAA Air Resources Laboratory, Silver Spring, MD. Model access via NOAA ARL READY Website: <http://ready.arl.noaa.gov/HYSPLIT.php> (last accessed on 10 March 2012).

Durant, A.J., Rose, W.I., 2009. Sedimentological constraints on hydrometeor-enhanced particle deposition: 1992 eruptions of Crater Peak, Alaska. *Journal of Volcanology and Geothermal Research*. 186, 40–59.

- Fisher, R.V., Schminke, H.-U., 1984. *Pyroclastic Rocks*. Springer-Verlag, New York, NY.
- Folch, A., Costa, A., Durant, A., Macedonio, G., 2010. A model for wet aggregation of ash particles in volcanic plumes and clouds: 2 Model application. *Journal of Geophysical Research*. 115, 148-227.
- Fuchs, N.A., 1964. *The Mechanics of Aerosols*. Dover Publications, New York, NY.
- Galindo, I., Ivlev, L.S., Gonzalez, A., Ayala, R., 1998. Airborne measurements of particle and gas emissions from the December 1994–January 1995 eruption of Popocatepetl volcano, Mexico. *Journal of Volcanology and Geothermal Research*. 83, 197–217.
- Gislason, S.R., Hassenkam, T., Neidel, S., Bovet, N., Eiriksdottir, E.S., Alfredsson, H.A., Hem, C.P., Balogh, Z.I., Dideriksen, K., Oskarsson, N., Sigfusson, B., Larsen, G., Stipp, S.L.S., 2011. Characterization of Eyjafjalljökull volcanic ash particles and a protocol for rapid risk assessment. *Proceedings of the National Academy of Science*. 108, 7307-7312.
- Heiken, G., Wohletz, K., 1985. *Volcanic Ash*. University of California Press, Berkeley, CA.
- Hobbs, P.V., Radke, L.F., Lyons, J.H., Ferek, R.J., Coffman, D.J., Casadevall, T.J., 1991. Airborne measurements of particle and gas emissions from the 1990 volcanic eruptions of Mount Redoubt. *Journal of Geophysical Research*. 96, 18,735-18,752.
- Horwell, C.J., Baxter, P.J., 2006. The respiratory health hazards of volcanic ash: A review for volcanic risk mitigation. *Bulletin of Volcanology*. 69, 1-24.
- Hunton, D.E., Viggiano, A.A., Miller, T.M., Ballenthin, J.O., Reeves, J.M., Wilson, J.C., Lee, S.-H., Anderson, B.E., Brune, W.H., Harder, H., Simpas, J.B., Oskarsson, N., 2005. In-situ aircraft observations of the 2000 Mt. Hekla volcanic cloud: Composition and chemical evolution in the Arctic lower stratosphere. *Journal of Volcanology and Geothermal Research*. 145, 23-34.
- James, M.R., Gilbert, J.S., Lane, S.J., 2002. Experimental investigation of volcanic particle aggregation in the absence of a liquid phase. *Journal of Geophysical Research*. 107, 148-227.
- Lawson, D., 1980. Impaction surface coatings intercomparison and measurements with cascade impactors. *Atmospheric Environment*. 14, 195-199.

- Lewis, E.R., Schwartz, S.E., 2004. Sea Salt Production: Mechanisms, Methods, Measurements and Models. Geophysical Monograph 152. American Geophysical Union, Washington, D.C.
- Mastin, L.G., Schwaiger, H., Schneider, D.J., Wallace, K.L., Schaefer, J.R., Denlinger, R.P., in review. Injection, transport and deposition of tephra during event 5 at Redoubt Volcano, 23 March 2009. *Journal of Volcanology and Geothermal Research*, Special Issue on the 2009 Redoubt Eruption.
- Mastin, L.G., Guffanti, M., Servranckx, R., Webley, P.W., Barsotti, S., Dean, K., Durant, A., Ewert, J.W., Neri, A., Rose, W.I., Schneider, D.J., Siebert, L., Stunder, B., Swanson, G., Tupper, A., Volentik, A., Waythomas, C.F., 2009. A multidisciplinary effort to assign realistic source parameters to model of volcanic ash-cloud transport and dispersion during eruptions. In: Mastin, L.G., Webley, P.W. (Eds.), *Journal of Volcanology and Geothermal Research: Special Issue on Volcanic Ash Clouds*. 186, pp. 10–21.
- Mauer, R., 13 July 2009. Drift River Terminal may resume shipping, platforms start up. *Anchorage Daily News*. <http://www.adn.com> (last accessed on 10 March 2012).
- McGimsey, R.G., Neal, C.A., Riley, C.M., 2002. Aerial distribution, thickness, mass, volume and grain size of tephra-fall deposits from the eruption of Crater Peak vent, Mt. Spurr volcano, Alaska. U.S. Geological Survey Open-File Report 01-370.
- MetOne Inc., 2009. E-BAM datasheet. http://www.metone.com/documents/E-BAM_Datasheet_Rev_Aug09.pdf (last accessed on 10 March 2012).
- Municipality of Anchorage, Air Quality Program, Environmental Services Division, Department of Health and Human Services, 2009. Air Quality in Anchorage, A Summary of Air Quality Monitoring Data and Trends, 1980–2008. <http://www.muni.org/iceimages/healthesd/2009%20report%20final.pdf> (last accessed on 10 March 2012).
- Newhall, C.G., Self, S., 1982. The Volcanic Explosivity Index (VEI): An estimate of explosive magnitude for historical volcanism. *Journal of Geophysical Research*. 87, 1231-1238.
- Peterson, R.A., Dean, K.G., 2007. Forecasting exposure to volcanic ash based on ash dispersion modeling. *Journal of Volcanology and Geothermal Research*. 170, 230-246.

- Power, J., Stihler, S., Haney, M., in review. Seismic observations of Redoubt Volcano, Alaska - 1989 - 2010 and forecasting of the 2009 eruption. *Journal of Volcanology and Geothermal Research*, Special Issue on the 2009 Redoubt Eruption.
- Raabe, O.G., Braaten, D.A., Axelbaum, R.L., Teague, S.V., Cahill, T.A., 1988. Calibration studies of the DRUM impactor. *Journal of Aerosol Science*. 19, 183-195.
- Reed, S., 2005. *Electron Microprobe Analysis and Scanning Electron Microscopy in Geology*. Cambridge University Press, New York, NY.
- Reist, P.C., 1993. *Aerosol Science and Technology*, Second Edition. McGraw-Hill, New York, NY.
- Riley, C.M., Rose, W.I., Bluth, G.J.S., 2003. Quantitative shape measurements of distal volcanic ash. *Journal of Geophysical Research*. 108, 2504-2519.
- Rolph, G.D., 2011. Real-time Environmental Applications and Display sYstem (READY) NOAA Air Resources Laboratory, Silver Spring, MD. <http://ready.arl.noaa.gov> (last accessed on 10 March 2012).
- Rose, W.I., Durant, A.J., 2009. Fine ash content of explosive eruptions. *Journal of Volcanology and Geothermal Research*. 186, 32-39.
- Russ, J., 1990. *Computer Assisted Microscopy: The Measurement and Analysis of Images*. Plenum Press, New York, NY.
- Siebert, L., Simkin, T., 2002-. *Volcanoes of the World: An Illustrated Catalog of Holocene Volcanoes and their Eruptions*. Smithsonian Institution, Global Volcanism Program, Digital Information Series, GVP-3. <http://www.volcano.si.edu/world/> (last accessed on 10 March 2012).
- Sparks, R.S.J., Bursik, M.I., Carey, S.N., Gilbert, J.S., Glaze, L.S., Sigurdsson, H., Woods, A.W., 1997. *Volcanic Plumes*. Wiley, New York, NY.
- Stith, J.L., Hobbs, P.V., Radke, L.F., 1977. Observations of a nuée ardente from the St. Augustine Volcano. *Geophysical Research Letters*. 4, 259-262.
- Vietch, G., Woods, A.W., 2001. Particle aggregation in volcanic plumes. *Journal of Geophysical Research*. 106, 26,425-26,441.
- Wallace, K.L., Schaefer, J.G., in review. Event chronology, plume heights, and preliminary report of distribution, thickness, and mass of ash fall from the 2009 eruption of Redoubt volcano, Alaska. *Journal of Volcanology and Geothermal Research*, Special Issue on the 2009 Redoubt Eruption.

Webley, P., Mastin, L., 2009. Improved prediction and tracking of volcanic ash clouds. *Journal of Volcanology and Geothermal Research*. 186, 1-9.

Webley, P.W., Lopez, T.M., Dean, K.G., Rinkleff, P., Dehn, J., Cahill, C.F., Wessels, R.L., Schneider, D.J., Ekstrand, A., Bailey, J.E., Izbekov, P., Worden, A., in review. Remote Sensing observations of eruptive clouds and surface thermal activity during the 2009 eruption of Redoubt volcano. *Journal of Volcanology and Geothermal Research*, Special Issue on the 2009 Redoubt Eruption.

Woods, D.C., Chuan, R.L., 1983. Size-specific composition of aerosols in the El Chichon volcanic cloud. *Geophysical Research Letters*. 10, 1041-1044.

4.9 Figures

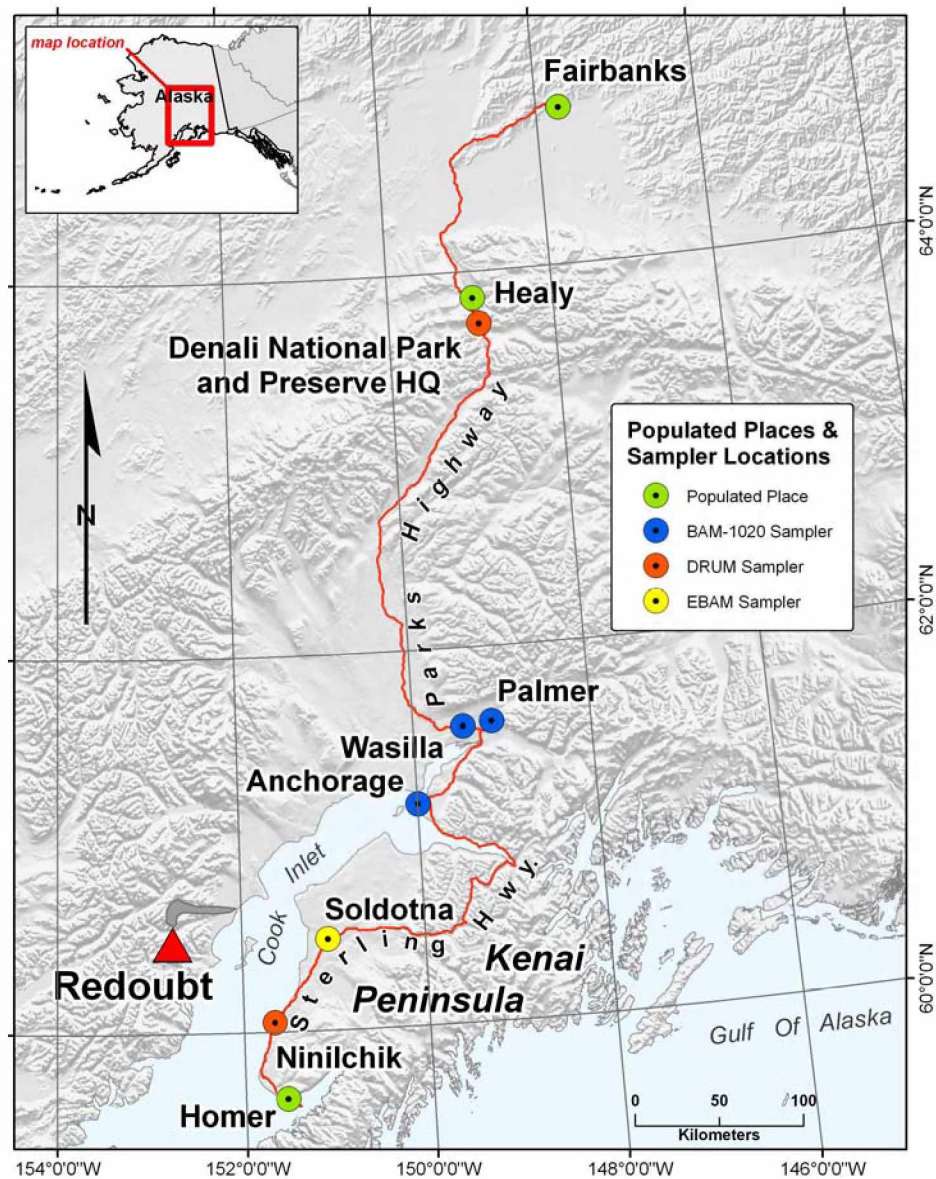


Figure 4.1. Location map of Redoubt Volcano, Alaska and sampling locations used in this study. Redoubt is located on Cook Inlet 170 km southwest of Anchorage.

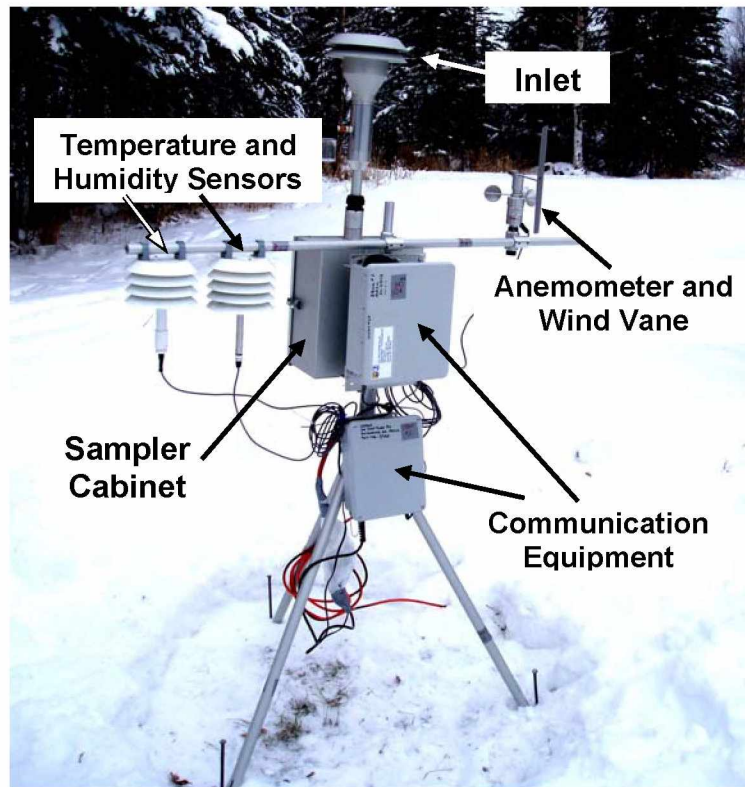


Figure 4.2. Exterior view of an EBAM equipped with a meteorological station. The unit consists of a louvered inlet (top) which is attached to the sampler cabinet. Attached to the sampler cabinet by two horizontal arms are weather station components. A communications unit is also attached to the main sampler cabinet. Photo credit: Drew Grimes, U.S. Fish and Wildlife Service.

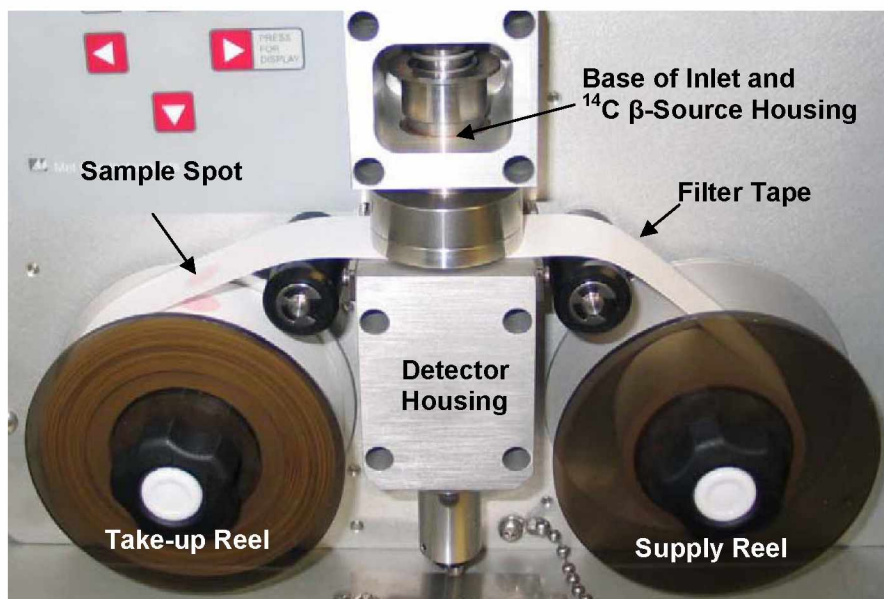


Figure 4.3. Interior view of the EBAM filter tape, β -source and detector. The assembly shown in the upper center of the cabinet contains the base of the inlet tube shown in Figure 4.2 and a ^{14}C source which emits a constant source of β -particles. The β -particles are attenuated as they collide with particles collected on the filter tape. Two dark sample spots are visible on the take-up roll of the filter tape spool. Aerosols are the filter tape which is located between the base of the inlet and the β -particle detector assembly. Photo Credit: MetOne Inc.

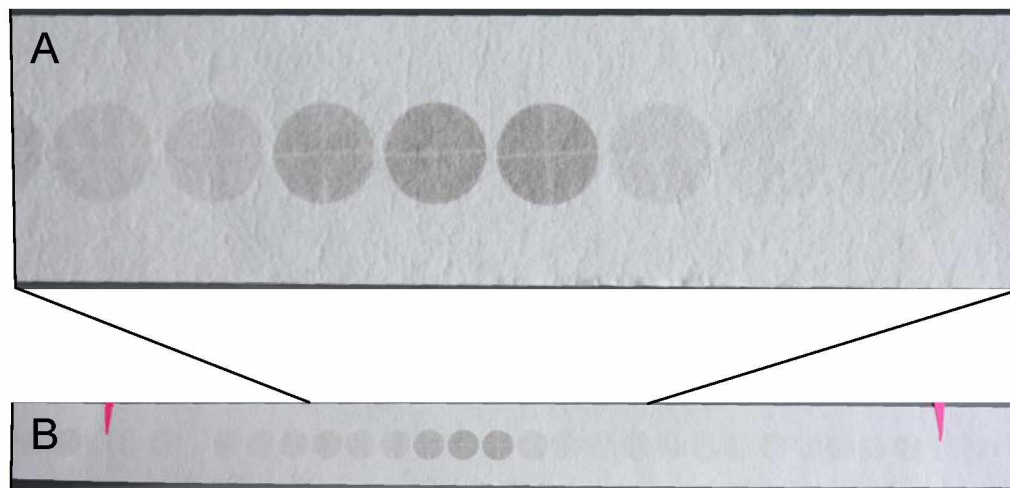


Figure 4.4 A and B. EBAM filter sample spots from the MOA Garden site $PM_{2.5}$ configured EBAM with Redoubt ash present. These spots are about 1 cm in diameter and represent a one hour interval. 4A shows a close-up of individual filter spots. The dark spot was collected over the 11:00 (AKDT) hour during a high mass loading episode while the lighter and virtually blank spots were collected during low mass loading episodes. B shows an entire 24 hour sample period. Note the arrows bracketing the 24 hour period. At each 24 hour interval, the EBAM advances 2 spaces to indicate the date change.

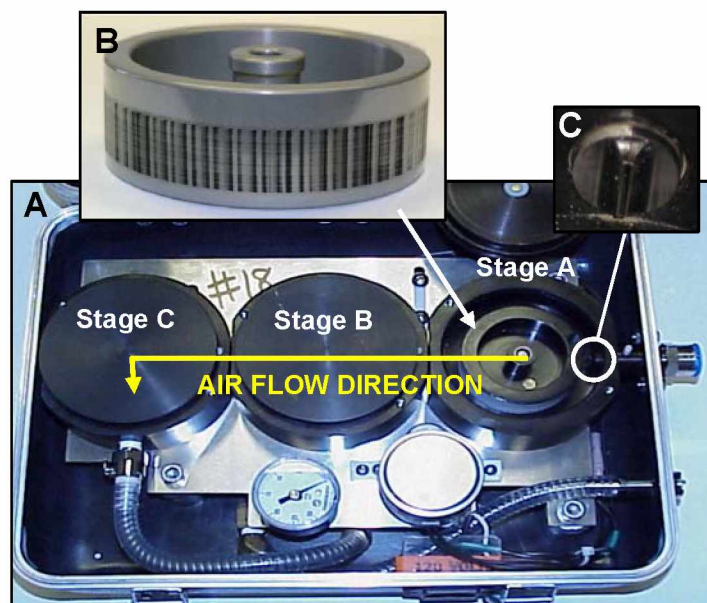


Figure 4.5. Three-stage DRUM sampler (A), sample drum (B), and chamber inlet (C). The sampler (A) connects to a vacuum pump and inlet/cyclone unit which imparts the initial size cut. The 3 circular chambers contain rotating drums that provide the sampling impaction surface. The first chamber (opened) collects the largest size fraction ($2.5\text{-}1.15\ \mu\text{m}\ \text{Ø}_A$). Subsequent stages collect smaller aerosol ($1.15\text{-}0.34$ and $0.34\text{-}0.1\ \mu\text{m}\ \text{Ø}_A$). The outer case is $30 \times 20 \times 10$ cm. The sample drum (B) has a MylarTM strip affixed to the outer surface. The dark lines on the outer drum surface are combustion aerosol particles that have collected on the MylarTM strip.

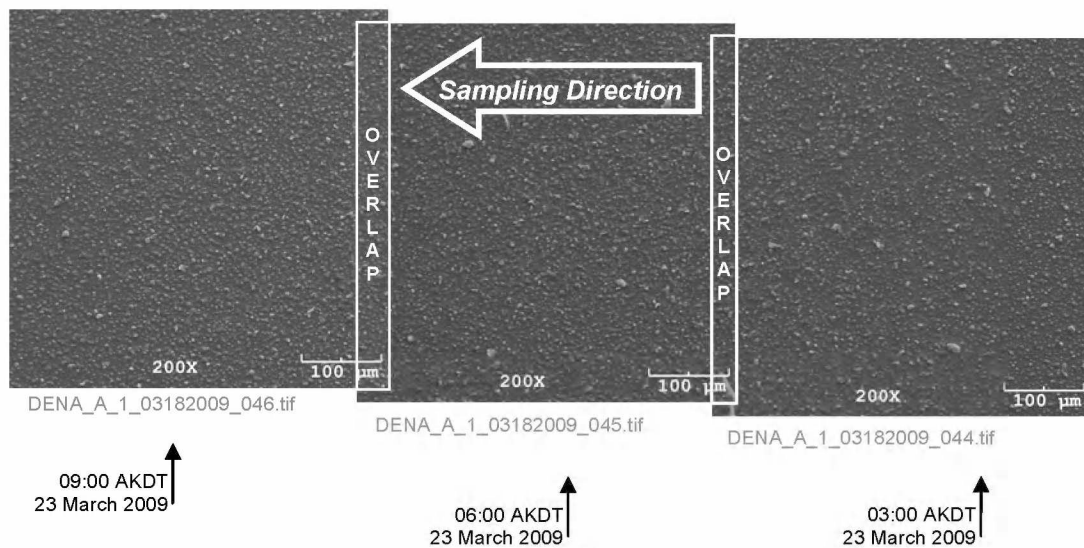


Figure 4.6. SEM DRUM sample image mosaic. The large particles are salts, smaller particles are volcanic ash. Each individual image represents about 3.5 hours of sampling time based on a rotation rate of 4 mm/day. The entire mosaic represents about 9 hours of sampling time after taking the image overlaps into account.

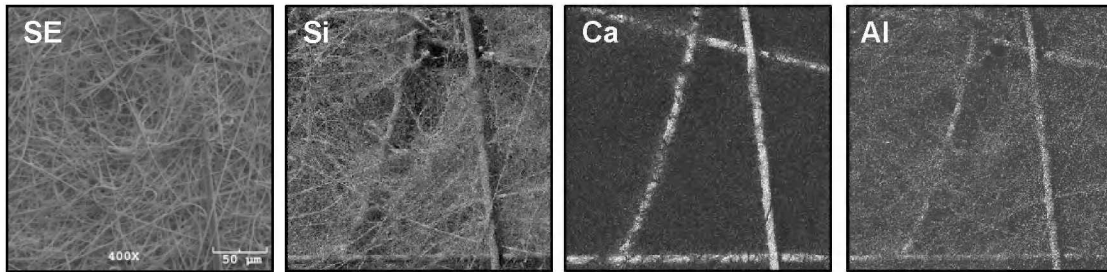
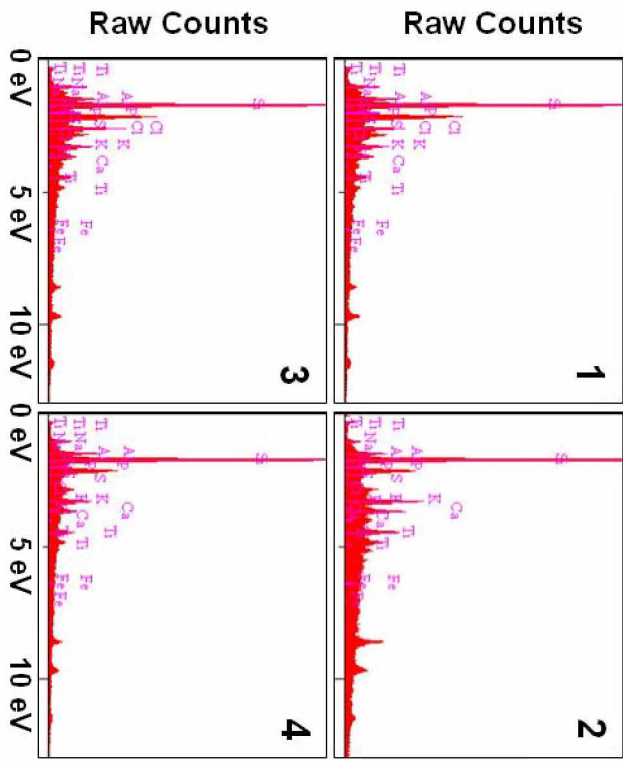


Figure 4.7. SEM secondary electron (SE) image and EDS element maps of EBAM filter tape. Si, Ca, and Al element maps are shown. The entire filter media is silica rich, while the thicker fibers also contain significant amounts of Ca and Al.



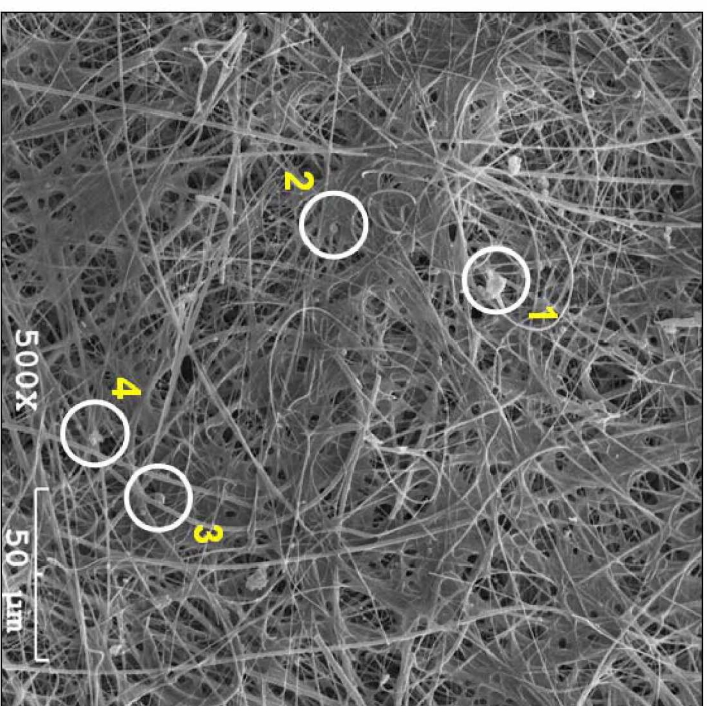


Figure 4.8. Secondary electron image of PM₁₀ EBAM filter tape and aerosol sample collected on 28 March 2009 at 05:00 AKDT at the MOA Air Quality Monitoring Program Garden site and corresponding EDS spectra from circled particles. Note the prominent silicon, aluminum, and calcium peaks in each spectrum regardless of particle composition. Particles indicated by 1 and 3 are likely salt aerosols due to the high chlorine counts, but the spectra are still dominated by background silicon counts. Particles indicated by 2 and 3 are possibly volcanic ash particles. Silicon is detected in all particles since the background (filter media) is made of silicon, aluminum, and calcium-rich glass fibers.

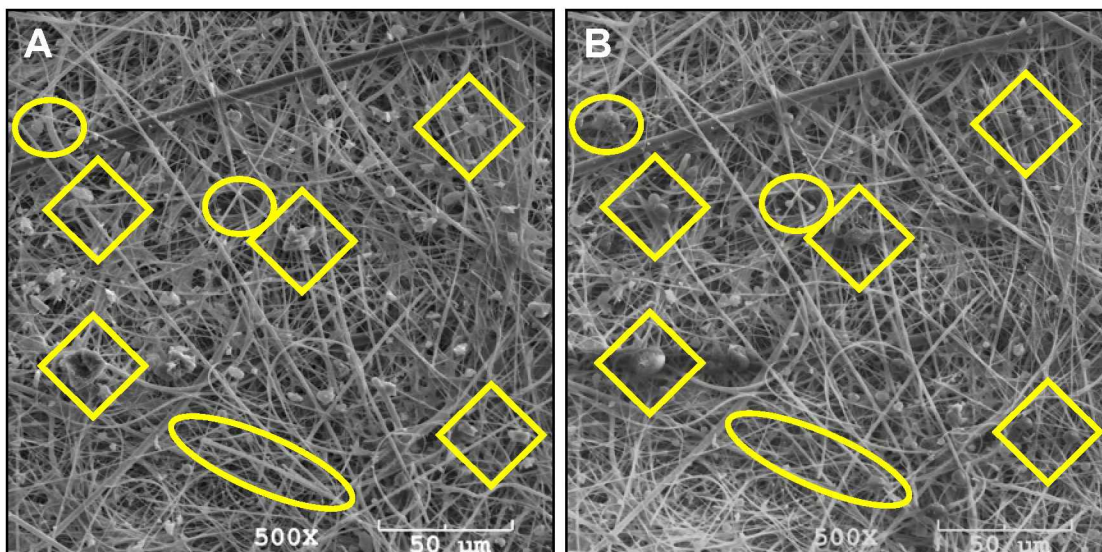


Figure 4.9. Secondary electron image of PM₁₀ EBAM filter tape and aerosol sample collected on 28 March 2009 at 18:00 AKDT at the MOA Air Quality Monitoring Program Garden site. Image A is the filter tape before analysis. Image B is the same area imaged after the collection of a 6 minute EDS spectra scan of approximately 25,000 counts per second, with the largest beam spot size setting and maximum accelerating current. Note the extensive fusing of aerosols and filter media. Some minor shifting of filter fibers is also present. Scan time, spot size, and accelerating current were set to collect sufficient x-ray counts to produce element maps with enough resolution for reliable image processing.

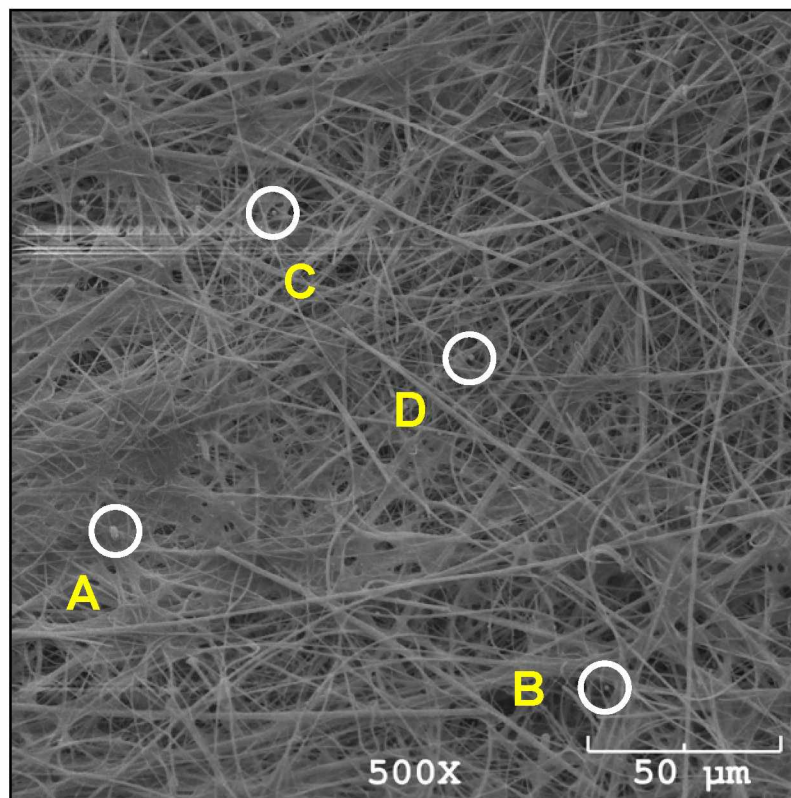


Figure 4.10. Secondary electron image of PM_{2.5} EBAM filter tape and aerosol sample collected on 28 March 2009 at 05:00 AKDT at the MOA Air Quality Monitoring Program Garden site. Few particles are present in the sample due to the low PM_{2.5} mass concentration (3 µg/m³). Those particles that are present are found on the surface of thick fiber mats (A) or imbedded in the media (B, C, and D).

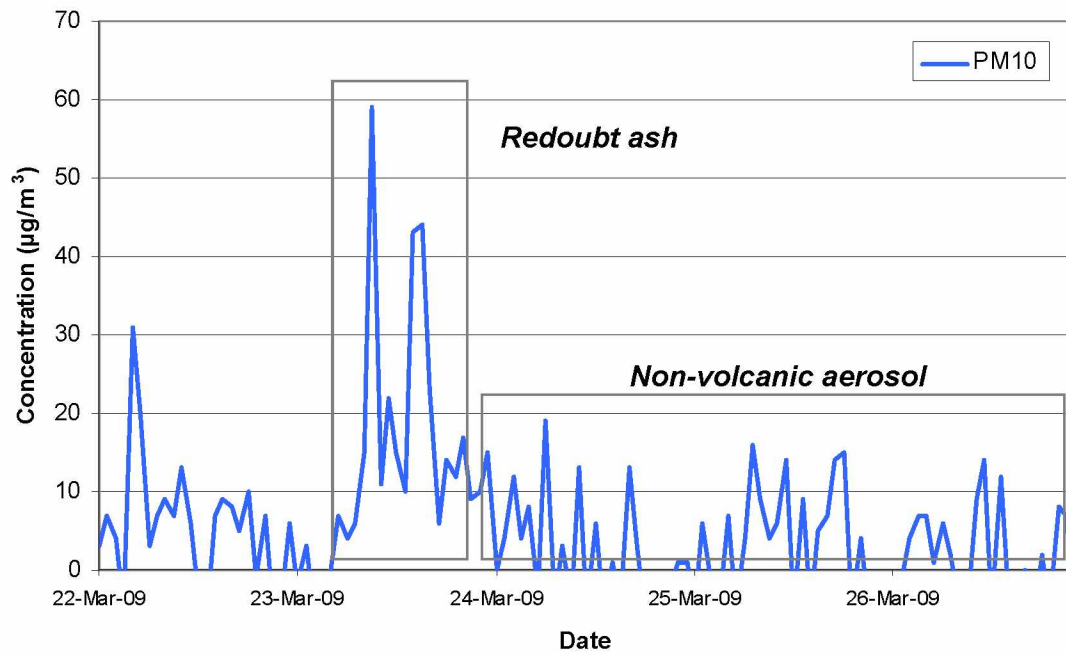


Figure 4.11 A. Hourly EBAM PM₁₀ levels in Soldotna, Alaska from 22 through 26 March 2009. Mass concentration spikes on 23 March are due to Redoubt ash at the sampling site. Mass concentrations after March 23 are from non-volcanic aerosols.

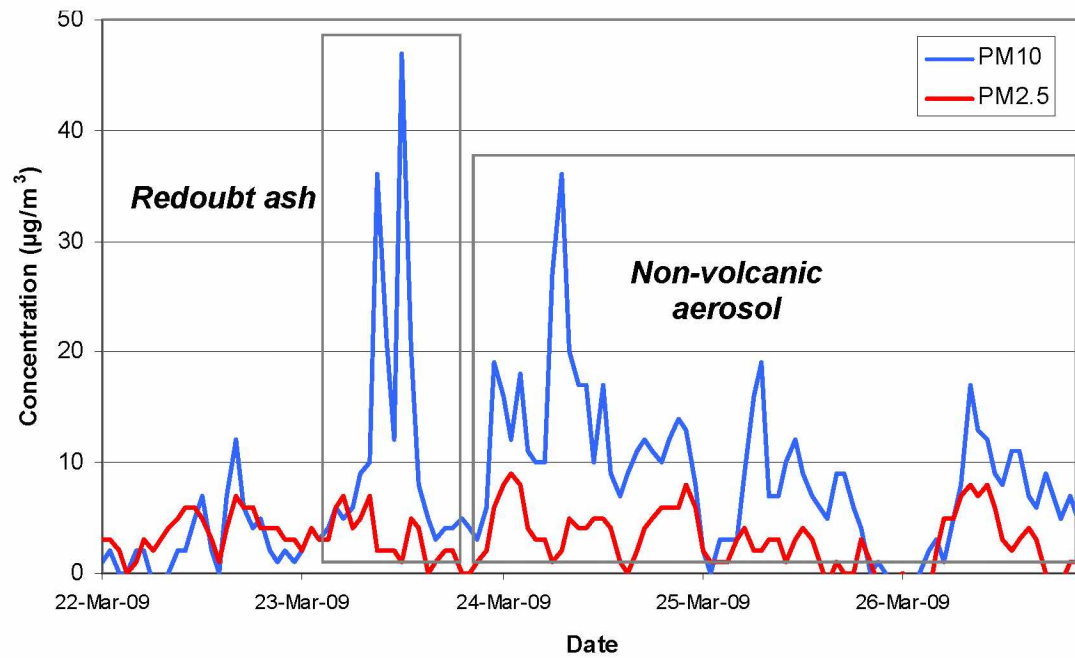


Figure 4.11 B. Hourly BAM-1020 PM₁₀ and PM_{2.5} levels in Anchorage, Alaska from 22 through 26 March 2009. Mass concentration spikes on 23 March are due to Redoubt ash at the sampling site. Non-volcanic aerosol was responsible for the elevated aerosol mass concentrations after 23 March 2009.

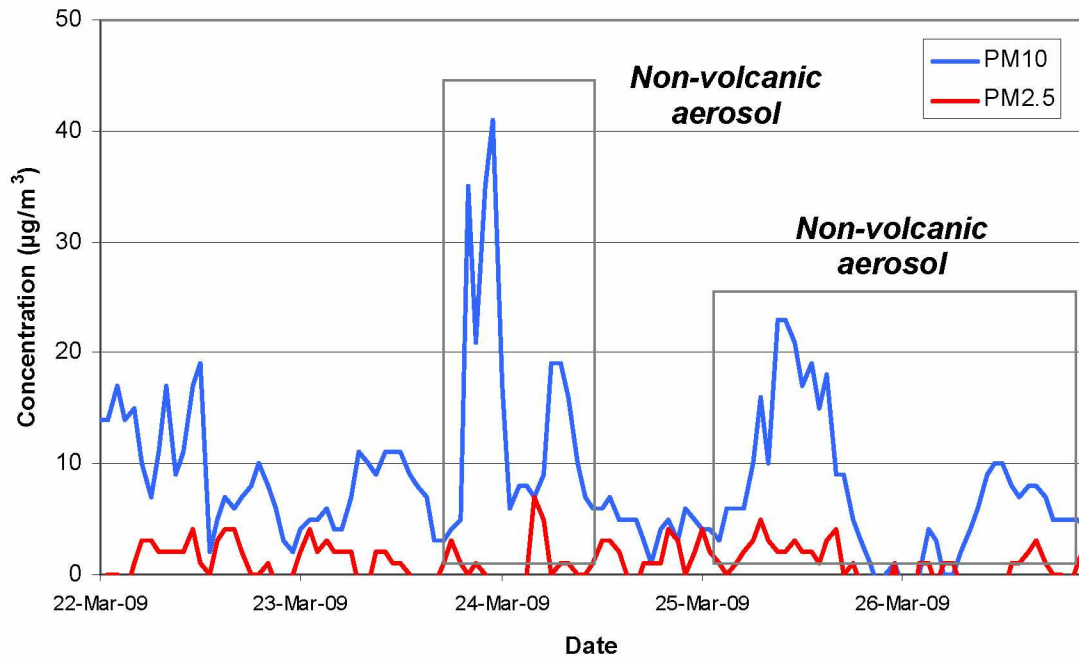


Figure 4.11 C. Hourly BAM-1020 PM₁₀ and PM_{2.5} levels in Wasilla, Alaska from 22 through 26 March 2009. No distinct increase in mass concentration coincides with HYSPLIT model predictions for 23 March. Non-volcanic aerosol was responsible for the elevated aerosol mass concentrations after 23 March 2009.

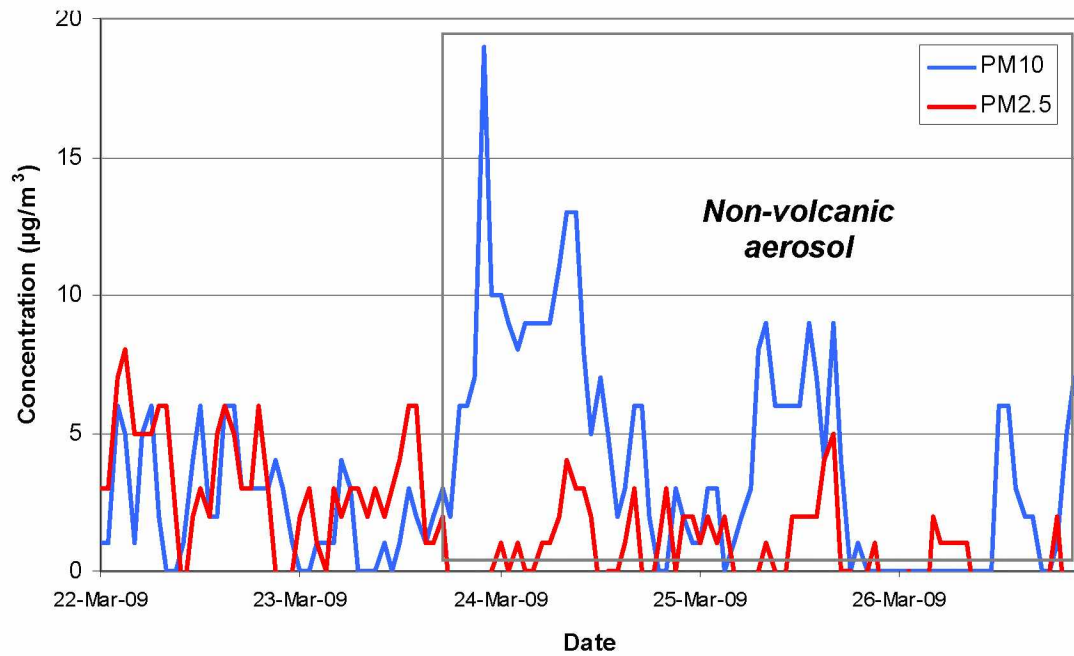


Figure 4.11 D. Hourly BAM-1020 PM₁₀ and PM_{2.5} levels in Palmer, Alaska from 22 through 26 March 2009. No mass concentration spikes were observed on 23 March despite HYSPLIT predicted arrival of air masses from Redoubt. Non-volcanic aerosol was responsible for the elevated aerosol mass concentrations after 23 March 2009.

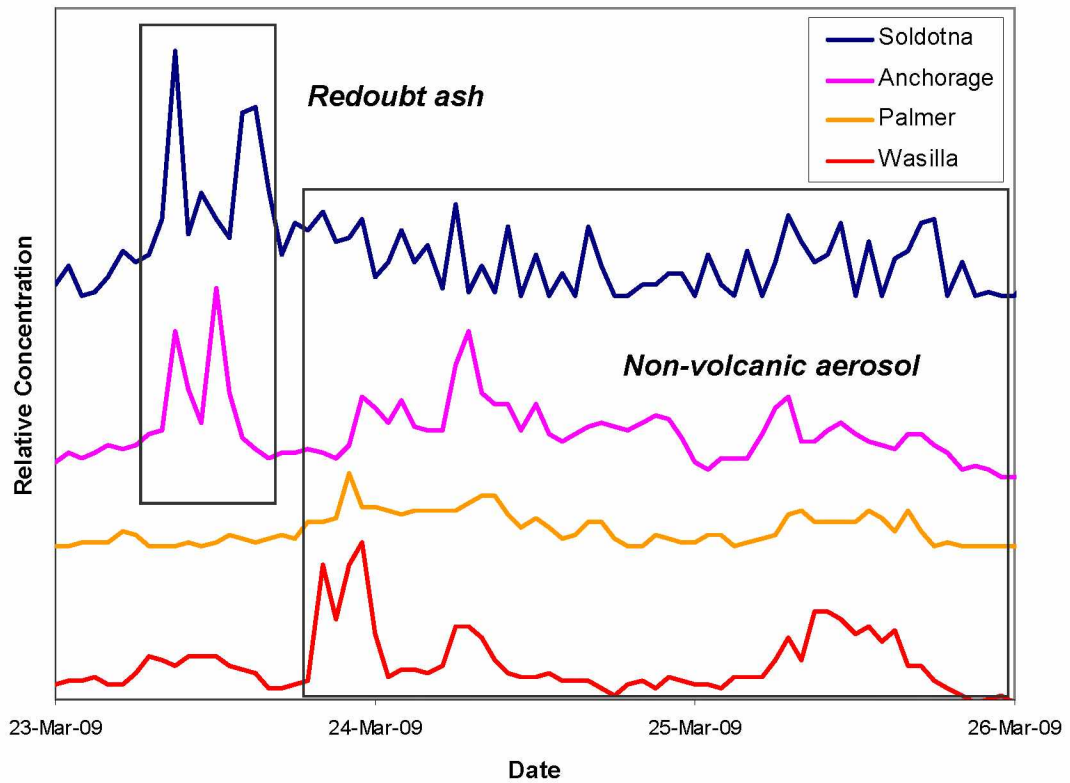


Figure 4.12. Relative hourly PM_{10} levels in Soldotna, Anchorage, Wasilla, and Palmer, Alaska from 23 to 26 March 2009. Mass concentration spikes (indicated by the box) on 23 March are due to Redoubt ash at the sampling site in Soldotna and Wasilla. No mass concentration spikes were observed in Palmer and Wasilla on 23 March. Aerosol mass concentrations after March 23 are from non-volcanic aerosol.

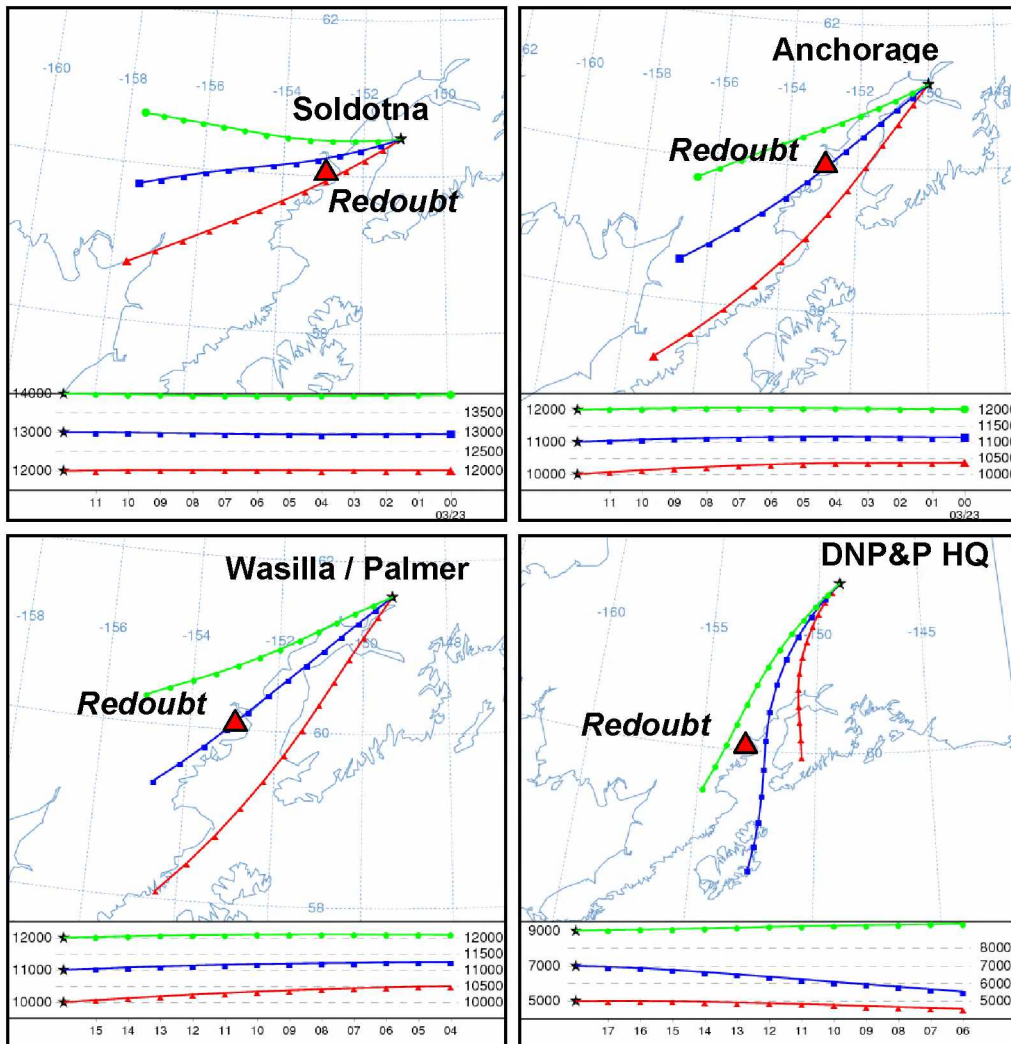


Figure 4.13. HYSPLIT backward trajectories for Soldotna, Anchorage, Wasilla/Palmer, and DNP&P HQ for the 23 March 2009 Redoubt eruption events. Trajectory altitudes are in meters above ground level.

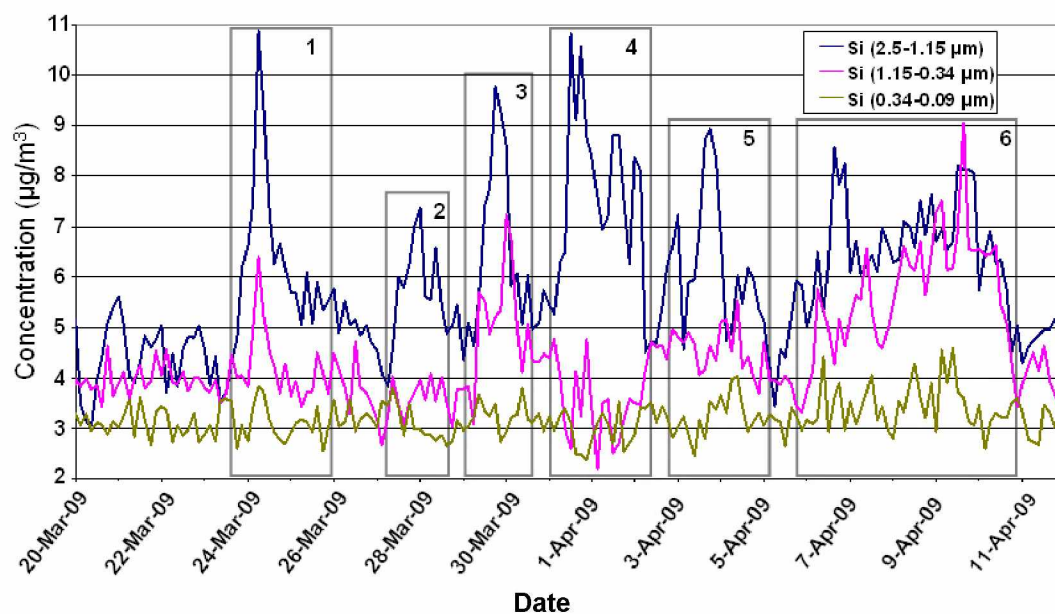


Figure 4.14. Time series of Si aerosol concentration collected by the DRUM sampler located at DNP&P HQ from 20 March-11 April 2009. The mass concentrations in boxes 1–3 are likely due to volcanic ash from Redoubt. This is confirmed by HYSPLIT trajectories presented in Figure 4.16. Silicon mass concentrations indicated in boxes 4–6 are from non-volcanic sources such as glacial dust and windblown river sediments. Note the relatively low silicon mass concentrations in the smallest (0.34-0.09 $\mu\text{m } \text{O}_A$) size fraction relative to the other stages.

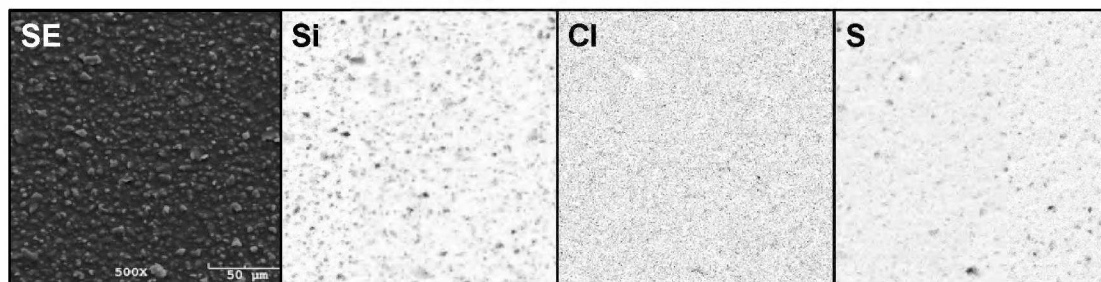


Figure 4.15 A. SEM secondary electron image and EDS element maps of aerosol collected at DNP&P HQ by DRUM sampler in the 2.5-1.15 μm O_A stage at 09:00 AKDT 23 March 2009. Sampling direction is from right to left. Volcanic glass shards are visible in the SE image and are visible in the EDS Si map. Some large sulfate particles are also present and evident in the S map. Minor chlorine salts are present, but most of the field of view is below the detection limit for Cl. No aggregation of particles is observed.

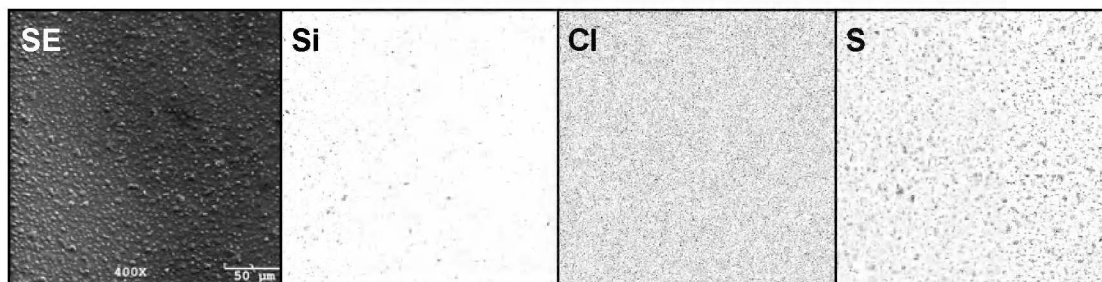


Figure 4.15 B. SEM secondary electron image and EDS element maps of aerosol collected at DNP&P HQ by DRUM sampler in the 1.15-0.34 μm O_A stage at 08:00 AKDT 23 March 2009. Sampling direction is from right to left. Some volcanic ash particles are visible in the SE image and the EDS Si map, but are very small and do not distinctly show shard shapes. Many large sulfate particles are also present and evident in the S map. No Cl is evident. The concentration of Si particles increases from right to left indicating a change in aerosol mass load. The sulfate mass load does not seem to change systematically with Si indicating that S and Si mass concentrations in this sampling interval are independent.

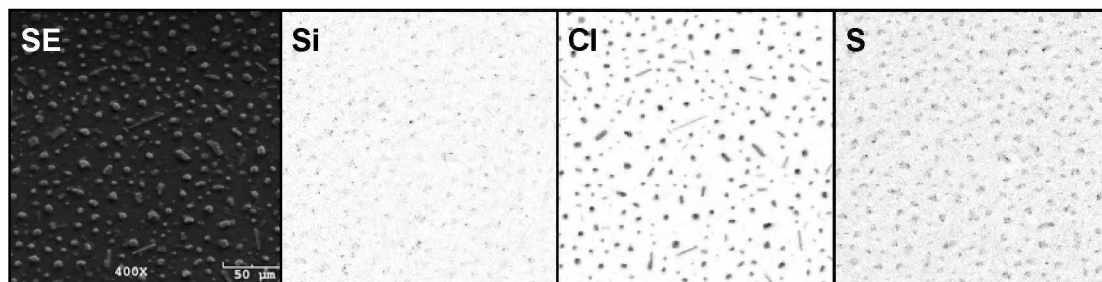


Figure 4.15 C. SEM secondary electron image and EDS element maps of aerosol collected at Ninilchik, Alaska by DRUM sampler in the 2.5-1.15 μm O_A stage at 17:00 AKDT 26 March 2009. Sampling direction is from right to left. Some Si is present and associated with S particles. Circular, ellipsoid, and rod-shaped Cl sea salt particles are abundant in the field of view. The S+Si particles are separate from the Cl particles indicating that Si and S aerosols combined to form hybrid aerosol while the sea salt particles did not. It is possible that the sulfate particles were liquid and sea salt particles were crystalline when aggregation occurred which could influence the aggregation process.

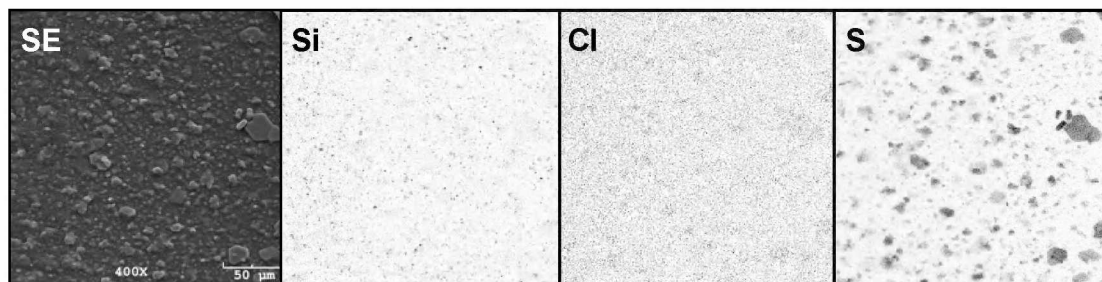


Figure 4.15 D. SEM secondary electron image and EDS element maps of aerosol collected at Ninilchik, Alaska by DRUM sampler in the 1.15-0.35 μm stage at 09:00 AKDT 27 March 2009. Sampling direction is from right to left. Large sulfate particles exhibiting distinct crystal shapes are evident in this image. There is no Cl aerosol present. Si aerosol is ubiquitous throughout the field of view. Sulfate may have been a dry aerosol when it was sampled due to the crystal shapes present in the image and that Si seems to be evenly distributed in the sample and not partitioned in sulfate particles. Sulfate particle sizes seem to decrease and particles become less crystalline as sampling progresses.

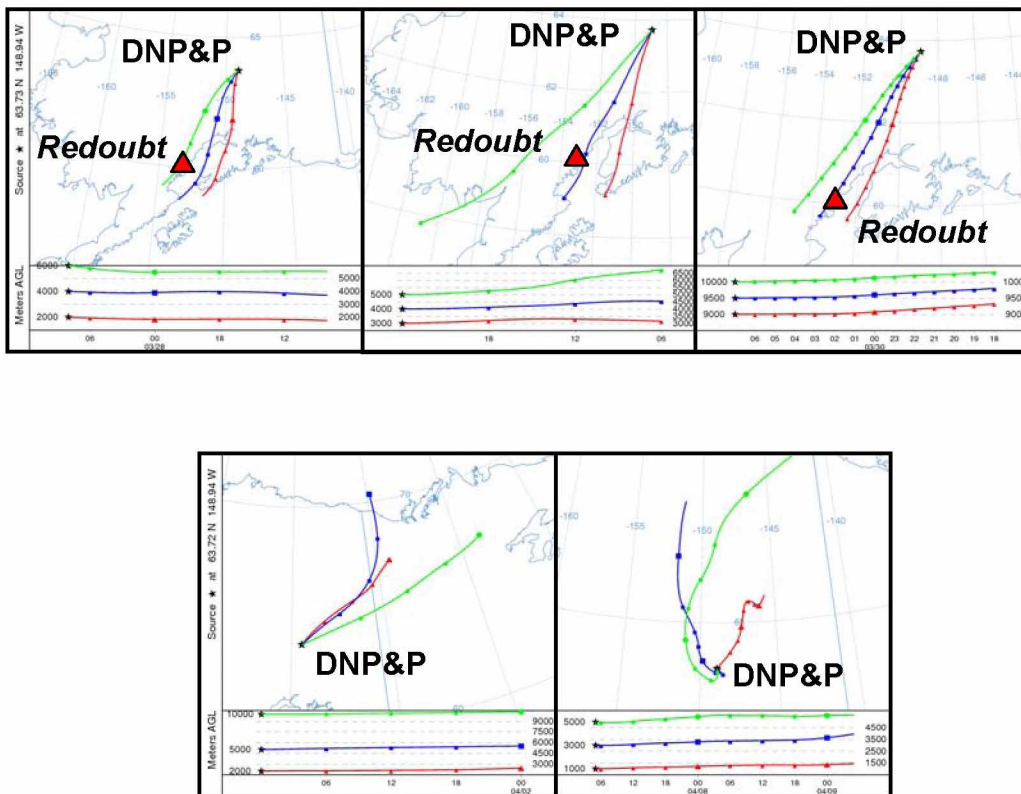


Figure 4.16. HYSPLIT backward trajectories for Denali National Park and Preserve (DNP&P) for 28-30 March 1 April and 7 April 2009. Trajectories from the 28-30 March show air masses transporting from Redoubt to DNP&P. Trajectories from 1 and 7 April 2009 show air masses transporting from the northeast and north, respectively.

Chapter 5 Conclusions

Three main conclusions are derived from the studies presented in this dissertation: 1) particle aggregation is influenced by eruptive style and atmospheric conditions, 2) fine ash volumes and settling rates used in volcanic ash tracking and dispersion models may be misleading, and 3) current satellite ash detection methods do not detect respirable ash mass concentrations in dispersed clouds.

5.1 Ash Aggregation Processes

Volcanic ash forms aggregates in ways that are influenced by eruption type and weather conditions (Sparks et al., 1997). Three types of particles containing ash were observed: single ash grains, ash aggregates, and hybrid aggregates. Single ash grains could be either in their original state of formation, having not undergone any post-eruptive aggregation, or could have been shed from an aggregate that had been subsequently degraded or destroyed.

Ash aggregates could form by a number of means, but they were only sampled over a specific size range in plumes from pyroclastic flows, which indicates the possibility of unique conditions for formation. Though no definitive means of formation at this specific size range is known, it is possible that the individual ash grains which formed these aggregates were formed in the pyroclastic flow by clast-to-clast milling and were not part of the ash initially produced by explosive processes (Darteville et al., 2002). Another possibility is that these particles most efficiently

retain their charge relative to particles of smaller or larger sizes (James et al., 2002; Fuchs, 1964). Speculation about how these particles form could lead to any number of possibilities; however, more investigation into the root processes of aggregate formation is needed to determine why these particles were sampled over such a narrow aerodynamic size range.

Hybrid aggregates likely form when downward mixing ash combines with maritime aerosol containing sea salt or non-sea sulfate mixing upwards from the marine boundary layer (Rose and Durant, 2009). The sulfate found in hybrid aggregates is thought to have a maritime source for three reasons: 1) sea salt is present in larger size fraction hybrid aerosols sampled at the same time as the sulfate-bearing hybrid aerosols, 2) no systematic change is observed in sulfate aerosol load relative to sea salt and volcanic ash mass concentrations relative to the timing of an eruption and 3) SO_2 to sulfate conversion rates during high-latitude, low solar flux wintertime conditions are too slow to produce substantial amounts of volcanic-source sulfate relative to the transport times needed for ash to reach the samplers used in these studies (Finlayson-Pitts and Pitts, 1986). Alternately, volcanic SO_2 may separate from a volcanic plume at altitude and be transported separately from the ash plume component (Mather et al., 2003; Rose et al., 2000).

5.2 Fine Ash Volume and Settling Rate Underestimation

Volcanic ash transport and dispersal models dependent on tephra collection data for model inputs may underestimate the volume of fine ash particulates because

large aggregates settle several orders of magnitude more quickly than fine ash. Therefore, tephra samples closer to the volcano do not contain fine ash because it may not have settled out of the dispersing cloud at the sampling location.

Model volume and settling time underestimation is due to five possible issues: 1) underestimating ash plume volume and particle size distribution when fine ash is not found during post-eruptive tephra sampling, 2) overlooking aggregation processes, 3) overestimating settling velocity when micron and smaller sized ash is not assumed to be produced by an eruption, 4) local weather influencing mass concentrations more than eruption rates when those rates are relatively low, and 5) meteorologic and topographic controls influencing the transport of ash-laden air parcels.

Particle aggregates are formed from ash particles and background aerosols smaller than the overall aggregate size. The larger aggregate is removed from the eruption cloud at a rate faster than the rate of removal for the individual particles. After removal, the aggregate structure is destroyed by impact, rain washing, compaction, loading, pedogenesis, and bioturbation (James et al., 2003; Shoji et al., 1993; Sorem, 1982). In general, only accretionary and cored lapilli remain intact in ash deposits (Schumacher and Schminke, 1991). Other atmospherically-formed ash aggregates are too weakly bound to survive after they are removed from the atmosphere (Rose and Durant, 2011; Taddeucci et al., 2011; James et al., 2003; Sorem, 1982). Sampling and analytical techniques used for tephra studies further disaggregate atmospherically aggregated ash by sieving and particle resuspension

methods (Riley et al., 2003; Heiken and Wohletz, 1985). Also, not all ash participates in aggregation processes at the same time; some of the ash remains as individual particles and undergoes long range transport. Indeed, some eruptions may produce ash that does not aggregate before sedimenting from the plume. In addition, these models do not address possible aggregate disintegration in the cloud due to particle collision, electrostatic charge relaxation, particle drying, or turbulence. Diurnal heating and radiative cooling of air masses can bring airborne ash to ground level or send it higher in the atmosphere at different times of the day which may influence ash and other aerosol mass concentrations in air masses being sampled (Seinfeld and Pandis, 2006). Other local effects such as an interposing topographic high region may divert air masses and cause mass concentrations to be different than model predictions that do not account for topography. For volcanic ash distribution models to more closely forecast ash fall and ash cloud evolution these factors would have to be quantified and incorporated.

5.3 Satellite Detection Method Limitations

The Brightness Temperature Difference (BTD) satellite volcanic ash detection method can miss the long-range transported ash mass due to low ash mass concentrations or the overall particle diameter being smaller than the thermal infrared wavelengths used for its detection algorithm: $\sim 2.5 \mu\text{m}$ for particles, versus AVHRR band 4 (10.3-11.3 μm) and band 5 (11.5-12.5 μm) (Prata, 1989).

Particles with diameters \geq than 10.3 μm are easily detected in translucent volcanic clouds. But, since the diameter of a substantial number of volcanic particles in the plume are well below these wavelengths, a dilute plume consisting of fine ash cannot be reliably detected by the BTD method (Simpson et al., 2000). As the plume is transported and larger particles are removed, the plume becomes dilute and dominated by fine ash less than 10.3 μm in diameter. The volcanic ash then falls below the detection limit of the BTD method even though ash is present. Therefore lower concentration plumes, or plumes consisting of fine ash particles, cannot be reliably tracked by current ash detection and monitoring satellite detection techniques. Alternate detection and tracking means are needed to monitor these plumes.

In addition to alternate detection and tracking means, a suite of forecasting, detection, measurement, and sampling methods, some with real-time reporting capabilities, are needed to fully address the range of incident management and scientific research needs during a volcanic eruption. While some methods and techniques are already incorporated into standard volcano observatory operations during an eruption response, a suite of formalized, scalable forecasting, detection, and tracking instruments and techniques needs to be developed and implemented during future eruptions.

5.4 References

- Dartevelle, S., Ernst, G.J., Stix, J., Bernard, A., 2002. Origin of the Mount Pinatubo climactic eruption cloud: Implications for volcanic hazards and atmospheric impacts. *Geology*. 30, 663-666.
- Finlayson-Pitts, B.J., Pitts J.N., 1986. *Atmospheric Chemistry: Fundamentals and Experimental Techniques*. Wiley-Interscience, New York, NY.
- Fuchs, N.A., 1964. *The Mechanics of Aerosols*. Dover Publications, New York, NY.
- Heiken, G., Wohletz, K., 1985. *Volcanic Ash*. University of California Press, Berkley, CA.
- James, M.R., Lane, S.J., Gilbert, J.S., 2003. Density, construction, and drag coefficients of electrostatic volcanic ash aggregates. *Journal of Geophysical Research*. 108, 2435-2447.
- James, M.R., Gilbert, J.S., Lane, S.J., 2002. Experimental investigation of volcanic particle aggregation in the absence of a liquid phase. *Journal of Geophysical Research*. 107, 148-227.
- Mather, T.A., Pyle, D.M., Oppenheimer, C., 2003. Tropospheric Volcanic Aerosol. In: Robock, A., Oppenheimer, C. (Eds.), *Volcanism in the Earth's Atmosphere*. American Geophysical Union, Washington D.C., pp. 189-212.
- Prata, A.J., 1989. Observations of volcanic ash clouds in the 10-12 μm window using AVHRR/2 data. *International Journal of Remote Sensing*. 10, 751-761.
- Riley, C.M., Rose, W.I., Bluth, G.J.S., 2003. Quantitative shape measurements of distal volcanic ash. *Journal of Geophysical Research*. 108, 2504-2519.
- Rose, W.I., Durant, A.J., 2011. Fate of volcanic ash: Aggregation and fallout. *Geology*. 39, 895-896.
- Rose, W.I., Durant, A.J., 2009. Fine ash content of explosive eruptions. *Journal of Volcanology and Geothermal Research*. 186, 32-39.
- Rose, W.I., Bluth, G.J.S., Ernst, G.G.J., 2000. Integrating retrievals of volcanic cloud characteristics from satellite remote sensors: a summary. *Philosophical Transactions of the Royal Society of London*. 358, 1585-1606.

Schumacher, R., Schminke, H.-U., 1991. Internal structure and occurrence of accretionary lapilli: A case study at Laacher See Volcano. *Bulletin of Volcanology*. 53, 612-636.

Seinfeld, J.H., Pandis, S.N., 2006. *Atmospheric Chemistry and Physics*. Wiley, Hoboken, NJ.

Seuss, D., 1949. *Bartholomew and the Oobleck*. Random House Publishers, New York, NY.

Shoji, S., Nanzyo, M., Dahlgren, R., 1993. *Volcanic Ash Soils: Genesis, Properties and Utilization*. Elsevier, New York, NY.

Simpson, J., Hufford, G., Pieri, D., Berg, D., 2000. Failures to detect volcanic ash from a satellite-based technique. *Remote Sensing of the Environment*. 72, 191-217.

Sorem, D.K., 1982. Volcanic ash clusters: Tephra rafts and scavengers. *Journal of Volcanology and Geothermal Research*. 13, 63-71.

Sparks, R.S.J., Bursik, M.I., Carey, S.N., Gilbert, J.S., Glaze, L.S., Sigurdsson, H., Woods, A.W., 1997. *Volcanic Plumes*. John Wiley, Hoboken, N. J.

Taddeucci, J., Scarlato, P., C. Montanaro, C., Cimarelli, C., Del Bello, E., Freda, C., Andronico, D., Gudmundsson, M.T., Dingwell, D.B., 2011. Aggregation-dominated ash settling from the Eyjafjallajökull volcanic cloud illuminated by field and laboratory high-speed imaging. *Geology*. 39, 891-894.